POLITECNICO DI MILANO
School of Industrial and Information Engineering
Master of Science in Nuclear Engineering

An Innovative Route for Uranium Carbide Synthesis and Densification using Spark Plasma Sintering

Supervisors: Prof. Lelio Luzzi
Dr. Vaclav Tyrpekl
Dr. Jean-François Vigier
Dr. Marco Cologna

Author: Daniele Salvato Matr. 817164

Academic year
2014-2015

This page is intentionally left blank

This page is intentionally left blank

Contents

This page is intentionally left blank

Acknowledgements

First of all, I would like to thank my supervisor at Politecnico di Milano, Prof. Lelio Luzzi, who supported me in being involved in this beautiful experience. I am very thankful to him for his precious advices during the supervision of the thesis.

I express my gratitude towards Dr. Maria Betti, Director of the Institute for Transuranium Elements (ITU, Karlsruhe, Germany) and Dr. Joe Somers, Head of the Nuclear Fuel Safety Unit of ITU, for giving the opportunity to complete this seven-months traineeship.

I am thankful for being involved in a training grant funded by the Euratom GENTLE (Graduate and Executive Nuclear Training and Lifelong Education) project.

I wish to thank also my supervisors at ITU, Dr. Vaclav Tyrpekl, Dr. Jean-François Vigier, and Dr. Marco Cologna, for their guidance and assistance during these months, for all the efforts and encouragement.

I would like to express my acknowledgment also to the rest of the Unit and ITU staff for their technical and scientific support. In particular, I would thank Michael, Andrea, Laura, Damien, Hervin, Co, Sarah, Chris, Elena, Olaf, Karin, Anthony, Bert, Oliver, and Thierry. It was a pleasure to work and collaborate with them.

I warmly thank also the administrative ITU staff, especially Anna, who has been of great help regarding whatever administrative issues, and Encarni, who helped me with bureaucratic practices.

I would like to thank also the fantastic friends I have met at ITU, especially Davide, Sara, Elisa, Luca, Fabiola, Donato.

Un sentito grazie va alla mia famiglia, a mio padre, a mia madre e a mia sorella, per il loro incoraggiamento e supporto. Grazie a Luchino con cui ho condiviso fantastiche esperienze a Karlsruhe. Un immenso grazie va ai miei compagni delle superiori, belli e brutte. Ringrazio Lone, amico di sempre, sempre, amico.

Infine, Eve, Ti ringrazio. Per la pazienza, per il conforto, per l'aiuto e per il Tuo Amore.

This page is intentionally left blank

Sommario

I carburi misti di uranio e plutonio sono considerati una possibile alternativa agli ossidi misti come combustibile di reattori veloci di quarta generazione (Generation IV). Tuttavia, diversi fattori hanno ostacolato la loro affermazione. Tra questi, uno dei più importanti è rappresentato dalla loro difficile e dispendiosa fabbricazione. Convenzionalmente, polveri di ossido di uranio e grafite vengono usate come precursori per la sintesi dei carburi, sfruttando una reazione chimica detta riduzione carbotermica. Tipicamente, per favorire il contatto fra le due fasi, e quindi migliorare la cinetica della reazione, le polveri di partenza vengono a lungo mescolate. Nonostante ciò, i trattamenti termici successivi, necessari alla produzione dei carburi, richiedono alte temperature e lunghe durate. Questa tesi si pone come obiettivo quello di sviluppare e analizzare un nuovo metodo di sintesi e densificazione di carburi d'uranio, volto a risolvere i problemi sopracitati. In particolare, per migliorare la reattività dei precursori, sono state impiegate soluzioni di nitrato di uranile e acido citrico, come sorgenti, rispettivamente, di ossido di uranio e carbonio. La natura liquida dei precursori, unita all'azione complessante del gruppo citrato nei confronti dello ione uranile, ha consentito di ottenere, dopo una decomposizione termica in argon, un composto (UO_2/C) caratterizzato da un'omogenea dispersione delle due fasi. La produzione di carburi di uranio é stata condotta attraverso diverse tipologie di trattamenti termici, che hanno visto l'impiego anche di un dispositivo di *Spark Plasma Sintering* (SPS), attraverso una configurazione di prova opportunamente adattata allo scopo. L'elevata reattività del composto di partenza e l'efficacia dei suddetti trattamenti hanno consentito di ridurre sensibilmente le temperature e i tempi usualmente richiesti, consentendo anche di ottenere una polvere di carburo estremamente sinterizzabile. Diverse tecniche sperimentali sono state impiegate per ricavare informazioni riguardanti la composizione, la struttura e la morfologia dei campioni prodotti, quali diffrazione a raggi X (XRD), microscopia elettronica a scansione (SEM) e a trasmissione (TEM), tomografia a raggi X.

This page is intentionally left blank

Abstract

Mixed uranium-plutonium carbides are considered as potential fuels for Generation IV fast reactors. However, high temperature and long periods are required to fabricate them, thus heavily hindering their success as a concrete alternative to mixed oxides fuels. Conventionally, UO_2 and C powders, precursors for carbide synthesis, are mechanically blended together through a long milling step to facilitate their interaction. In this thesis, a new synthesis and sintering route for carbides production is proposed. At first, a mixture of nanocrystalline UO_2 embedded in amorphous carbon was obtained by thermal decomposition of a solution of uranyl nitrate and citric acid. The liquid nature of the precursors assured an intrinsic homogeneity at a molecular scale, thus enhancing their reactivity, avoiding any milling step. The effects of initial composition, temperature, dwell time, gas/vacuum atmosphere, and thus the overall reaction kinetics were studied performing the carbide synthesis in a conventional furnace or in a modified Spark Plasma Sintering (SPS) facility. The latter turned out to be very suitable for this kind of material, allowing a drastic reduction of the time and temperature usually needed. Furthermore, a fine uranium carbide powder was produced with significantly increased sinterability. In fact, the densification was also performed in SPS reaching high densities in very short times. The occurring phenomena, the phase compositions, the morphology, and the structure of the produced samples have been characterized by different experimental techniques, as (among all) X-ray powder diffraction, scanning and transmission electron microscopy, and X-ray tomography.

This page is intentionally left blank

Estratto in Italiano

1. Introduzione

I carburi misti di uranio e plutonio, insieme ai nitruri e alle leghe metalliche, sono considerati un'alternativa agli ossidi misti (MOX) come combustibili avanzati per i reattori veloci di nuova generazione (Gen IV). In particolare, se confrontati con i MOX, essi presentano una più elevata densità di atomi pesanti (12.9 contro 9.8 g/cm^3) e una migliore conducibilità termica (tra le 5 e le 8 volte maggiore), oltre a una migliore compatibilità con fluidi termovettori quali metalli liquidi (Na) e gas (He). Queste proprietà consentono un migliore sfruttamento delle potenzialità di un reattore veloce, sia questo inteso come fertilizzante (*breeder*), che, ancor più interessante, come bruciatore (*incinerator*) di attinidi minori (Np, Cm, Am).
Nonostante questi vantaggi, l'affermazione dei carburi come vera alternativa agli ossidi è da sempre ostacolata dalle gravi difficoltà legate alla loro fabbricazione. Queste ultime, di fatto, vanno ad offuscare qualsiasi vantaggio in termini neutronici e di performance di questa categoria di combustibile.
In particolare, il metodo convenzionale di produzione di carburi si basa sul fenomeno della riduzione carbotermica, dove polvere di ossido di uranio (e plutonio) e grafite reagiscono a dare carburo di uranio (e plutonio) e monossido di carbonio attraverso due successive reazioni:

$$UO_2 + 4C \rightarrow UC_2 + 2CO \quad (1)$$
$$UO_2 + 3UC_2 \rightarrow 4UC + 2CO \quad (2)$$

Diverse difficoltà riguardano tale processo di fabbricazione. Innanzitutto, da studi dettagliati (Suzuki *et al.*, 1981) è emerso che i principali fattori che ostacolano la cinetica della reazione sono la diffusione dell'ossigeno negli agglomerati di UO_2 verso l'interfaccia di reazione e la difficoltosa diffusione del CO attraverso strati compatti.
Per questi motivi, nel tentativo di migliorare la reattività, è usualmente prevista la macinazione delle polveri in un mulino a palle (*ball milling*), per un lungo intervallo (fino a 24/48h), in modo da ridurre la dimensione dei grani e promuovere un contatto intimo fra i precursori e quindi agevolare il procedimento della reazione (Sengupta *et al.*, 1981). Peraltro, è obbligatoria l'adozione del vuoto durante il trattamento termico, in quanto questo favorisce la liberazione di CO. Nonostante ciò, alte temperature (>1450°C) e lunghi tempi di residenza (5-15h) sono richiesti per completare la suddetta riduzione carbotermica (Duguay *et al.*, 2015).
Inoltre, date le alte temperature e i lunghi tempi richiesti, le polveri di carburo così prodotte risultano essere parzialmente sinterizzate. Per questo motivo, la loro successiva densificazione, dopo la pressatura in forma di pastiglie, risulta essere ostacolata. Infatti, per raggiungere le densità richieste (80-85% TD (Manara *et al.*, 2012)) si procede con una ulteriore macinazione, prima della sinterizzazione finale a temperature maggiori di 1700°C con una permanenza di 5 o più ore (Burkes *et al.*, 2009).
Tutti questi fattori rendono sicuramente meno competitivo questo tipo di combustibile rispetto ai ben più affermati e facilmente realizzabili ossidi misti di uranio e plutonio.

L'obiettivo raggiunto da questo lavoro di tesi è stato quello di proporre e sviluppare un nuovo metodo di sintesi e densificazione per i carburi, dimostrando la migliore efficacia in termini di tempi e temperature richieste e studiando i vari fenomeni fisico/chimici coinvolti.
La principale innovazione è rappresentata dall'impiego di soluzioni liquide come precursori di partenza (nitrato di uranile e acido citrico, come fonte, rispettivamente, di uranio e di carbonio). L'idea è di sfruttare l'azione complessante del gruppo citrato nei confronti dello ione uranile (Lenhart *et al.*, 2000; Bailey *et al.*, 2005). In questo modo, dopo una decomposizione delle soluzioni ad alte temperature, si è ottenuto un composto di ossido di uranio e carbonio intimamente miscelato che consente quindi di incrementare la reattività dei precursori della riduzione carbotermica, evitando le lunghe fasi di macinazione usualmente necessarie. Un'altra innovazione deriva dall'utilizzo della tecnica di *Spark Plasma Sintering* (SPS) per condurre sia la sintesi che la sinterizzazione dei carburi.
Negli esperimenti svolti, si è studiata la produzione di carburi di uranio, e non di carburi misti (U, Pu), data la minore radiotossicità dei primi e quindi la più facile esecuzione degli esperimenti.

2. Procedura sperimentale

La procedura sperimentale è riassunta nella *Figura 1*.

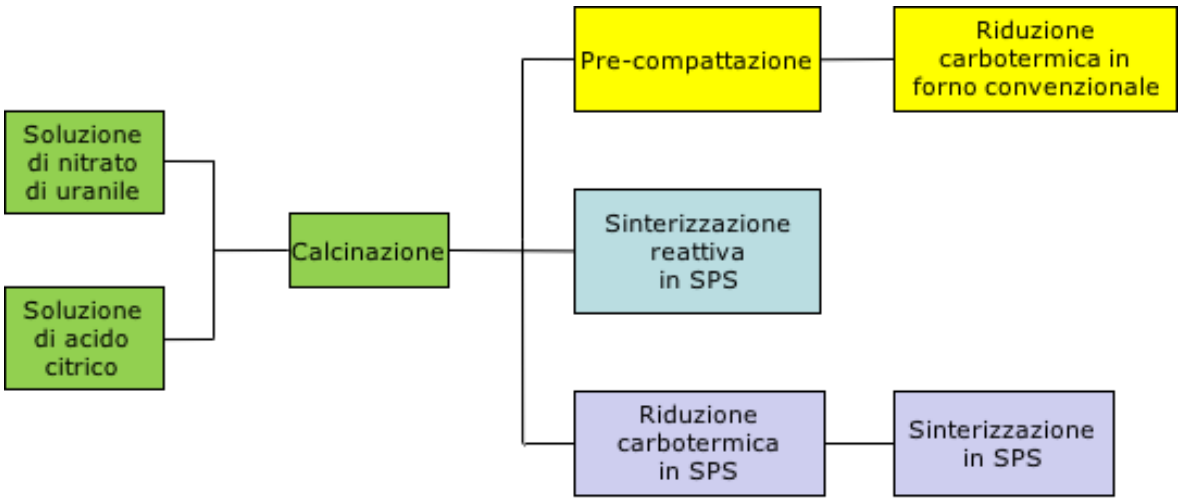

Figura 1: Schema generale degli esperimenti svolti.

2.1 Preparazione dei campioni

Le due soluzioni di partenza sono una soluzione di nitrato di uranile (- $UO_2(NO_3)_2$ -) e una di acido citrico ($C_6H_8O_7$) con concentrazioni molari rispettivamente di 2.076 mol/L e 2.611 mol/L. La preparazione dei campioni è avvenuta all'interno di una scatola a guanti predisposta all'impiego di sostanze radiotossiche. La composizione dei campioni è stata variata miscelando diverse quantità di acido citrico e nitrato di uranile, al fine di determinare il rapporto ottimale per massimizzare il grado di completamento della riduzione carbotermica.

2.2 Calcinazione

Dopo la miscelatura, i campioni sono stati sottoposti a un trattamento termico di calcinazione, per liberare tutte le sostanze volatili (H_2O, CO, CO_2, N_2, NO_x, C_xH_y), ottenendo infine un miscuglio di UO_2 e C.

Il processo è avvenuto all'interno di un forno convenzionale, in atmosfera inerte (argon). Il trattamento termico consiste in un riscaldamento con un tasso di 50°C/h da temperatura ambiente fino a 200°C e 200°C/h fino a 1000°C, con un tempo di residenza di due ore e infine un raffreddamento con un tasso di 400°C/h.

La polvere ottenuta è stata analizzata per mezzo di diverse tecniche. La composizione e la cristallinità del composto sono state valutate tramite analisi XRD, mentre SEM e TEM hanno consentito di studiarne la morfologia e la struttura.

2.3 Sintesi di carburo di uranio

Il composto calcinato di UO_2 e C è stato sottoposto a tre diverse tipologie di trattamenti termici, al fine di valutare quella più efficace: (i) riduzione carbotermica in un forno

convenzionale, (ii) sinterizzazione reattiva (*reactive-sintering*) in SPS, per sintetizzare e al tempo stesso sinterizzare i carburi di uranio, e infine (iii) riduzione carbotermica in SPS, attraverso una configurazione di prova appositamente sviluppata durante questo lavoro, seguita dalla sinterizzazione, sempre in SPS, utilizzando una configurazione *standard* (tipicamente adottata per sinterizzare ossidi di uranio, torio e zirconio).

2.3.1 Riduzione carbotermica in forno convenzionale

Prima del riscaldamento, la polvere calcinata è stata pressata con una pressa automatica idraulica fino a una pressione compresa fra 400 e 500 MPa. Tale precompattazione è servita per migliorare il contatto tra i precursori (Majunmdar *et al.*, 2006) e quindi favorire il procedimento della reazione.
La ricetta adottata ha previsto il riscaldamento in argon a 1600°C per un'ora, con un tasso di +200°C/h, seguito da un raffreddamento fino a temperatura ambiente con un tasso di -200°C/h. In letteratura si afferma chiaramente che l'utilizzo del vuoto migliora la cinetica della reazione (Matzke *et al.*, 1986), ma nel nostro caso questo non è stato possibile a causa di problemi tecnici legati alla tenuta del forno.
Il grado di completezza della reazione è stato stimato tramite delle analisi XRD del prodotto finale.

2.3.2 Sinterizzazione reattiva in SPS

Alcune prove sono state effettuate in SPS sul composto di UO_2+C, ricavato dopo la calcinazione, in cui si è provato simultaneamente a produrre il carburo e a densificarlo. Questo tipo di reazione è stata effettuata con successo su altri tipi di carburi, come mostrano i lavori di Majunmdar *et al.* (HfC), Sun *et al.* (WC), He *et al.* (VC), e Guo *et al.* (SiC).
L'apparato utilizzato per questi esperimenti è stato quello *standard*. È stata studiata l'influenza di diversi fattori, quali la pressione applicata, l'atmosfera e la durata dell'esperimento.
In aggiunta alle analisi XRD sui campioni prodotti, in questo caso si sono potute usare le informazioni normalmente registrate dal *software* dell'SPS, quali lo spostamento dei pistoni di grafite e la loro velocità. Queste grandezze possono essere utilizzate per monitorare l'evoluzione del processo, come un'eventuale reazione allo stato solido o una densificazione in atto.

2.3.3 Riduzione carbotermica in SPS

La parte finale di questo lavoro sperimentale si è focalizzata sulla sintesi dei carburi di uranio in SPS utilizzando una configurazione appositamente progettata (*Figura 2*), seguita dalla sinterizzazione in SPS, in una configurazione convenzionale. Quindi, diversamente dal processo descritto precedentemente (paragrafo 2.3.2), in questo caso si sono eseguiti i due processi separatamente, analogamente al lavoro di Feng *et al.* (2015) con carburi di afnio.
L'apparato sviluppato comprende due modifiche significative rispetto a quello *standard*. La prima consiste nell'impiego di pistoni in grafite con dei fori opportunamente posizionati. La seconda, nell'utilizzo di uno spaziatore in grafite, da posizionarsi all'interno dello stampo, con l'obiettivo di evitare che la pressione esercitata dai pistoni sia applicata sulla polvere trattata.

Entrambe le modifiche hanno lo scopo di favorire la rimozione del CO prodotto durante la riduzione carbotermica.
Quindi, in tali esperimenti, l'SPS è stata utilizzata come un forno per la riduzione carbotermica, ma con alcuni vantaggi rispetto al forno convenzionale precedentemente usato. Infatti, se confrontato con quest'ultimo, l'SPS consente l'adozione del vuoto e tassi di riscaldamento/raffreddamento molto elevati (>100°C/min). Il primo aspetto favorisce la cinetica della reazione, mentre il secondo permette di ridurre drasticamente i tempi necessari al trattamento, e quindi ridurre la crescita dei grani e il loro grado di *necking* durante il riscaldamento, aumentando considerevolmente la loro predisposizione alla densificazione (Feng *et al.*, 2015).
Grazie alla facilità e velocità del trattamento, è stato possibile valutare l'influenza di diversi parametri, quali la temperatura massima raggiunta e il tempo di stazionamento a tale temperatura.
Sono state effettuate analisi XRD su tutti i campioni prodotti per valutarne la composizione e immagini SEM su campioni selezionati per indagare l'effetto di diverse storie termiche sulla morfologia.

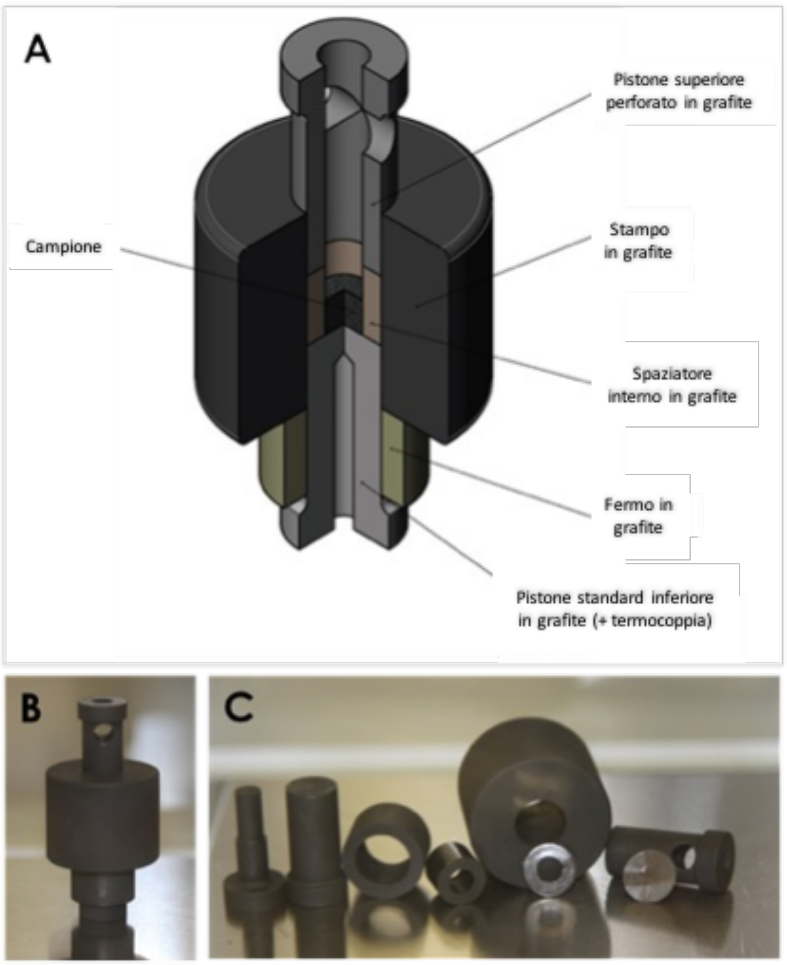

Figura 2: Disegno tecnico della configurazione di prova progettata per la riduzione carbotermica in SPS (A), fotografia della configurazione assemblata (B) e disassemblata (C).

2.3.4 Sinterizzazione dei carburi di uranio in SPS

I carburi realizzati in SPS sono stati successivamente sinterizzati con lo stesso macchinario. Lo scopo di tali esperimenti è stato quello di confrontare la sinterizzabilità di polveri prodotte a diverse temperature.

La procedura ha previsto un riscaldamento fino a 1700°C, con un tasso di 200°C/min, una permanenza di 10 minuti e, infine, un raffreddamento con tasso identico. La pressione applicata durante la sinterizzazione è stata di 100 MPa.

La temperatura di inizio sinterizzazione è stata stimata attraverso il *software* dell'SPS stessa. Le densità raggiunte sono state invece misurate tramite una tomografia a raggi X, dato che la loro estrazione dallo stampo di grafite è risultata essere difficoltosa. Dopo tale misura, misure XRD sono state effettuate per valutare eventuali cambiamenti nella composizione.

3. Discussione dei risultati ottenuti

3.1 Caratterizzazione del prodotto della calcinazione

Il diffrattogramma relativo alla polvere calcinata (1000°C, 2h, argon) è mostrato in *Figura 3*. Come si può notare, emergono solo i picchi caratteristici della struttura cristallina dell'ossido di uranio. Nessuna linea di diffrazione del carbonio è presente: nonostante il trattamento termico a 1000°C, il carbonio non è cristallizzato, ma piuttosto è rimasto come fase amorfa. Un'altra informazione importante si ricava dalla notevole larghezza dei picchi dell'UO_2 (misurata a metà altezza del picco, cosiddetta *Full Width at Half Maximum*, FWHM). Tale fatto può essere dovuto ad una dimensione nanometrica dei cristalliti dell'ossido. Utilizzando la formula di Williamson-Hall, tale grandezza può essere stimata a partire dalla FWHM. In questo caso, la grandezza media dei cristalliti è risultata essere 10 nm. Questo valore risulta essere particolarmente piccolo, se si considerano le alte temperature impiegate nel processo (1000°C), che invece ne avrebbero dovuto comportare una significativa crescita tramite processi diffusivi. Questi risultati inducono a ipotizzare che il composto sia costituito da una matrice di carbonio amorfo, all'interno della quale si trovano nano-cristalli di UO_2, e indicano che il contatto fra le due fasi e la dispersione della fase UO_2 sono ottimali: la matrice di carbonio impedisce efficacemente il contatto fra i nanograni di urania e quindi la loro crescita. Informazioni sulla morfologia e sulla struttura della polvere vengono fornite dalle immagini SEM e TEM. Le prime, mostrate in *Figura 4*, mostrano degli agglomerati di dimensioni fino ai 100 μm, dove l'ossido di uranio e il carbonio appaiono organizzati in strutture a fiocchi sottili (*flake shape*). Inoltre, tali agglomerati risultano essere molto porosi, con un'elevata porosità aperta, probabilmente dovuta al rilascio di diverse sostanze gassose durante la decomposizione delle soluzioni di partenza. L'ipotesi di una struttura costituita da nano-cristalli di UO_2 circondati da carbonio amorfo viene supportata anche dalle immagini TEM (*Figura 5*), dove la misura massima dei cristalliti risulta essere di 100 nm.

Riassumendo, il metodo proposto fornisce un composto di UO_2/C definito da una omogenea distribuzione a livello nanometrico delle due fasi (senza necessità di macinazione) e da una struttura altamente porosa. Entrambe le proprietà vanno nella direzione di migliorare la reattività del materiale: la prima garantisce una maggiore superficie di reazione fra le due fasi e limita la distanza media che i reagenti devono percorrere per reagire a dare i prodotti, mentre la seconda facilita l'eventuale rilascio del monossido di carbonio prodotto (spostando ulteriormente la reazione verso i prodotti).

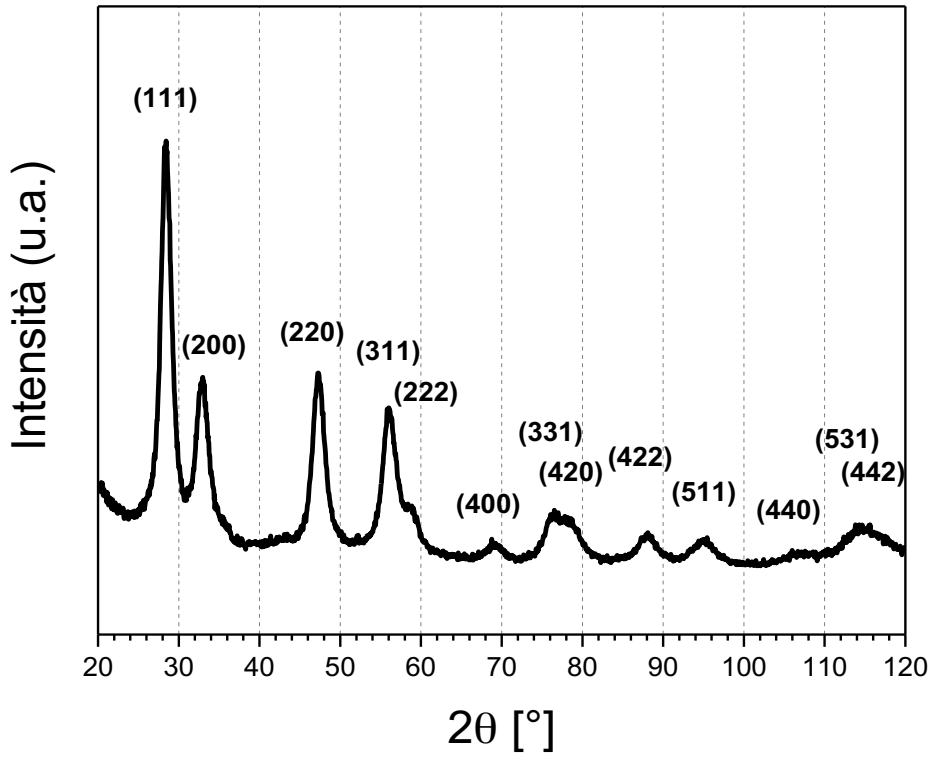

Figura 3: Diffrattogramma del composto UO_2/C ottenuto dopo la calcinazione delle soluzioni di acido citrico e nitrato di uranile a 1000°C, per 2 ore, in argon. Vengono riportati gli indici di Miller della struttura cristallina dell'urania.

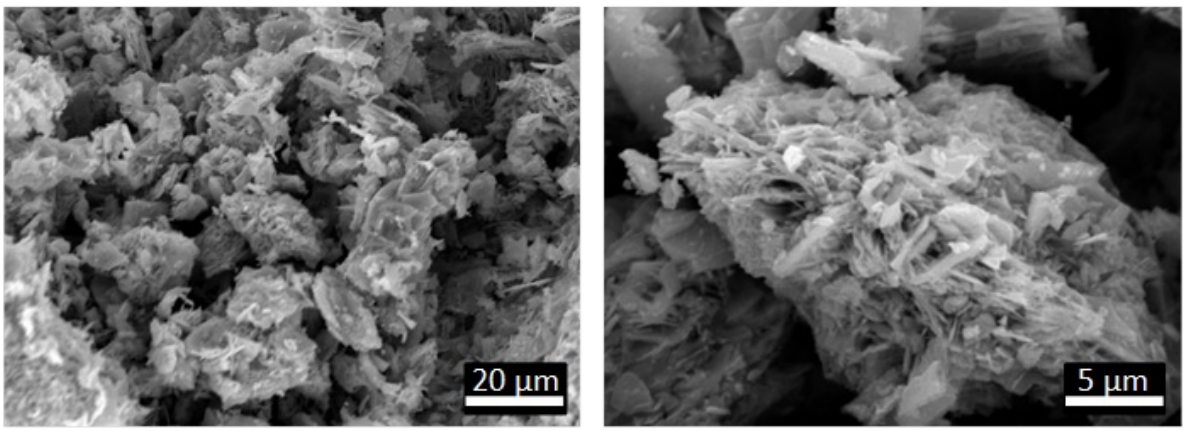

Figura 4: Immagini SEM (a diverso ingrandimento) del composto UO_2/C ottenuto dopo la calcinazione delle soluzioni di acido citrico e nitrato di uranile a 1000°C, per 2 ore, in argon.

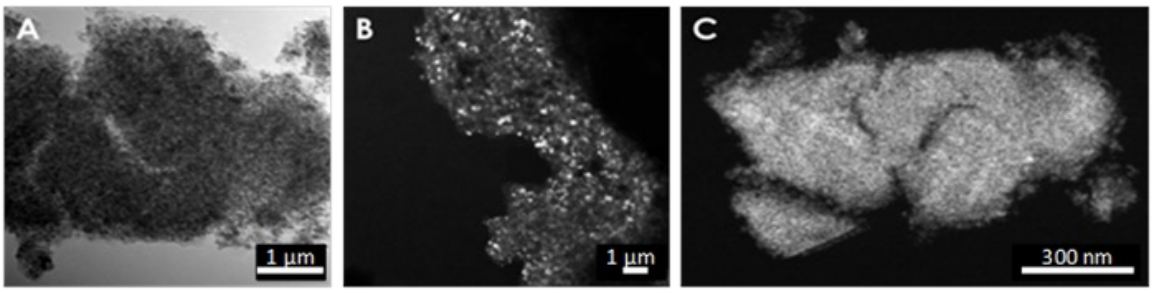

Figura 5: Immagini TEM del composto UO_2/C ottenuto a 1000°C in argon. I cristalliti sono osservabili nelle immagini in campo chiaro (A) e scuro (B). La morfologia e la porosità generale sono state catturate dalla modalità a "scansione e trasmissione"(C).

3.2 Ottimizzazione del rapporto acido citrico/uranio nel forno convenzionale

L'ottimizzazione del rapporto fra acido citrico e nitrato di uranile è stata effettuata sottoponendo diversi campioni (calcinati a 1000°C) a un trattamento termico a 1600°C in argon, per 1 ora, in un forno convenzionale. I rapporti molari considerati nella fase preliminare sono stati: 1.1, 1.4, 1.7, 2.0, 2.3. La percentuale delle fasi presenti, e quindi il grado di avanzamento della reazione, è stata stimata tramite XRD. Tre diverse fasi sono state identificate: UO_2, UC_2 e UC. La presenza di UO_2 e quella eventuale di UC_2 sono state correlate a una incompletezza della reazione (vedi eq. (1) e (2)). L'ossido potrebbe essere anche dovuto a un'ossidazione del carburo, che è noto ossidarsi con estrema facilità (Berthinier *et al.*, 2011).
Lo studio preliminare ha mostrato come la percentuale maggiore di carburo di uranio si trovasse nel campione con un rapporto 2.0. Alla luce di questi risultati, sono stati studiati i rapporti attorno a tale valore: 1.90, 1.95, 2.00, 2.05, 2.10. I risultati dell'analisi XRD sono presentati in *Figura 6*. Anche qui il risultato migliore è stato ottenuto per un rapporto pari a 2.00. Si ritiene che i rapporti maggiori (2.05 e 2.10) siano stati affetti da un'importante ossidazione, durante lo stoccaggio, la misura, o ancor più probabile, durante il trattamento termico ad alte temperature (quando il carburo è maggiormente sensibile a impurezze di ossigeno). Infatti un rapporto maggiore di quello ottimale avrebbe dovuto portare a una permanenza di UC_2. È da notare che l'atmosfera di azoto nelle scatole a guanti utilizzate per condurre tali esperimenti tipicamente ha un contenuto di ossigeno compreso fra 0.5-2% (molto maggiore delle specifiche consigliate per la produzione di carburi di uranio, che si attestano a 25 ppm).
Questi esprimenti, oltre a essere serviti a stimare quale fosse il rapporto ottimale, hanno messo in luce anche l'elevata reattività della polvere prodotta secondo il metodo innovativo proposto. Infatti, si è riusciti ad ottenere quasi il 100% della fase desiderata, nonostante il trattamento termico fosse durato solo un'ora e il vuoto non fosse stato utilizzato, il tutto senza una fase preliminare di macinazione delle polveri.

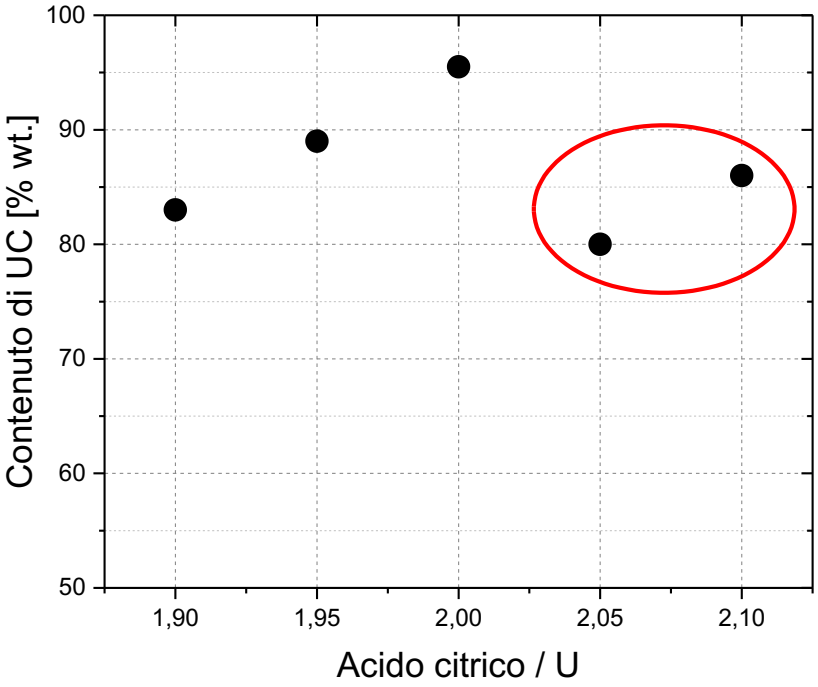

Figura 6: Percentuale in peso di UC dall'analisi XRD della seconda fase di ottimizzazione del rapporto acido citrico/nitrato di uranile nel forno convenzionale a 1600°C per un'ora, in argon. Nel cerchio rosso sono evidenziati i due risultati affetti da una sospetta ossidazione.

3.3 Considerazioni sulle prove di sinterizzazione reattiva in SPS

Diverse prove sono state effettuate con l'SPS sul composto di UO_2/C calcinato, nel tentativo di condurre contemporaneamente la produzione e la sinterizzazione dei carburi. Nonostante siano state provate diverse condizioni (durata dell'esperimento, atmosfera nella camera dell'SPS, pressione applicata durante il trattamento) nessuno di questi esperimenti ha avuto esito positivo, sia in termini di carburo prodotto che in termini di densità raggiunte. Nonostante ciò, queste prove sono risultate molto utili, in quanto si è notato che l'adozione del vuoto durante il processo ha determinato sempre un miglioramento, seppur in piccola misura. Gli esperimenti hanno evidenziato che uno dei problemi determinanti è la permanenza del monossido di carbonio in prossimità della zona di reazione: in presenza del vuoto il monossido di carbonio ha maggiori possibilità di essere rilasciato attraverso i giochi tra stampo e pistoni in grafite, favorendo quindi il procedimento della reazione. Alla luce di tali risultati si è messo a punto una nuova configurazione di prova per l'SPS, dove condurre esclusivamente la riduzione carbotermica.

3.4 Riduzione carbotermica in SPS (tramite apparato di prova modificato)

Il composto di UO_2+C è stato infine sottoposto a un trattamento termico in vuoto in SPS, tramite l'apparato sopra descritto (paragrafo 2.3.3). In queste prove, grazie alla rapidità di esecuzione, si è potuto studiare a fondo la cinetica della reazione chimica considerata, andando

a valutare l'effetto della temperatura massima e del tempo di residenza. Sono state provate diverse combinazioni, i cui risultati sono esposti in *Figura 7*.
Come si può notare, per gli esperimenti a 1600°C, la produzione del carburo di uranio è quasi completata già con tempo di stazionamento nullo. Questo dimostra come la reazione, di fatto, proceda significativamente già durante la rampa di riscaldamento e raffreddamento (±200°C/min). Riducendo la temperatura massima è possibile notare una certa progressione ma solo negli esperimenti più brevi, dato che sia a 1400°C che a 1200°C il grado di completezza della reazione supera il 90% già dopo i primi 5 minuti. Per quanto riguarda la prova a 1000°C, al contrario, nessuna traccia di carburo è stata trovata. Questo suggerisce che la temperatura di inizio della reazione è da localizzarsi tra i 1000°C e i 1200°C in questa particolare configurazione.

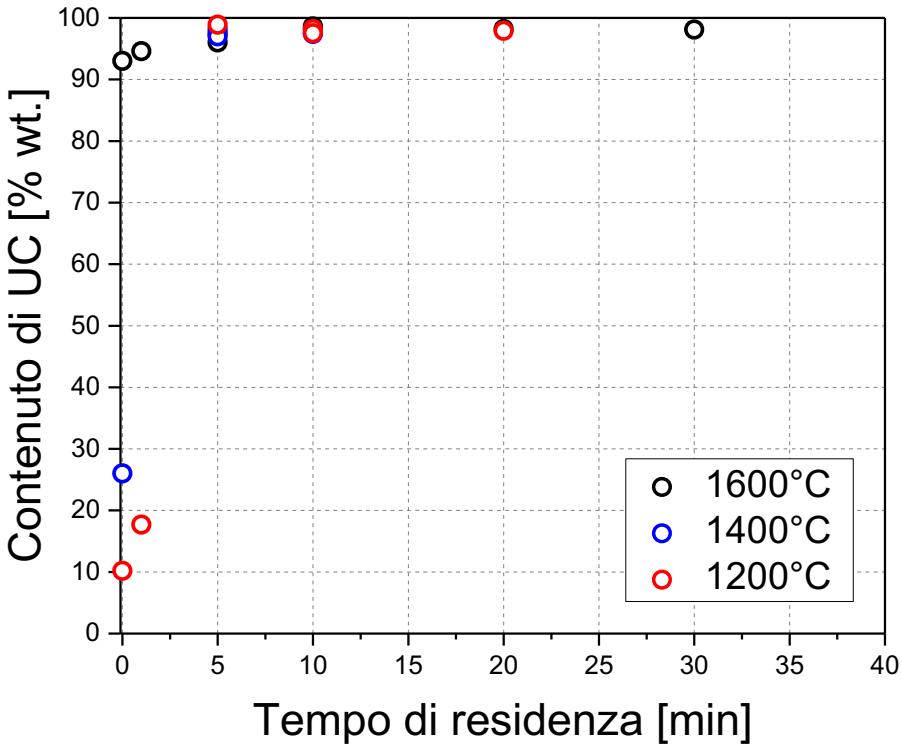

Figura 7: Quantità di carburo di uranio prodotta in SPS a diverse temperature massime per diversi tempi di stazionamento.

Tra i campioni prodotti, sono state selezionate tre polveri da analizzare tramite SEM: quelle prodotte a una temperatura massima di 1200°C, 1400°C e 1600°C con 10 minuti di permanenza. Le immagini SEM sono mostrate in *Figura 8*. La struttura generale presenta degli agglomerati porosi con dimensioni caratteristiche tra i 10 e i 100 µm, indipendentemente dalla temperatura di produzione. La differenza maggiore che può essere notata è la quantità di colletti (*necks*) e il grado di sinterizzazione dei grani, che aumentano progressivamente tra 1200°C e 1600°C. Per questo motivo è prevista una sinterizzabilità minore per le polveri prodotte a temperatura maggiore.

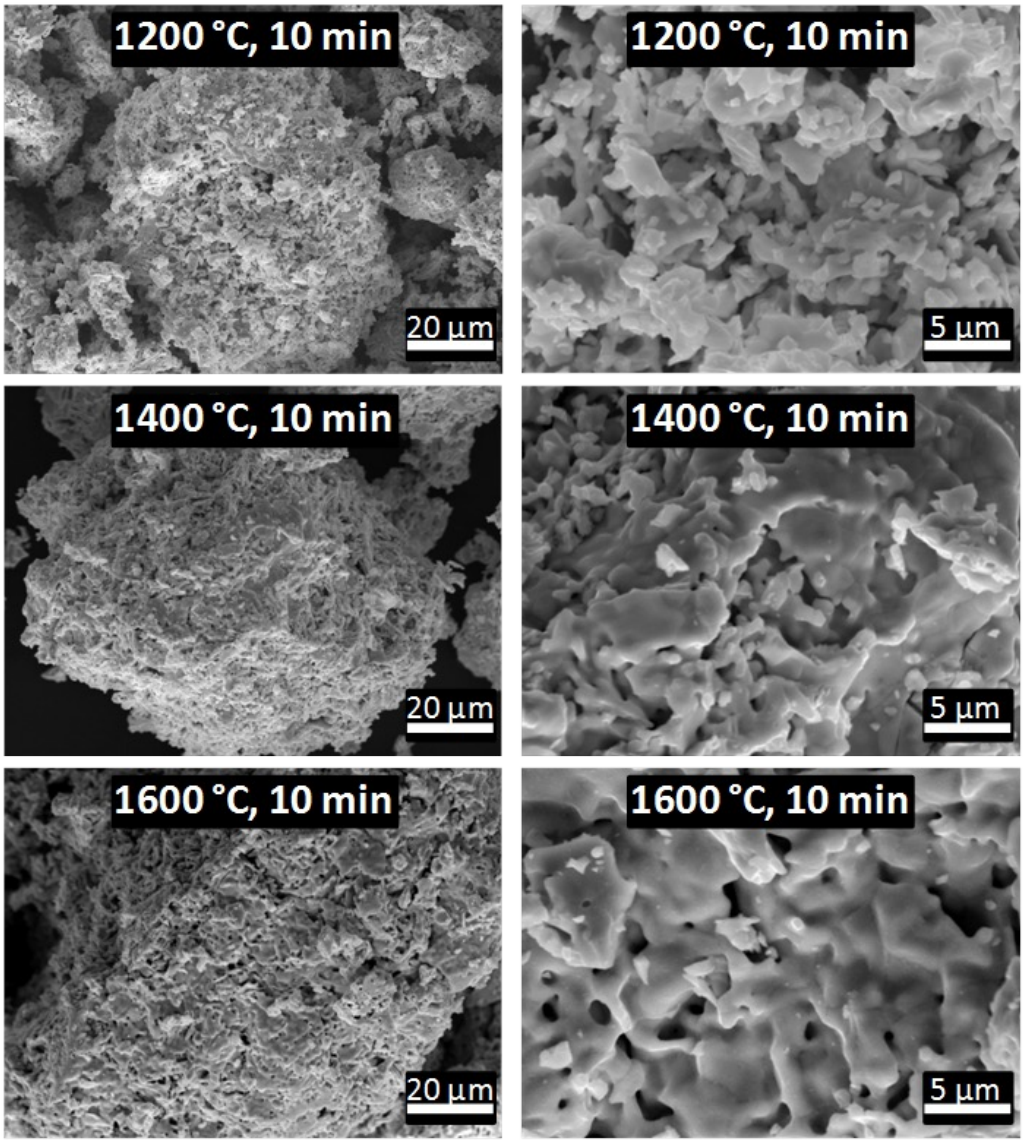

Figura 8: Immagini SEM dei carburi prodotti in SPS a diverse temperature in 10 minuti di stazionamento.

Per avere una prova ulteriore della maggiore reattività del composto di UO_2/C ottenuto partendo da acido citrico e nitrato di uranile, si è utilizzata la configurazione di prova modificata per trattare delle polveri di UO_2 e grafite, macinate manualmente con pestello in un mortaio. Il trattamento termico adottato è stato di 1600°C per 10 minuti. Il confronto fra i risultati ottenuti con la polvere derivante dal metodo proposto e quella invece derivante dal metodo convenzionale è mostrato in *Figura 9*. Mentre nel primo caso si è ottenuto più del 98% in peso di UC, nel secondo la quantità di UC non supera il 42%.
Riassumendo quanto ottenuto, si può affermare che il procedimento proposto consente di ridurre notevolmente le temperature e i tempi richiesti per la produzione di carburi di uranio. Questo risultato è dovuto a un più intimo contatto fra i precursori della reazione e, inoltre, anche all'impiego di un opportuno apparato in grado di consentire un'efficace rimozione del CO prodotto.

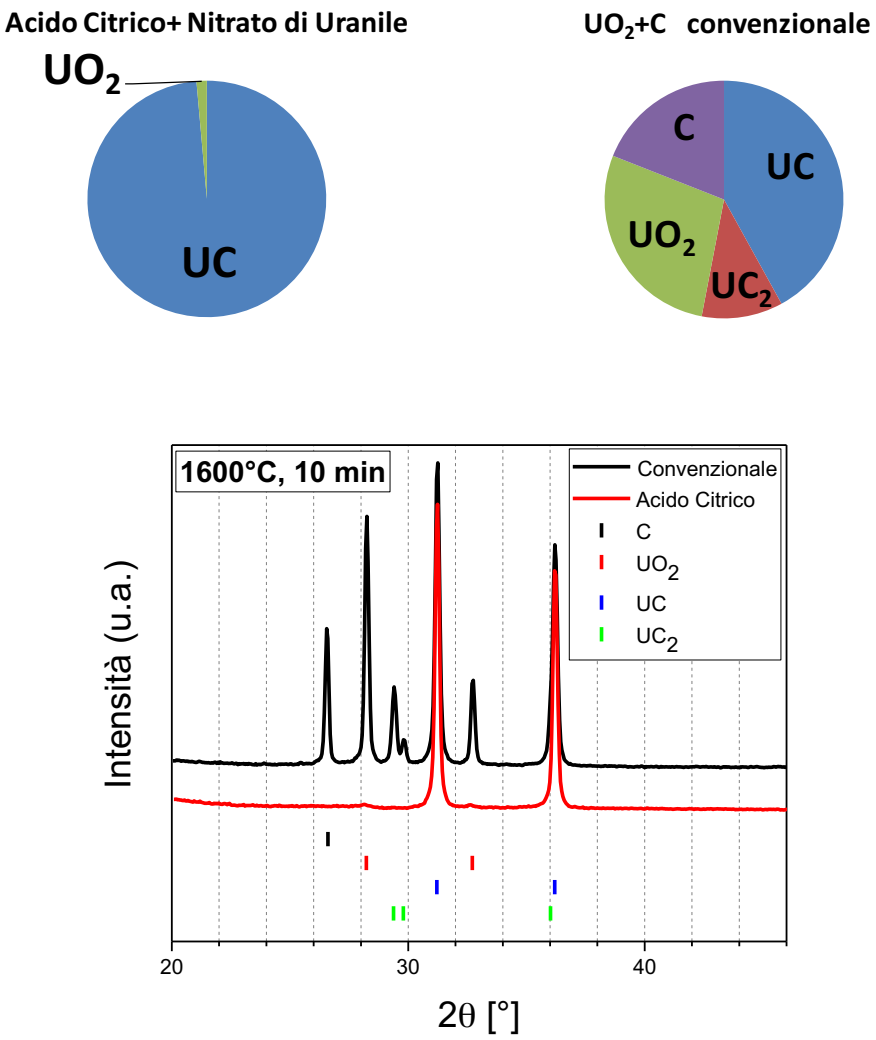

Figura 9: Confronto fra i diffrattogrammi XRD e la composizione delle fasi delle polveri trattate in SPS a 1600°C per 10 minuti, ricavate dal metodo convenzionale di mescolamento di UO_2 e grafite e dal metodo proposto (acido citrico/ nitrato di uranile).

3.5 Sinterizzazione in SPS

I carburi sintetizzati nell'SPS a diverse temperature sono stati poi sinterizzati nello stesso macchinario, utilizzando una configurazione *standard*.

In particolare, si è studiato il comportamento di sinterizzazione delle polveri, attraverso i dati registrati dal *software* dell'SPS stessa (spostamento relativo dei pistoni e loro velocità), le densità finali, ricavate dalle analisi di tomografia a raggi X, e le immagini SEM sui prodotti sinterizzati. Questi dati hanno confermato che le polveri prodotte a 1200°C sono caratterizzate da una notevole sinterizzabilità, la quale ha consentito di raggiungere elevate densità (≈95%TD), con una temperatura di inizio del processo di sinterizzazione di gran lunga inferiore alle altre (T_{onset}≈1100°C), come mostrato in *Figura 10* e *Figura 11*. L'andamento delle densità finali dei carburi sinterizzati è supportato anche dalle immagini SEM (*Figura 12*). In queste si può notare un livello progressivamente decrescente del numero e delle dimensioni dei pori visibili sulla

superficie di frattura osservata, fino ad arrivare a una porosità quasi nulla per il campione sintetizzato a 1200°C.

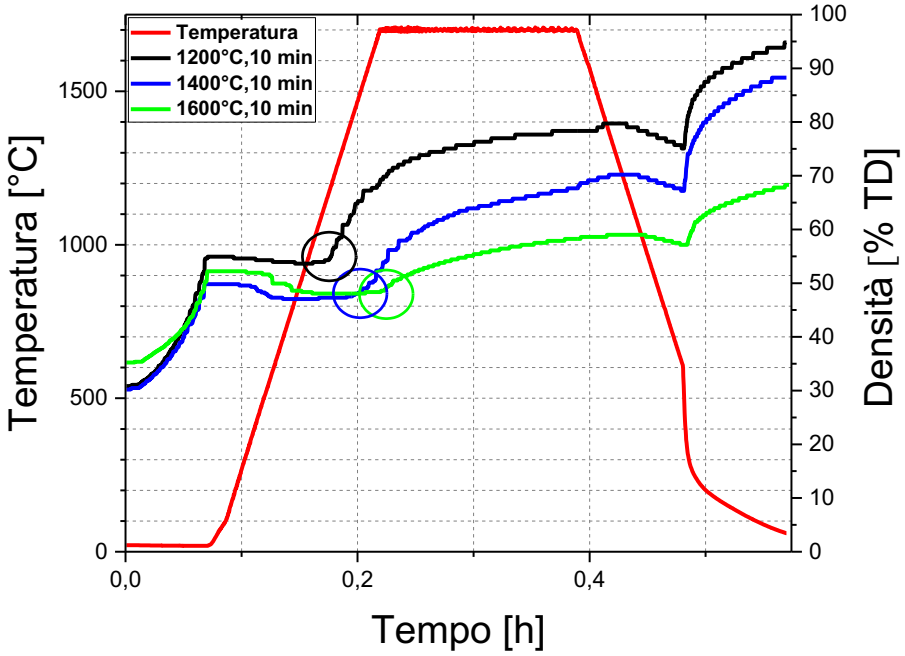

Figura 10: Andamento della temperatura e della densità dei carburi di uranio durante la sinterizzazione in SPS (andamento non corretto per l'espansione e contrazione termica del sistema). L'inizio della densificazione per le tre diverse polveri è evidenziato dai cerchi.

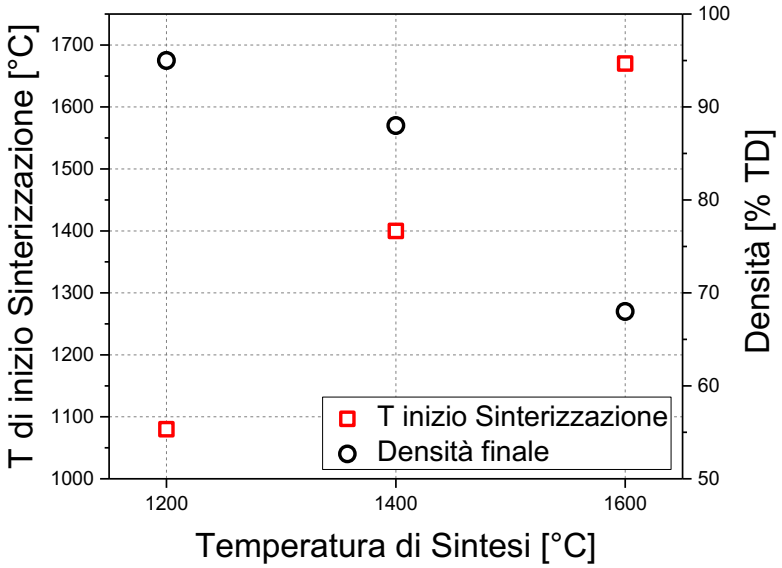

Figura 11: Studio di sinterizzabilità in SPS: densità finali e temperature di inizio della sinterizzazione per i carburi di uranio sintetizzati a diverse temperature.

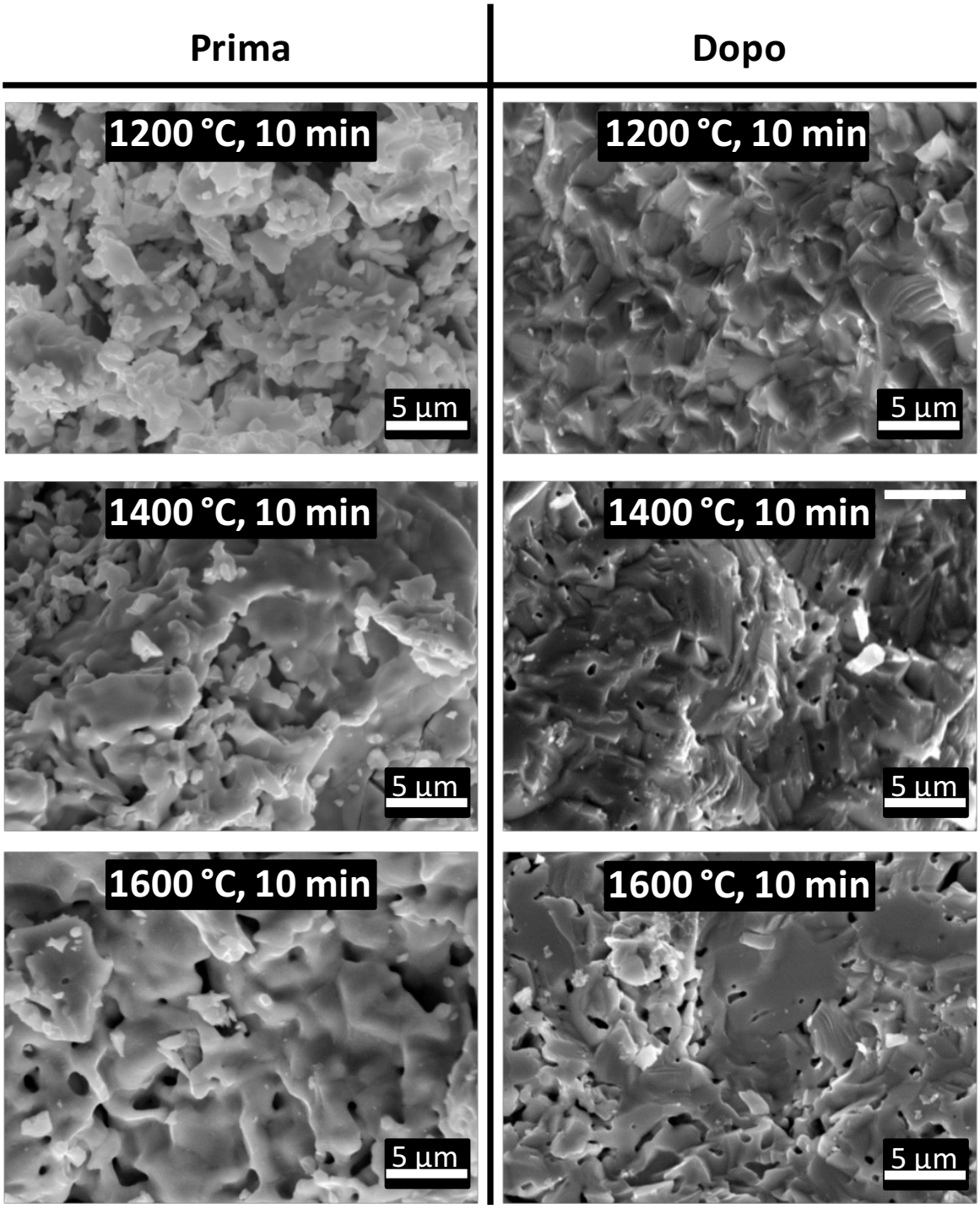

Figura 12: Immagini SEM dei carburi, prodotti a diverse temperature, prima (SX) e dopo (DX) il processo di densificazione in SPS.

4. Conclusioni

Tramite questo lavoro di tesi, si è sviluppato un nuovo metodo di sintesi e densificazione di carburi di uranio. L'impiego di soluzioni liquide di acido citrico e nitrato di uranile come materiali di partenza ha consentito di ottenere, dopo un processo di calcinazione a 1000°C, un composto intrinsecamente omogeneo di nano-particelle di UO_2 ben disperse in una matrice di carbonio amorfo, che ha reso superfluo il processo tradizionale di macinazione. Tale composto, grazie anche all'elevata superficie di reazione tra carbonio e UO_2, è risultato essere particolarmente efficace come precursore per la formazione di carburi. Infatti, ottimi risultati sono stati ottenuti provando la riduzione carbotermica in un forno convenzionale e, soprattutto, nell'SPS, tramite un innovativo apparato di prova progettato allo scopo. In quest'ultimo caso, si è riusciti a ottenere, a 1200°C con 5 minuti di permanenza, più del 99% di carburo nel prodotto finale. Quindi, con una durata complessiva di meno di 20 minuti (comprendendo anche la rampa di riscaldamento e raffreddamento), si è portata a termine una reazione che usualmente, con i metodi convenzionali, richiede più di 15-20 ore.
Inoltre, grazie alla rapidità del trattamento termico e alle basse temperature richieste, è stata prodotta una polvere di carburo estremamente sinterizzabile. Infatti, sia la polvere prodotta a 1400°C che, soprattutto, quella prodotta a 1200°C (con 10 minuti di stazionamento) hanno dimostrato un'elevata sinterabilità, senza che su di esse fosse stato eseguito alcun processo di macinazione. In soli 10 minuti a 1700°C in SPS si sono raggiunte delle densità relative superiori all'88%, mentre, convenzionalmente, sono richieste diverse ore a una temperatura compresa tra 1700°C e 1900°C e laboriosi processi di macinazione per raggiungere risultati analoghi.
In conclusione, lo scopo iniziale di questa campagna sperimentale è stato pienamente raggiunto, sviluppando e ottimizzando una nuova procedura per la produzione e sinterizzazione di carburi, che si è dimostrata essere estremamente efficace e rapida. Una sinossi del lavoro svolto è presentata in *Figura 13*.

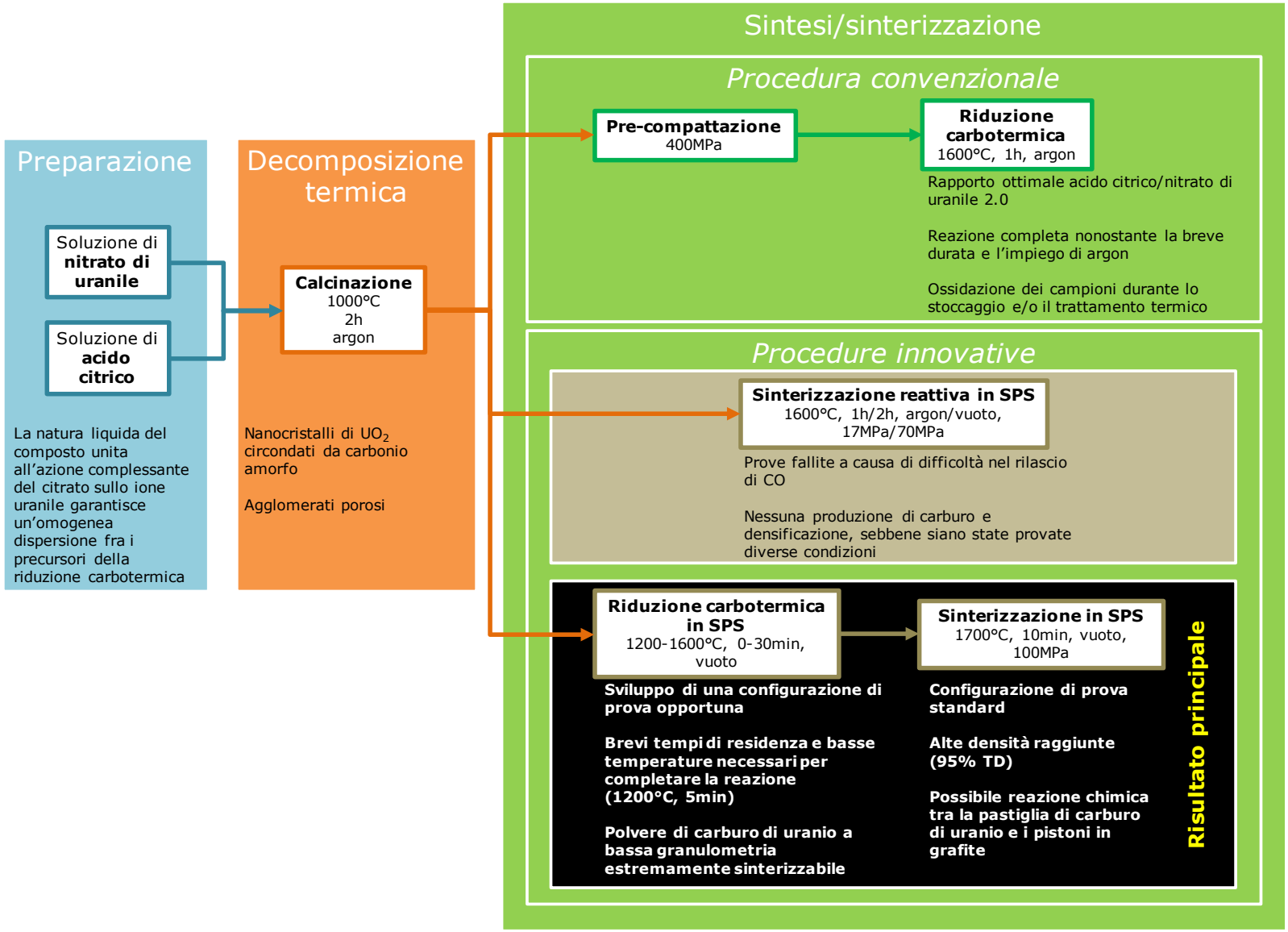

Figura 13: Sinossi del lavoro svolto.

5. Sviluppi Futuri

Diversi miglioramenti o studi ulteriori possono essere programmati a partire dai risultati ottenuti:

- sarebbe opportuno tentare di limitare ogni possibile fonte di ossidazione dei carburi prodotti, per esempio prevedendo l'impiego esclusivamente di contenitori metallici a migliore tenuta per lo stoccaggio dei materiali, e operando su di essi esclusivamente quando il livello di ossigeno all'interno dell'atmosfera della scatola a guanti è al di sotto dei limiti consigliati (25 ppm). Questo consentirebbe di limitare una possibile fonte di ossidazione e ottenere, quindi, un carburo di uranio di più alta qualità;

- un altro possibile miglioramento deriverebbe dallo sviluppo di un nuovo apparato sperimentale per l'SPS in grado di incrementare la quantità di carburo prodotta. Aumentare la massa di materiale trattato comporterebbe aumentare la quantità di monossido di carbonio liberata. Quindi, per evitare di intaccare la cinetica della reazione, occorrerebbe rendere più efficace l'asportazione del gas, aumentando per esempio il diametro o il numero dei fori applicati al pistone di grafite, preservando, al tempo stesso, le sue proprietà di resistenza termo-meccanica (viste le alte temperature e pressioni in gioco);

- prospettiva di estremo interesse sarà dimostrare la fattibilità del metodo proposto per la produzione di pastiglie di carburi misti ((U,Pu)C o caricati con MAs) per una futura applicazione in reattori veloci. In quest'ottica, il metodo sviluppato presenterebbe il vantaggio di consentire la produzione di carburi a basse temperature (1200°C) e con brevi tempi di stazionamento (5-10 minuti), limitando quindi ogni possibile vaporizzazione di Pu o MAs. Tale fatto rappresenta un problema rilevante dei metodi convenzionali attualmente seguiti.

List of Acronyms

AGR	Advanced Gas Reactor
BR	Breeding Ratio
BSE	Back-Scattered Electron
CR	Conversion Ratio
CT	Computed Tomography
CTR	Carbo-Thermal Reduction
EDX	Energy-Dispersive X-ray
FAST	Field Assisted Sintering Techniques
fcc	face-centred cubic
FCCI	Fuel-Cladding Chemical Interaction
FCMI	Fuel-Cladding Mechanical Interaction
FR	Fast Reactor
FWHM	Full Width at Half Maximum
GIF	Generation IV International Forum
HAADF	High-Angle Annular Dark-Field
HBS	High Burn-up Structure
HMTA	HexaMethyleneTetrAmine
HP	High Pressure
HV	Vickers Hardness
HWR	Heavy Water Reactor
LWR	Light Water Reactor
MAs	Minor Actinides
MOX	Mixed Oxide fuel
PHWR	Pressurized Heavy Water Reactor
PUREX	Plutonium Uranium Redox EXtraction
PWR	Pressurized Water Reactor
R&D	Research and Development
RDT	Reactor Doubling Time
SE	Secondary Electron
SEM	Scanning Electron Microscopy
SFR	Sodium Fast Reactor
SIMFUEL	SIMulated high burn-up FUEL
SPS	Spark Plasma Sintering
TD	Theoretical Density
TEM	Transmission Electron Microscopy
TGA	Thermo-Gravimetric Analysis
XRD	X-Ray powder Diffraction

This page is intentionally left blank

List of Figures

This page is intentionally left blank

List of Tables

This page is intentionally left blank

Introduction

The very difficult fabrication process of carbides is one of the most serious issues that has affected their success as nuclear fuels. Among the different ways of carbide production, the most used one is the powder-metallurgical route. In this process, uranium dioxide and carbon powder are mixed together as precursors for the carbothermal reduction (CTR). A long milling step is crucial to provide enough reactivity and, then, enhance the synthesis of carbide. However, the homogeneity achievable is limited, thus demanding conditions are required for the heat treatments of this mixture. As a matter of fact, high temperatures (>1450°C) and long holding times (>4 h) are needed to complete the synthesis and densification processes.

In this thesis, a new synthesis process for uranium carbide production has been developed. The idea behind this method is to provide an intrinsic contact between the two starting precursors for the carbothermal reduction, UO_2 and C. This intimate contact is reached starting from liquid solutions, where appropriate chemical compounds containing uranium and carbon are dissolved.

Uranyl nitrate solution is used as uranium source, while, as Matovic *et al.* (2013) did for hafnium carbide synthesis, citric acid is used as carbon source. The two main advantages of using this carboxylic acid are its high solubility in aqueous solutions and its complexation of uranyl ions (Lenhart *et al.*, 2000; Bailey *et al.*, 2005). Thus, a homogeneity at molecular scale between uranium and carbon may be achieved.

The aim of this work was then the achievement of a better reactivity of the precursors, in order to decrease the dwell times and temperatures needed to complete the carbothermal reduction (CTR) for carbide synthesis. Together with the particular nature of the starting materials, another innovation was represented by the employment of a spark plasma sintering (SPS) device to carry on the CTR. For this purpose, a new SPS set-up has been designed to improve the kinetics of the reaction, which, as clearly stated in literature (Sengupta *et al.*, 2012), strongly depends on the partial pressure of the produced CO. Then, the better is the removal of CO, the faster is the CTR. Furthermore, thanks to the very short times and low temperatures, the as-synthesised uranium carbides were supposed to be highly sinterable. Thus, their densification was performed and studied in SPS, which has never been applied to such material.

The thesis is structured in four main chapters. The first one summarizes the reasons of the interest in uranium carbide as nuclear fuel for fast reactors. The advantages and disadvantages of this alternative fuel are presented, focusing the attention on the issues of conventional fabrication. The second and third chapters are instead focused on the particular techniques used to analyse and characterize the produced samples and on the description of the adopted experimental procedures, respectively. Finally, the fourth and last chapter presents the results and their discussion.

This page is intentionally left blank

1 Carbides: Advanced Fuel for Fast Reactors

Abstract *In the last years, especially after Fukushima accident and because of the growing public concern about waste management and the increasing building costs, the research in nuclear field has been focused on the development of new reactor and fuel designs characterized by increased safety, sustainability, and economics. For these purposes, interest in advanced nuclear fuels (metallic alloys, nitrides, and carbides), already employed in the early ages of nuclear, is gradually increasing. However, besides many advantages if compared to MOX in physical properties and irradiation behaviour, efforts are still needed to solve some issues concerning their fabrication. In fact, demanding conditions are usually needed to produce these kinds of fuel and to guarantee a high purity composition.*

1.1 Introduction

In this chapter an overview on the fast reactor technology is given and the principles of transmutation and breeding are briefly described. Then, the different applicable fuels for these reactors are presented, focusing the attention on mixed carbides and the advantages and concerns linked to this choice, in particular to their fabrication issues. Finally, the thermo-physical properties of uranium carbide are discussed.

1.2 Nuclear Birth and Concerns

The birth of nuclear power plants could be set in 1942, when a team of scientist led by Enrico Fermi demonstrated the possibility of controlling nuclear chain reactions. This experiment was conducted in the Chicago-Pile 1 (CP-1), a graphite-moderated reactor, and was part of the Manhattan Project in US. In fact, during its first stages, the growth of nuclear industry was mostly driven by military purposes, which led to the development and use of the atomic bomb in the Second World War. In 1953, U.S. President Eisenhower delivered a famous speech to the United Nations, known to history as "Atoms for Peace", where he stated the need of supporting and developing a civil use of nuclear energy. Since then, commercial power plants started to be built all over the world, providing a relevant fraction of electricity demands. This initial rapid spread was justified by the economic competitiveness of nuclear energy production. Moreover, the lack of emissions of carbon dioxide and other air pollutants represented an important advantage over classical gas/oil-burning plants. However, such strong and growing interest in building nuclear power plants had and still has to deal with several difficulties.

First of all, among the years, the popularity of nuclear energy has been subjected to different severe events. In particular, the accidents of Three Mile Island (1979), Chernobyl (1986) and Fukushima (2011) have pointed out the weakness of nuclear power plants, resulting in increase of safety requirements - firstly from a design point of view, with the adoption of

engineering solutions enhancing an intrinsic safety, and then through the development of advanced materials to withstand the conditions, during both normal and off-normal operations. Furthermore, these severe accidents had a strong impact on public opinion. They made commercial nuclear power stations appear as a hazard to the human life and the environment. Such a negative public attitude, together with the economical drawbacks, contributed to slow down further expansion of the nuclear energy.

Moreover, public opinion is concerned about the issue of nuclear waste. In particular, the main problem lies in the long-term radiotoxicity and heat-production of spent fuel. Long-lived elements, such as Pu and Minor Actinides (MAs), namely Np, Am, Cm, are responsible of these phenomena.

The exploitation of uranium resources represents another issue. In fact, the current nuclear power plants use less than 1% of the natural uranium processed to fabricate their fuel (Sengupta *et al.*, 2012). This lack of efficiency poses a reasonable question on the sustainability of nuclear power.

In this context, a new interest in Fast Reactors (FRs) has grown up in the last decades. FRs have been selected as a suitable technology for the future power plants, and they play a fundamental role in the framework of the Generation IV International Forum (GIF-2001). The new generation of reactors should address public concerns and economical issues to fully realize the potential of nuclear energy as a safe, clean, reliable and low-cost source of energy. In particular, (six) goals have been identified for Gen IV systems in the area of sustainability, economics, safety and reliability, proliferation resistance, and physical protection.

Two unique features have sparked renewed interest in FRs: the ability to transmute MAs and to breed fuel. Thus, their palliation would reduce the radiotoxicity of spent fuel (with a potential decrease of time in repository from hundreds of thousands of years down to less than a thousand) and allow a better exploitation of natural resources. However, efforts are still needed to meet the strict requirements in reliability, economy and safety. In this perspective, new fuel concepts have been studied and designed leading to the development of the so-called advanced fuels, namely, metallic alloys, nitrides, and carbides, which are characterized by intrinsic physical properties that facilitate the fulfilment of those requirements.

1.3 Fast Reactors

The history of FRs started in the forties (Clementine, Los Alamos, USA, 1946), concurrently with thermal reactors. As shown in *Figure 1*, since then, many design and fuel concepts were studied and tested, and some commercial and prototype plants were built. However, thermal reactors, namely Light Water Reactors (LWRs), Heavy Water Reactors (HWRs), and Advanced Gas Reactors (AGRs) soon established themselves as the leading nuclear

technology, mainly driven by the military purposes of plutonium production and submarine propulsion.

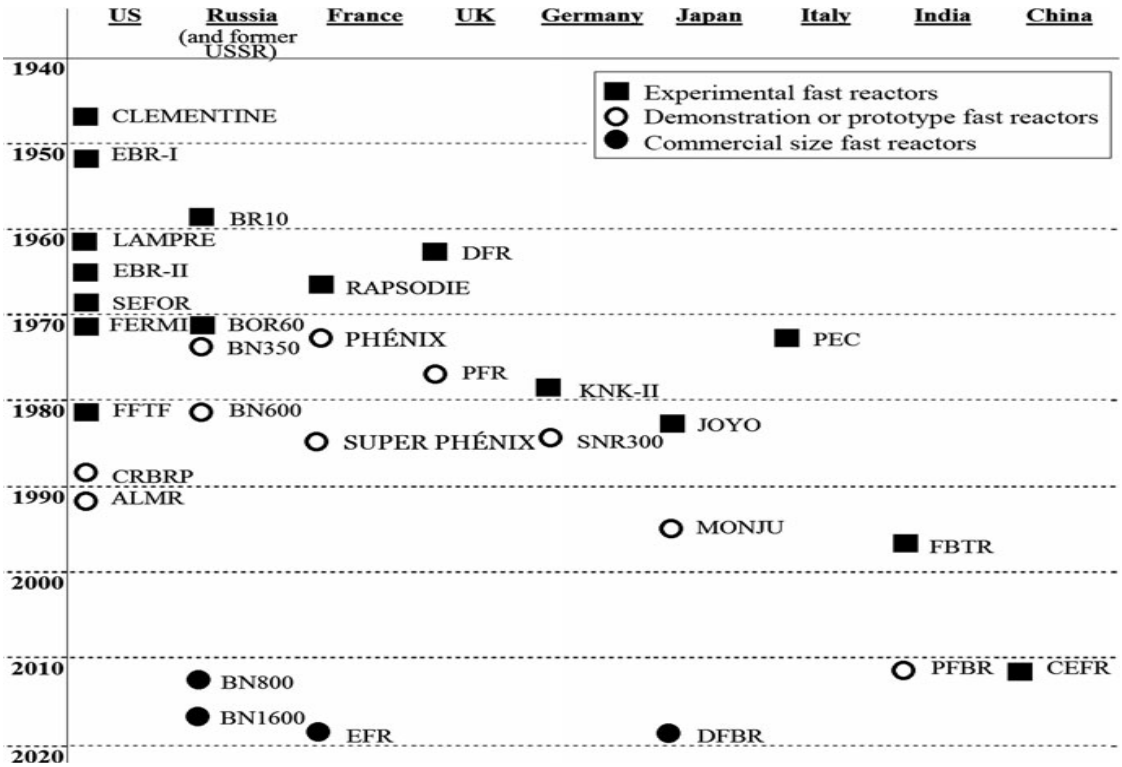

Figure 1: Built fast reactors among years and nations (Waltar et al., 2012).

Fast reactors represent an advanced concept of nuclear power plant. The main difference compared to thermal reactors is the absence of any moderator to provide a fast neutron spectrum. Actually, neutron slowing-down is unavoidable because of the inelastic collisions with the nuclei of coolant and structural materials. Hence, the real spectrum is not properly the fission one, but still the mean energy is high enough to allow the transmutation of long-lived heavy radionuclides and fissile breeding. A more detailed description of these two phenomena and their figures of merit will be given in the following.

1.3.1 Transmutation

The process of transmutation generally involves the conversion of a radionuclide into another one, through a nuclear process. In particular, in Fast Reactor's technology, this term refers to the transmutation of a long half-life isotope into stable or short-lived isotopes by a fission reaction. Since Cm and Am are fissionable at high energy, only fast neutrons could fission them. It was this specific feature that has driven a renewed interest towards FRs at the beginning of 21st century, more than the breeding capability. In fact, this could help nuclear energy to be more accepted by people, in an overall context where the protection of the environment is becoming the most relevant concern.

Actually, transmutation takes place in thermal reactors too. A fraction of neutrons has high energy to fission some heavy nuclei. However, the most appropriate parameter to evaluate the efficiency of transmutation is the ratio between fission and absorption. As shown in *Figure 2*, unlike FRs, in thermal reactors, the build-up of MA elements prevails over their elimination.

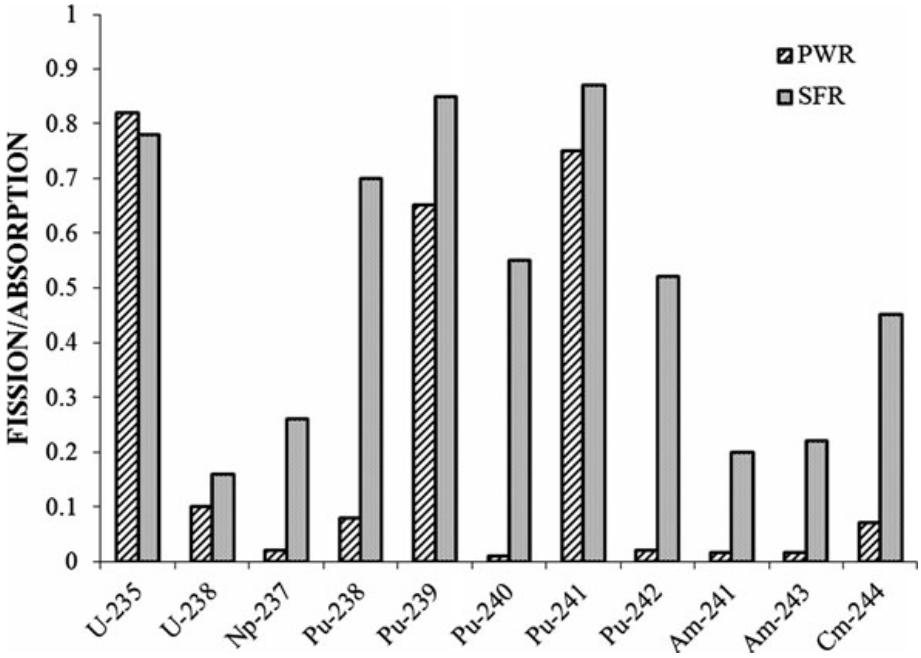

Figure 2: Fission to neutron absorption ratio for different actinides in PWR and Sodium Fast Reactors (SFR) (Waltar et al., 2012).

1.3.2 Breeding

The breeding principle was demonstrated by Enrico Fermi in 1946. In nuclear reactors, fertile materials could be converted into fissile isotopes, via a neutron capture and following β^- decays. Neutron spectrum, fuel composition and core design contribute to fix the breeding capability of a reactor.

Different parameters have been introduced to evaluate the degree of conversion of a reactor system. First of all, the effectiveness of a reactor to produce new fissile isotopes is represented by the *conversion ratio* CR, defined as:

$$CR = \frac{\text{Produced fissile}}{\text{Destroyed fissile}} \quad (1)$$

For a *breeder* this ratio should be greater than one. In this case, CR is called *breeding ratio* BR. Common thermal reactors have a CR less than 1, typically 0.5 and 0.7 for LWRs and PHWRs, respectively.

Different configurations of thermal reactors can allow BR to be greater than 1. However, neutronic considerations lead to higher values for fast reactors. In fact, in order to achieve the breeding, the average number of neutrons produced per fission should be high enough to ensure the proceeding of the chain reactions and the conversion of fertile isotopes to fissile, taking into account also the unavoidable losses. Thus, the neutron yield per neutron adsorbed, η, must be greater than 2. Looking at the evolution of η with energy, shown in *Figure 3*, it is worth noting why fast reactors fuelled with ^{238}U-^{239}Pu are the best choice for the production of new fissile.

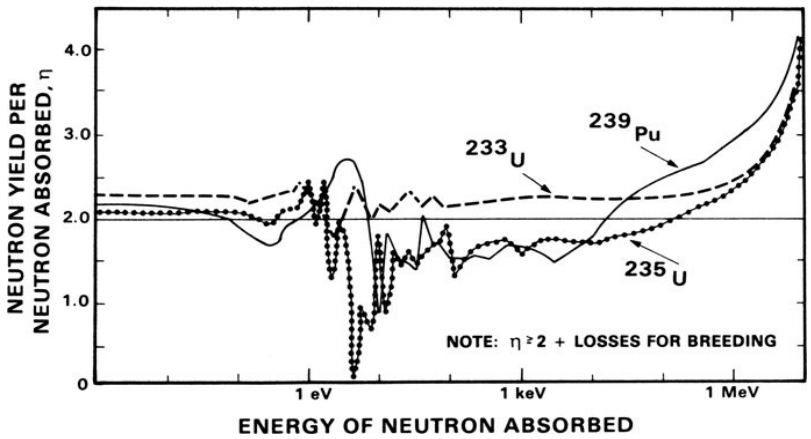

Figure 3: Neutron yield per neutron adsorbed in function of energy for different fissile isotopes (Waltar et al., 2012).

The Reactor Doubling Time (RDT) is another important parameter for the evaluation of the breeding capability. It is defined as the time required for a particular breeder reactor to produce enough fissile material in excess of its own fissile inventory to fuel an identical reactor. Hence, it is the time necessary to double the initial load of fissile fuel. It is strongly dependent on the BR, as will be later discussed, and it has a deep impact on the economic assessment, since it affects the time scale of an ideal chain of FRs (Lamarsh *et al.*, 2001).

Following the definition, RDT (in years) is given by the ratio between the initial fissile inventory M_0 and the fissile mass gained per year thanks to the breeding, M_g'. M_g' could be expressed as a function of the power in megawatts, P, the loading factor, f, the capture-to-fission ratio, α (= σ_f/σ_c), and the breeding ratio, BR, thus leading to the following expression of the RDT, suggested by Waltar *et al.* (2012):

$$RDT \approx \frac{2.7*M0}{(BR-1)*(1+\alpha)*P*f} \quad (2)$$

This dependence shows the importance of having, respectively, high breeding ratio and low specific fissile inventory (M_0/P) in order to reduce the doubling time.

1.4 Fuel for Fast Reactors

Among the years, different fuel concepts for fast reactors were tested. The main challenge was to develop a fuel that would operate safely without failure up to high burn-up, producing energy economically, enable to breed fissile material or transmute MAs efficiently, and be relatively easy to fabricate and reprocess (IAEA TECDOC No. 1374, 2003).

Meeting these requirements for fast reactor fuel could be more difficult than for thermal reactor, due to typically higher temperature of the fuel and high neutron fluence, which lead to more severe thermo-mechanical conditions.

In order to satisfy these features, heavy-atom density [$(g_U+g_{Pu})/cm^3$], breeding ratio, melting temperature and thermal conductivity should be very high. Similarly, if we analyse the fuel environment, a chemical compatibility with the chosen coolant and cladding and a stable behaviour under irradiation are required.

It should be pointed out that mixed uranium plutonium oxide (MOX) have been mostly used in commercial FRs. MOX's success is related to the well-established fabrication and reprocessing route of uranium dioxide fuel and the deeply studied irradiation behaviour. However, the use of MOX as driver fuel in fast reactors has some disadvantages, which set a limit in the reactor operation. These include poor heavy metal density and thermal conductivity, thus giving high doubling time and small breeding gain, and forcing the linear heat rate to be low (IAEA TECDOC No. 1374, 2003).

In fact, research programmes on new advanced fuel for fast reactors were actively pursued in the US, United Kingdom, France and Russia during 1960s and 1970s, and later in India and Japan. Until now, three different types of advanced fuel systems have been studied and tested, namely carbides, nitrides, and metallic alloys (Sengupta *et al.*, 2012).

1.4.1 Carbide Fuel

Uranium-plutonium mixed carbides are promising candidate fuels for fast reactors. Higher thermal conductivity and heavy-atom density lead to a better exploitation of fast reactors potentials, thus making them an attractive alternative to oxide fuels.

A large number of experiments have been carried out in different countries. These research programmes studied the influence of fabrication parameters on the final properties of carbides. In particular, the time and temperature of the heat treatments, the duration of milling process, the addition of sintering additives, and the pressure applied during the precompaction have been studied to discern the effects on the density, open porosity, impurities (O, N) concentrations and microstructure (Duguay *et al.*, 2015; Majumdar *et al.*, 2006; Vaudez *et al.*, 2008; Suzuki *et al.*, 1981). Besides the optimization of fabrication process, the irradiation

behaviour was deeply studied, by means of simulations and in-pile experiments. These were focused on the effect of pellet density, pin diameter, pellet-cladding gap, type of cladding alloy, and bond type (He or Na), on fuel and cladding swelling, fission product behaviour, fuel restructuring, and fuel-cladding mechanical (FCMI) and chemical (FCCI) interaction. Despite of some undesired features, these tests stated the feasibility of a fast reactor fuelled with carbides (Ganguly *et al.*, 1988; Bart *et al.*, 2008).

If compared to oxide fuels, the higher thermal conductivity of carbides allows increasing the linear power, allowing at the same time higher safety margin to melting (IAEA TECDOC No. 1374, 2003). The higher linear power leads to lower specific fissile inventory. Then, the presence of only one moderator atom per heavy metal atom instead of two for oxide, plus a higher metal density, lead to a harder spectrum and, therefore, to higher breeding ratio and higher transmutation efficiency. Higher breeding gain and lower specific fissile inventory both result in lowering the doubling time (Waltar *et al.*, 2012).

In-pile experiments stated that the most important drawback of carbide fuel is the high swelling rate due to its more compact lattice structure (Matzke *et al.*, 1986). The impact of this phenomenon could be reduced at a design level, adopting appropriate fuel-cladding gap and making use of a low-density fuel. In fact, carbide fuel specifications foresee the employment of pellet with a density 80-85% TD in order to partially accommodate the fuel swelling and limit the FCMI when the gap closure occurs. The carbon activity (C/M) is another key factor, since it could affect the fuel pin safety. For this reason, the recommended content of higher carbides ($(U,Pu)_2C_3$) is between 5 and 10 wt.%. This value comes from an optimization with the aim of avoiding the formation of a metallic phase with a low melting point, while reducing the intensity of clad carburization effect (Duguay *et al.*, 2015). The reprocessing of carbide fuel is another concerning issue. The implementation of the well developed PUREX process leads to the formation of complex organic compounds (e.g., hexacarboxylic acid, oxalic acid) during dissolution which could interfere during separation process by forming a third phase (Bokelund *et al.*, 1982). Thus, big efforts have been carried out to find a solution to this problem, and some advanced hydrometallurgical processes have been proposed (Natarajan *et al.*, 2007).

Beyond the advantages and disadvantages of carbides as nuclear fuel, and the adopted ways to solve them, it is important to describe their physical properties and the conventional routes to produce them, in order to better contextualise this work, underlining the addressed issues.

1.5 Actinide Carbides: General Properties and Applications

Carbides are classified as ceramic materials, as oxides and nitrides. They are chemical compounds in which carbon bonds with less electronegative elements. Different types of carbides exist depending mainly on the difference in electronegativity. There are *salt-like compounds* (where carbon bonds with very high electropositive elements), *covalent compounds* (as

SiC and B_4C), and *interstitial compounds* (with transition metals of the groups 4, 5, 6). Usually, carbides exhibit metallic properties (as a low electrical resistivity), high hardness, and very high melting points. Indeed, they are considered refractory materials. Thanks to these peculiar properties, they are used in different engineering fields: building, mechanics, aerospace, rockets, and nuclear (Manara *et al.*, 2012).

1.5.1 Actinide Carbides: Structure of the Matter

Actinides form three type of carbides: monocarbides of the type AnC, dicarbides of the type AnC_2 and sesquicarbides of the type An_2C_3. All these three different carbides are *salt-like* compounds. Then, carbon is present as a single anion C^{4-}, double anion C_2^{2-}, and three atom units C_3^{2-} in the mono-, di- and sesquicarbides, respectively.

Actinide carbides could have different crystallographic structures depending on the stoichiometry. Monocarbides $AnC_{1\pm x}$ crystallize in cubic NaCl-type space group *Fm*-3*m*, No. 225. The lattice parameter is influenced by the C/An ratio: it linearly increases with the dissolution of carbon in the lattice. However, it is difficult to correlate it to stoichiometry since also other factors affect it, such as oxygen and nitrogen impurities dissolved in the lattice. Actinide dicarbides AnC_2 show a large variety of structures, depending mainly on temperature. The possible AnC_2 crystallographic modifications include tetragonal dicarbides of the type CaC_2 (*I*4*mmm*, Group 139), cubic fcc of the type KCN (*Fm*-3*m*, Group 225) and monoclinic (*C*2/*c*, Group 15). Dicarbides are always substoichiometric, then, they are often represented as AnC_{2-x}. Finally, the sesquicarbides have been identified to be body-centred cubic (bcc) of the *I*-43*d* type. These compounds are more difficult to form than mono- and dicarbides. Complex preparation procedures are needed. Only Pu_2C_3 forms easily in appropriate ranges of temperatures and is the most stable among the Pu carbides (Manara *et al.*, 2012). As a summary, a list of the known actinide carbides and description of their structure is reported in *Figure 4*.

Compound and lattice parameters	*Composition and temperature range*	*Space group*	*Structure* ● - Actinide; ● - C
$ThC_{1\pm x}$ 508.8 pm (Th) to 534.4 pm ($ThC_{0.98}$ in equilibrium with ThC_2)	C/Th = 0–1.96 Eutectic $ThC_{1\pm x}$ = 1980 K Congruent T_m = 2780 K for C/Th = 0.975	NaCl-fcc $O_h^5 - Fm\bar{3}m$(Nr.225)	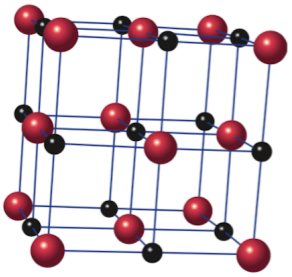
PaC 506.08 pm	–		
$UC_{1\pm x}$ 4.9605 Å ($UC_{1.0}$) 4.9563 Å ($UC_{0.93}$)	C/U = 0.82–1.86 T_m = 2780 K for C/U = 1		
$NpC_{1\pm x}$ 499.1 pm for $NpC_{0.82}$ to 501.0 pm for $NpC_{1.0}$	0.82 ≤ C/Np ≤ 1.0		
PuC_{1-x} $a = 498.13 - 1.50$ (1 − C/Pu)pm	C/Pu = 0.74–0.94 $T_{peritectic}$ = 1910 ± 20 K		
AmC_{1+x} 502 pm	$AmC_{1.04}$, $AmC_{1.25}$		
Th_2C_3 855.13 ≤ a ≤ 856.09 pm in a narrow homogeneity range	Th_2C_{3-y} (0 ≤ y ≤ 0.05) Under high p > 2.8 GPa	bcc – eight molecules per unit cell $T_d^6 - I\bar{4}3d$(Nr.220)	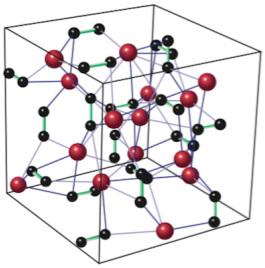
U_2C_3 808.99 pm	$U_2C_3 \rightarrow UC + UC_2$ (>2093 K)		
Np_2C_3 810.3 pm	–		
Pu_2C_3 812.1 ≤ a ≤ 813.4	C/Pu = 1.45–1.5 Stable under 2300 K		
Am_2C_3 827.57 pm	–		
Cm_2C_3 839.4 pm	–		
α-ThC_2 $a = 668.4 \pm 0.02$ pm; $b = 422.0 \pm 0.1$ pm; $c = 673.5 \pm 0.2$ pm; $\beta = 103.91 \pm 0.01°$	$ThC_{1.94}$ Stable up to 1713 K	Monoclinic $C2/c$ (No. 15)	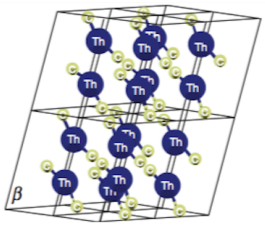
β-ThC_2 a = 422.1 pm; c = 539.4 pm (in equilibrium with graphite)	Stable for 1713 K ≤ T ≤ 1768 K	CaC_2-tetragonal $D_{4h}^{17} - I4/mmm$ (Nr. 139)	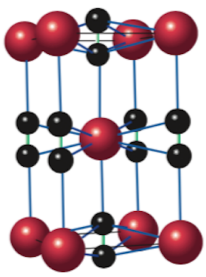
α-PaC_2 a = 361 pm; c = 611 pm	Observed around 2500 K		
α-UC_2 $a = 352.45 + 0.75$ (C/U-1.80) pm; $c = 1.702a$	C/U = 1.75–1.9 $UC_2 \rightarrow U_2C_3 + C$ (<1790 K)		
Stable in range 1790–2050 K T^m = 2720 K	$\alpha UC_2 \rightarrow UC + \beta UC_2$ (>2050 K)		
α-PuC_2 a = 363 pm; c = 6.094 Å	Stable for 1933 K ≤ T ≤ 1983 K		
γ-ThC_2 a = 581.3–584.1 pm	Stable above 1768 K $T_m \cong$ 2883 K	KCN-fcc $O_h^5 - Fm3m$(Nr.225)	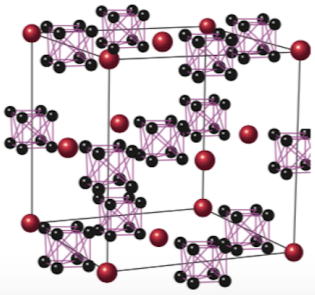
β-UC_2 a = 548.8 pm	Stable above 2050 K $T_m \cong$ 2750 K		
β-PuC_2 a = 572 pm	Stable above 1983 K $T_m \cong$ 2520 K		

Figure 4: Synopsis of the known actinide carbides (Manara et al., 2012).

1.6 Uranium Carbides

This thesis will focus on uranium carbides, which are regarded as a possible alternative to oxides as nuclear fuel for FRs. However, it is worth noting that uranium carbides in natural isotopic composition could not fuel a fast reactor, since a significant amount of starting fissile material is needed. Then, either enriched uranium or, as a more advisable option, mixed plutonium and uranium carbides should be considered. Here, only uranium carbide was studied as a typical representative of actinides and due to its easy handling compared to plutonium. Then, this work should be considered as a first characterization and optimization of a wider procedure that should later involve the more complex system of mixed carbides.

Hereafter, a brief description of the uranium-carbon system will be given. Particular attention is addressed to uranium monocarbide, UC, which is the main compound considered in the specifications of this type of advanced fuel.

1.6.1 Uranium - Carbon Phase Diagram

The latest U-C phase diagram is due to Chevalier *et al.* (2001), and it is presented in *Figure 5*. As shown in the diagram, depending on temperature and C-U content, different phases can be formed. From stoichiometric monocarbide $UC_{1.00}$ to hypo- or hyperstoichiometric $UC_{1\pm x}$, from sesquicarbide U_2C_3, for the higher C content, to hypostoichiometric UC_{2-x}.

This phase diagram was compiled from experiments and calculations following the thermodynamic equilibrium criteria. However, the thermodynamic stability of the sesquicarbide phase could be hardly achieved (Benz *et al.*, 1969), while $UC_{1\pm x}$ and UC_{2-x} are easily stabilized, even at room temperature. Then, it was decided to establish a "metastable" uranium-carbon phase diagram, reported in *Figure 6*. In this diagram, U_2C_3 has not been considered, and tetragonal α-UC_{2-x} is the only stable phases in equilibrium with $UC_{1\pm x}$ or C, depending on C portion, at room temperature (Laugier *et al.*, 1971)

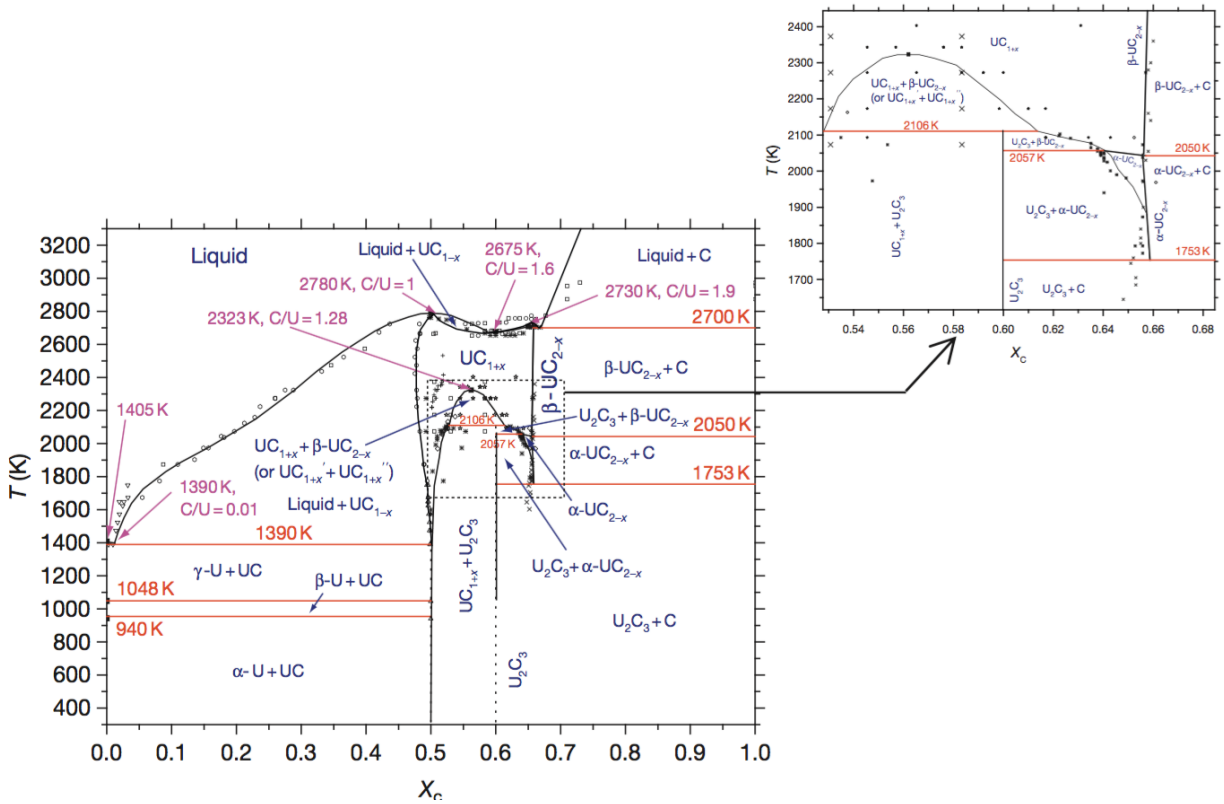

Figure 5: The equilibrium U-C phase diagram based on calculated and experimental data (Manara et al., 2012).

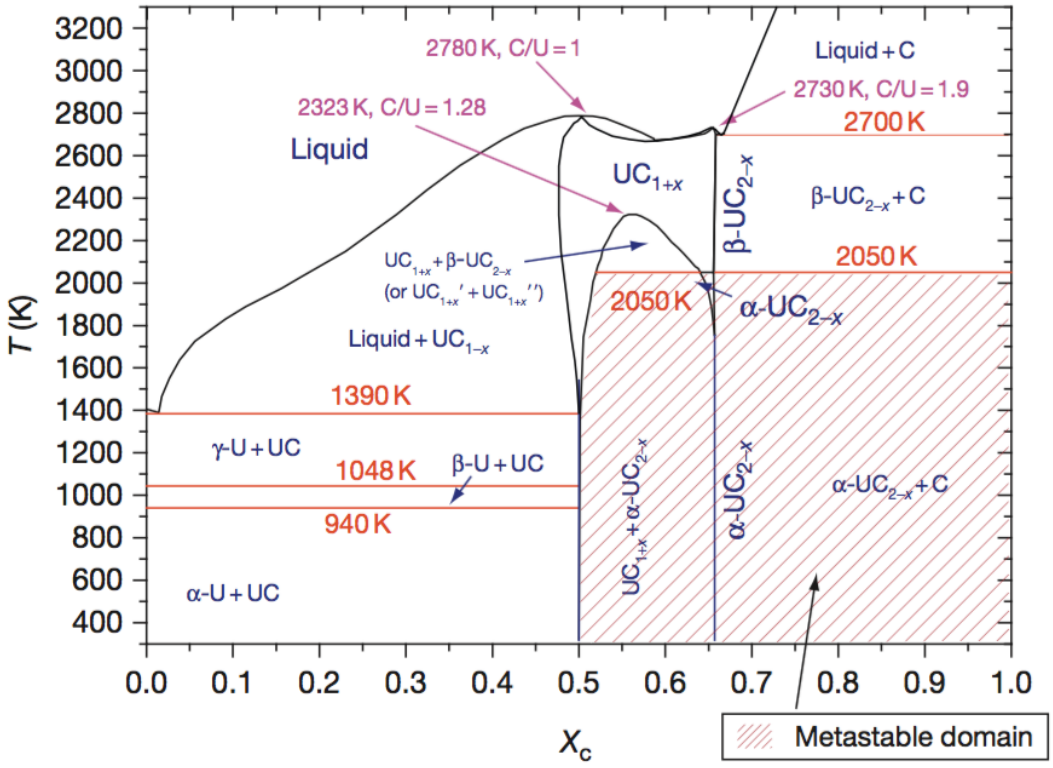

Figure 6: The metastable U-C phase diagram (Manara et al., 2012).

1.6.2 Crystallography of Uranium Carbides

Many authors studied the dependence of UC lattice parameter on temperature, C/U ratio, and O and N concentration as impurities (Holleck *et al*, 1987). Stoichiometric UC is characterized by a lattice parameter a = 4.9600 ± 0.0005 Å at room temperature (Williams *et al.*, 1960). Then, hypostoichiometric UC_{1-x} shows a lattice parameter linearly increasing with x, while hyperstoichiometric UC_{1+x} behaves almost homogenously, since substituting a single C with two C stabilizes the excess C. If O and N impurities are dissolved in the lattice, correlating the lattice parameter calculated from Rietveld refinement to the stoichiometry is not direct. In fact, O and N influence the lattice dimensions. In particular, they have opposite effects, since the substitution of C by O gives lattice dilation, while the substitution of C by N results in a decrease of a (Manara *et al.*, 2012).

For completeness, the tetragonal α-UC_{2-x} shows a lattice parameter a that increases linearly with x. The c/a ratio is 1.702 at room temperature (Tegawa *et al.*, 1970). The cubic β-UC_{2-x}, instead, is characterized by a = 5.4880 Å (Bowman *et al.*, 1966). Finally, the cubic structure of U_2C_3 presents a lattice parameter a = 8.0899 Å at room temperature (Boutard *et al.*, 1974).

1.6.3 Thermo-Mechanical Properties of Uranium Carbide

One of the most important advantage of employing uranium carbide as nuclear fuel is the high thermal conductivity. This property leads to a better heat exchange in the fuel pellet. Then, thanks also to the high melting point (T_m=2780 K), safer operations and higher performances are achievable.

In particular, thermal conductivity of uranium carbide slightly depends on temperature. This dependence is shown in *Figure 7*. However, many factors influence this tendency, among which the most important is the level of oxygen impurities. In fact, as shown in the figure, a decrease of a factor of two is observed when the oxygen impurities are 15 at.%. Another relevant parameter is the carbon content deviation from stoichiometry. Similarly to uranium dioxide, the thermal conductivity has been observed to decrease with both vacancies (UC_{1-x}) and interstitials (UC_{1+x}) in the crystal (Matzke *et al.*, 1986; Holleck *et al.*, 1987).

Another characteristic of uranium carbide is the higher theoretical density (ρ=13.60 g/cm^3). This feature has positive effects on neutronics, design and economy. In fact, together with the better thermal conductivity, it allows higher specific power, thus more compacted cores, and lower doubling time (Manara *et al.*, 2012).

Most of the mechanical properties of UC, like the Young, torsion and bulk moduli, the brittle-ductile transition, the Vickers hardness (HV) or creep behaviour have been determined analysing their dependence from thermal history, grain size, O and N impurity content, C/U ratio, and porosity (Matzke *et al.*, 1986; Holleck *et al.*, 1987; Hall *et al.*, 1970).

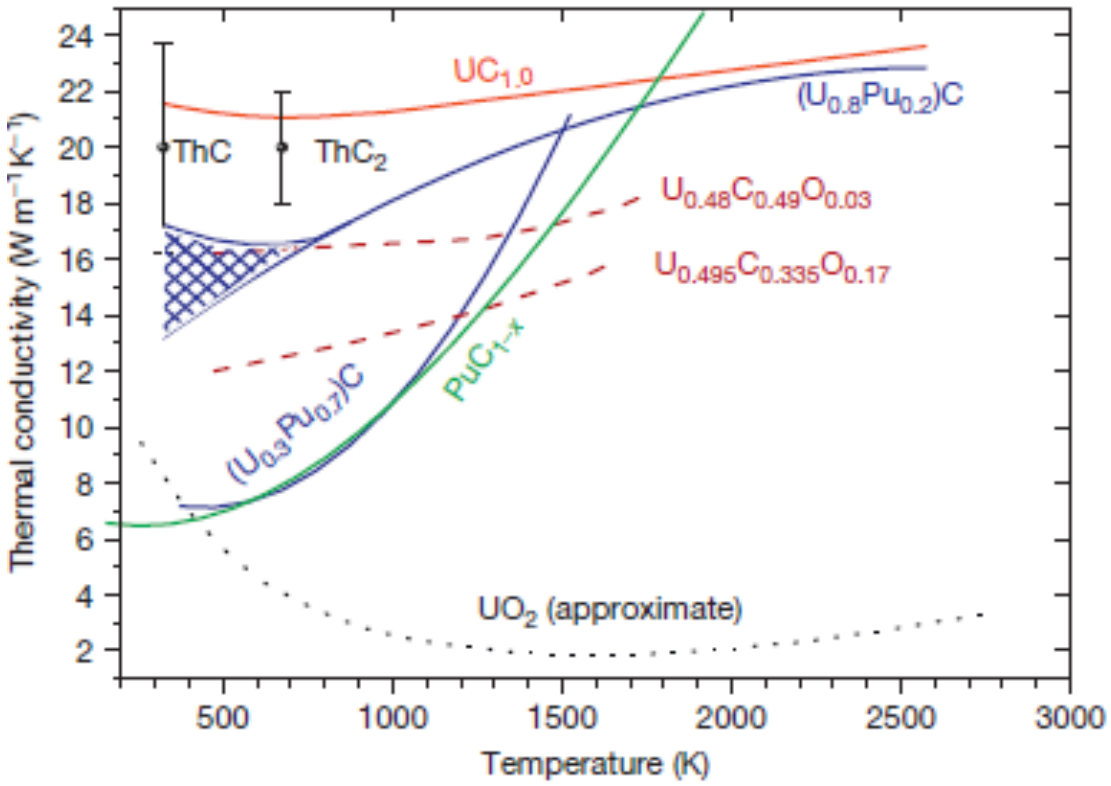

Figure 7: The thermal conductivity of some actinide carbides and oxycarbides compared to uranium dioxide (Manara et al., 2012).

1.6.4 Uranium-Plutonium Mixed Carbides

As already stated, an amount of fissile isotopes is needed to fuel a FR. Then, uranium and plutonium carbides should be considered. Phase relationships in the U-Pu-C system was studied in Los Alamos Scientific Laboratory of the University of California and Argonne National Laboratory (Rosen *et al.*, 1963; Reavis *et al.*, 1966). In these studies, it was stated that uranium carbide forms a complete solid solution with plutonium carbide, due to their very similar crystal structures.

As in MOX, there is a general worsening of thermal properties with increasing the plutonium content. Both the melting point and thermal conductivity decrease (Stahl *et al.*, 1964; Ohse *et al.*, 1976), as shown in the *Figure 7*.

1.7 Conventional Fabrication of Carbide Fuel

Fabrication of carbide fuel on commercial scale is a difficult task and needs additional care because of pyrophorocity and tendency to easily oxidize and hydrolyse. High-purity inert gas

(nitrogen or argon) in the fabrication line is mandatory. The oxygen and moisture content in the glove box atmosphere should be less than 25 ppm (Manara *et al.*, 2012) to minimize O pick up during the fabrication process.

From the beginning of the research on carbide fuel, different routes have been pursued to produce it: namely, melting casting, carbothermal reduction of oxide and graphite, and sol-gel.

In the melting casting process, metallic uranium and graphite are arc-melted many times until the desired homogeneity is reached, then melted and finally dropped into an appropriate mold. This method results to be uneconomical since the high cost of metal fabrication, and is conducted only for small-scale production (Frost *et al.*, 1963).

The carbothermal reduction (CTR) represents the most applied among the different fabrication routes, due to its higher economics and better predisposition to large-scale production. Uranium/plutonium dioxide and graphite are blended together through ball milling for 24-48h, as Suzuki *et al.* (1981) reported, to achieve a good homogeneity between the two precursors. Then, after a precompaction at 400-500 MPa, CTR is conducted at a temperature ranging between 1450°C and 1700°C for 5-13h (Vaudez *et al.*, 2015). Lower CTR temperatures are necessary to limit the plutonium (or MAs) losses by vaporization, but typically the content of unreacted oxide in the final powder is higher (Richter *et al.*, 1974). CTR is usually conducted under vacuum to enhance the kinetics of the reaction (Matzke *et al.*, 1986). The so-synthesised carbides are milled for several hours (3-48h as reported by Suzuki *et al.*, 1981) to increase their sinterability. Densification is performed in argon atmosphere at 1700-1900°C for 5-20 h (Burkes *et al.*, 2009). A reduction of the sintering temperature could be achieved if sintering aids are used, like nickel (Suzuki *et al.,* 1981).

The sol-gel is based on the internal gelation process. Concentrated feed solutions of uranium and plutonium nitrates are mixed together with solution of hexamethylenetetramine (HMTA), urea and dispersed carbon black. The mixture is dropped into a column of hot silicon oil (90°C). The temperature rise in the droplets triggers off the decomposition of HMTA to form ammonia, which precipitates ammonia-diuranate and plutonate within the droplets, forming small solid spheres. Washing steps are performed with carbon tetrachloride and ammonium nitrate to remove the silicon oil and other reaction products. A calcination step in argon/hydrogen drives off the volatile substances still present and adjusts the uranium/plutonium oxidation state. Here, the produced spheres could follow two different processes, depending on the type of fuel to be realized: sphere-pac (Stratton *et al.*, 1993) or pellet shape fuel (Ganguly *et al.*, 1996). The first foresees a reaction-sintering step at 1950°C for 8h in argon producing dense microspheres to be loaded directly into fuel pins. To obtain a pellet shape fuel, the material is first carboreduced at 1500°C in vacuum. The produced carbide spheres are first cold-pelletised at 1200 MPa and, then, heat treated at 1700°C in argon atmosphere.

1.8 Concluding Remarks

Despite the enhanced safety and power performances achievable with these so-called advanced nuclear fuels, interest in mixed carbides gradually decreased. A lot of factors contributed to that. First of all, fabrication process is more complicated if compared to oxide fuels. In fact, if we analyse the powder-metallurgic way, a further step is needed: the carbothermal reduction. Furthermore, due to the very high sensibility to oxygen and moisture, the use of high-purity dry inert cover gases such as argon or nitrogen in glove boxes is compulsory. Both these drawbacks heavily affect economics, representing the biggest obstacle to overcome for making carbide an attractive and economically viable option.

Then, further research activity is still needed to pass through these problems and to fill the gap between carbides and oxides. In particular, this thesis focuses on the development of a new synthesis method of uranium carbide. The main purpose was to increase the reactivity of the starting materials, thus lowering the time and temperatures needed for production.

This page is intentionally left blank

2 Tools and Techniques

Abstract *Different experimental techniques were adopted in this project. The obtained results gave qualitative and quantitative information which were useful to evaluate the effectiveness of the new proposed procedures for uranium carbide synthesis and densification, and at the same time to characterise the composition, crystallography, morphology and structure of the produced samples. Due to the high sensitivity of carbides to oxygen and moisture, different measures had to be taken in order to preserve them from degradation. Above all, the presence of an inert atmosphere (argon or nitrogen) was mandatory. Apart from the fact that an oxidation would have affect the results, thus leading to erroneous conclusions, also safety issues justify this care: uranium carbide is reported as pyrophoric material (Mazaudier et al., 2010).*
Most of the experiments were conducted in a spark plasma sintering (SPS) device through the development of a particular set-up designed for the purpose. To the author's knowledge, it was the first time that uranium carbides were synthesised and densified in SPS. However, the importance of SPS has been already established in the fabrication of uranium dioxide pellets thanks to the high sintering capability (Tyrpekl et al., 2014) and the possibility of simulating high burn-up structure (HBS) (Cologna et al., 2016) and spent nuclear fuel (SIMFUEL), incorporating volatile fission products (Wangle et al., 2015).

2.1 Introduction

In this chapter, the used measuring techniques are described. The basic principles of operation are briefly explained and particular specifications of the devices are given. Finally, the spark plasma sintering (SPS) technique is introduced. The SPS set-ups that have been used in this work are illustrated, focusing the attention on the new developed design for performing CTR.

2.2 Characterization Techniques

2.2.1 X-Ray Diffraction

X-ray powder diffraction (XRD) is a widely used technique based on scattering and interference of the X-rays on the atoms in a crystal lattice. During the interaction the electrons of these atoms starts to oscillate, thus emitting themselves X-rays with the same energy of the incident radiation. This phenomenon is called coherent scattering. The interaction between the scattered X-ray produces a diffraction pattern, which contain information about the atomic arrangement within the crystal. In fact, the reflected radiation gives a constructive interference, and then a diffraction peak, only in some particular directions. The angle of positive interference depends on the size and the shape of the unit cell characterizing the particular crystallographic structure. In general, the Bragg's law provides a simplistic model that shows the required conditions for diffraction.

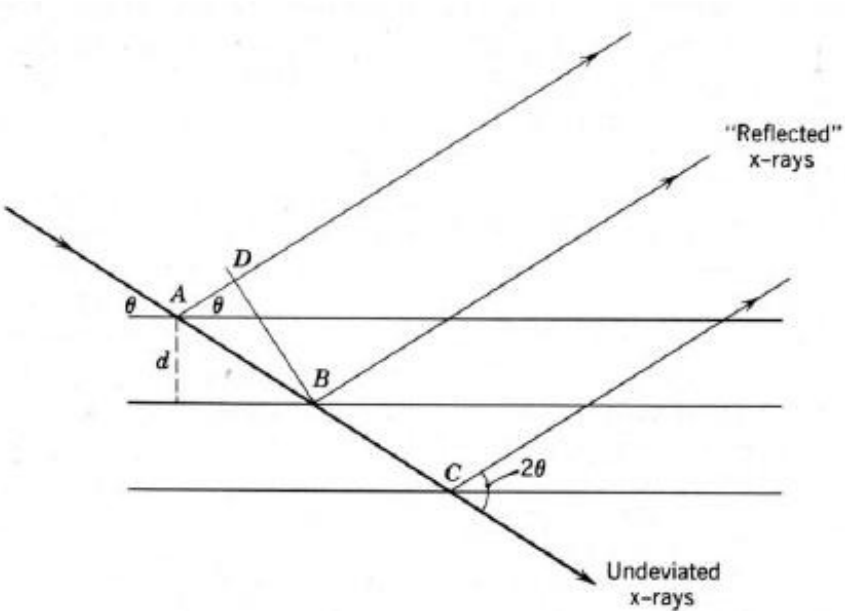

Figure 8: Bragg law: condition for constructive interference.

The constructive interference occurs only when the difference in the path between the X-ray reflected by the first plane in *Figure 8* and the X-ray transmitted and reflected by the second plane (AB - AD) is equal to an integer value of the wavelength λ of the incoming radiation:

$$AB - AD = n\lambda \tag{3}$$

Easy mathematical calculations lead to the final equation, calling θ the angle between the incident beam and the family of planes, and d the distance between two consecutive parallel planes:

$$n\lambda = 2d \sin\theta \tag{4}$$

While the position of the diffraction peak is determined by the distance between parallel planes, the intensity of each peak depends on the arrangement and the kind of atoms in the entire crystal.

XRD could be used to determine:
- Crystal structure;
- Phase composition;
- Unit cell lattice parameters;
- Residual macrostrain;
- Preferential orientation;
- Crystallite size and microstrain.

The calculation of crystallite size and microstrain can be done using the Williamson-Hall law, which originate from the principle that crystallite size and inhomogeneous strain can broaden the diffraction peaks, affecting their Full Width at Half Maximum (FWHM).

In this work, XRD patterns were recorded using a Bruker® D8 X-ray diffractometer mounted in a Bragg–Brentano configuration with a curved Ge monochromator (1, 1, 1), a ceramic copper tube (40 kV, 40 mA) equipped with a LinxEye position sensitive detector. For the measurement, the powder was deposited on a silicon wafer to minimize the background and dispersed on the surface with 2 or 3 drops of isopropanol. Structural analyses were performed by the Rietveld method with the JANA 2006 software suite (Petricek *et al.,* 2014).

2.2.2 Scanning Electron Microscopy

The scanning electron microscopy (SEM) is a technique that produces a high-magnification image by using electrons to form an image. Electron beam, coming from a heated W–filament called electron gun, is accelerated against the specimen in a strong potential (from kV to tens of kV). Thanks to this high energies, the electrons have a shorter De Broglie wavelength ($\sim 10^{-12}$ m) than that of visible light (characteristic of optical microscopes) resulting in a higher resolution. The electrons of the beam could be scattered by the sample both elastically and inelastically, and then be detected. In the first case, more energetic electrons are detected, called Back-Scattered Electron (BSE), whereas Secondary Electrons (SE) have a lower energy, since they are produced by the inelastic interactions. The low energy of these SE forces to perform the analysis under high vacuum. Then, if the material is not conductive, a coating with gold or graphite is needed. Since electrons strongly interact with matter, SEM provides only an analysis of the surface of the sample.

The device employed in the present work was a FEI (Philips®) XL40 scanning electron microscope using a tungsten filament, operating between 200 V and 30 kV and installed in a glove box.

2.2.3 Transmission Electron Microscopy

Transmission electron microscopy (TEM) is a microscopy technique which involves a high voltage beam of electrons to obtain information about the structure of the analyzed specimen. Contrary to SEM, here the detected electrons are the one transmitted through the material, which is located in a vacuum chamber. Thus the sample should be thin enough (up to hundred of nanometers thick) for electrons to pass through (electron transparency). Samples also need to be able to withstand the vacuum chamber and often require special preparation before viewing, depending on the nature of the material and type of investigated information. These include: dehydration, sputter coating of non-conductive materials, cryofixation, sectioning and staining.

The used device was a TecnaiG2 (FEI™) 200 kV equipped with field emission gun, modified during its construction to enable the examination of radioactive samples. The instrument is provided with a Gatan™ Tridiem GIF camera, an energy-dispersive X-ray (EDX) analysis system, and a high-angle annular dark-field (HAADF) detector for the scanning transmission electron microscope (STEM) imaging. The samples for the TEM investigations were prepared by crushing tiny fragments of the various compounds in methanol. The resulting suspension was allowed standing for decanting, and a droplet subsequently deposited on a copper grid coated with carbon.

2.2.4 Thermogravimetric Analysis

A thermogravimetric analysis (TGA) consists in heating the sample under pre-set atmosphere conditions and simultaneously measuring its mass. A small amount of material is powdered and put into the thermobalance alumina crucible. The crucible is seated in an oven, where a certain gas flow and a raising ramp of temperature are set, and it is connected to a high-sensitivity analytical balance that allows in situ weighing of the powder during the heating process. Different information could be provided, depending on the parameters of the heat treatment. Studies on decomposition, oxidation, reduction, and gas release are achievable.

TGA was conducted to follow the thermal behaviour of the uranyl-citrate solution in argon atmosphere. TGA was also used to perform an oxidation study under air on the UO_2/C nanocomposite after calcination. The measurements were performed using NETZSCH Simultaneous Thermal Analysis Apparatus STA 449C.

2.2.5 X-Ray Computed Tomography

X-ray computed tomography (CT) is a non-destructive technique for visualizing interior features within solid objects and obtaining information on their geometrical properties. During a CT acquisition, the sample is fixed on a rotary stage between an X-ray source and the detector. A sequence of 2D X-ray images is taken as the object rotates 360 degrees. The images then go through a reconstruction software that generates a 3D volumetric map composed of elementary units, called voxels. The radiation, passing through the sample, is subjected to different interaction phenomena resulting in the attenuation of both energy and intensity of the X-ray beam. The 2D image registered by the detector is composed of different shades of grey, which reflect the X-ray attenuation pattern. The probability of X-ray interaction depends on the volume/dimensions of the sample, its density, its atomic number, the presence of porosity or other type of defects.

We used a Nikon X-ray tomography system XT H 225 ST equipped with a microfocus source, a tungsten reflection target, and a 16 bit Perkin Elmer 1621 flat panel detector. The volume analysis was performed by means of Aviso 9 3D analysis software.

2.3 Spark Plasma Sintering Device

The spark plasma sintering (SPS) is a particular method used to produce high quality pellets from powders. The technique belongs to the so-called Field Assisted Sintering Techniques (FAST), which are characterized by an employment of an electric field as a facilitator of sintering (Tyrpekl *et al.*, 2015).

A typical SPS device consists of a uniaxial hydraulic press with graphite punches and dye in a steel containment. The graphite punches generate pressures up to 100 MPa and also serve as electrodes providing a pulsing current through the powder and the die. Usually the highest applicable voltage is 10 V, while the highest generated current is 10 kA (Guillon *et al.*, 2014). The heating is carried out by Joule effect inside the treated material if the latter is highly conductive (as metallic alloys or ultra-high-temperature ceramics), or, on the contrary, inside the graphite die and then quickly and efficiently transferred to the sample by conduction. A schematic draft of the tool is shown in *Figure 9*.

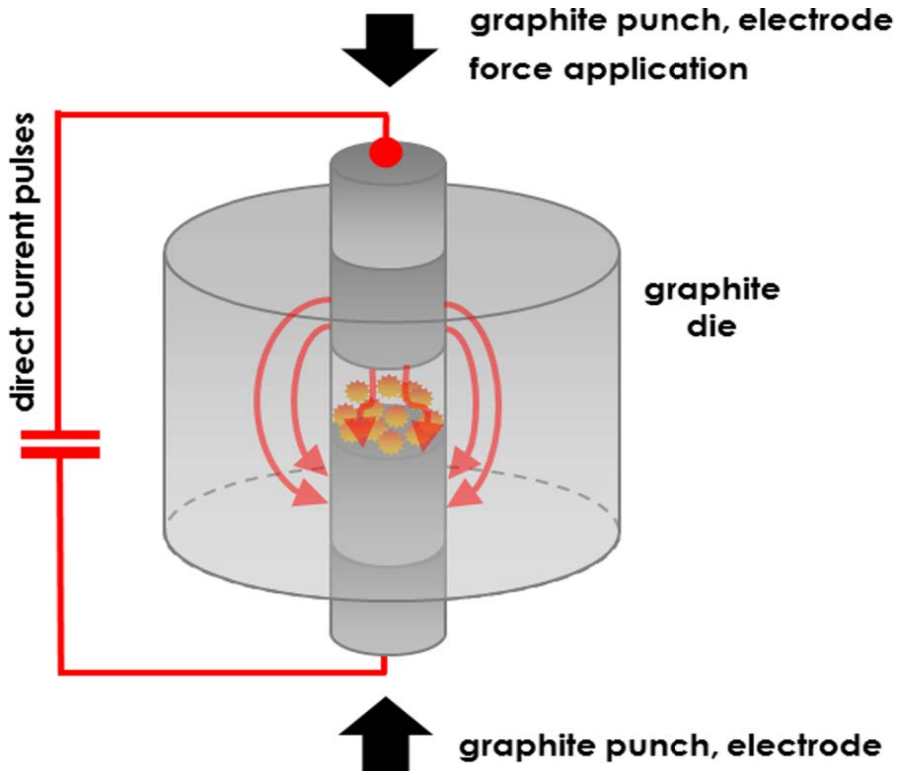

Figure 9: General principles of spark plasma sintering (Tyrpekl et al., 2015).

SPS resulted to be a very efficient technique for powder consolidation compared to classical sintering of green pellets (Rishi *et al.*, 2011). This efficiency may be justified by different reasons, going from mechanical to thermal and electrical effects. First of all, the compressive stress applied leads to a better contact between particles, thus enhancing the densification mechanisms already present in free sintering (like grain boundary diffusion, lattice diffusion,

and viscous flow), but also activating new mechanism, such as plastic deformation or grain boundary sliding (Rahaman *et al.*, 2003). Besides pressure, another advantage is the availability of high heating rates. Reaching quickly high temperatures could enhance densification rate while retarding the microstructure coarsening (Quach *et al.*, 2010; Shen *et al.*, 2002). Finally if high currents flow through the sample, interactions between the current and microstructure may occur, like percolation effects, which could improve the efficiency of the process (McWilliams *et al.*, 2008; Schwesig *et al.*, 2011).

SPS devices are mostly used in conventional industry, where the number of installed apparatuses is estimated to be 1800 (Guillon *et al.*, 2014). Concerning the nuclear research, SPS has been applied to consolidation of UN (Muta *et al.*, 2008), UO_2 (Ge *et al.*, 2013; Ge *et al.*, 2014), UO_2-SiC composites (Yeo *et al.*, 2013; Chen *et al.*, 2014), and W-UO_2 cermets (O'Brien *et al.*, 2013). In particular, the device used in this work is probably the only one that has been placed inside a glove box, thanks to appropriate modifications (Tyrpekl *et al.*, 2015). The isolation in a hermetic glove box enables handling of highly radiotoxic materials (as Pu and MAs), and make it suitable for the here studied uranium carbide, which are known to be very sensitive to oxygen.

In the present work, different set-ups have been used, depending on the particular process to be performed. The sintering test on uranium carbide and the reactive sintering on the nanocomposite UO_2/C mixture were performed in the standard set-up, shown in *Figure 10*. The used graphite punches and dies had a 6 mm diameter. High pressure sintering was conducted employing a particular set-up (Anselmi-Tamborini *et al.*, 2007; Grasso *et al.*, 2010), whose characteristic are presented in *Figure 11*. Finally, a new set-up (*Figure 12*) has been designed to carry out the carbothermal reduction on the UO_2/C powder. The main peculiarities of this set-up are the use of a perforated graphite punch (10 mm diameter), which allow the produced CO to be released, and an inner graphite spacer to avoid the pressure to be applied on the treated material.

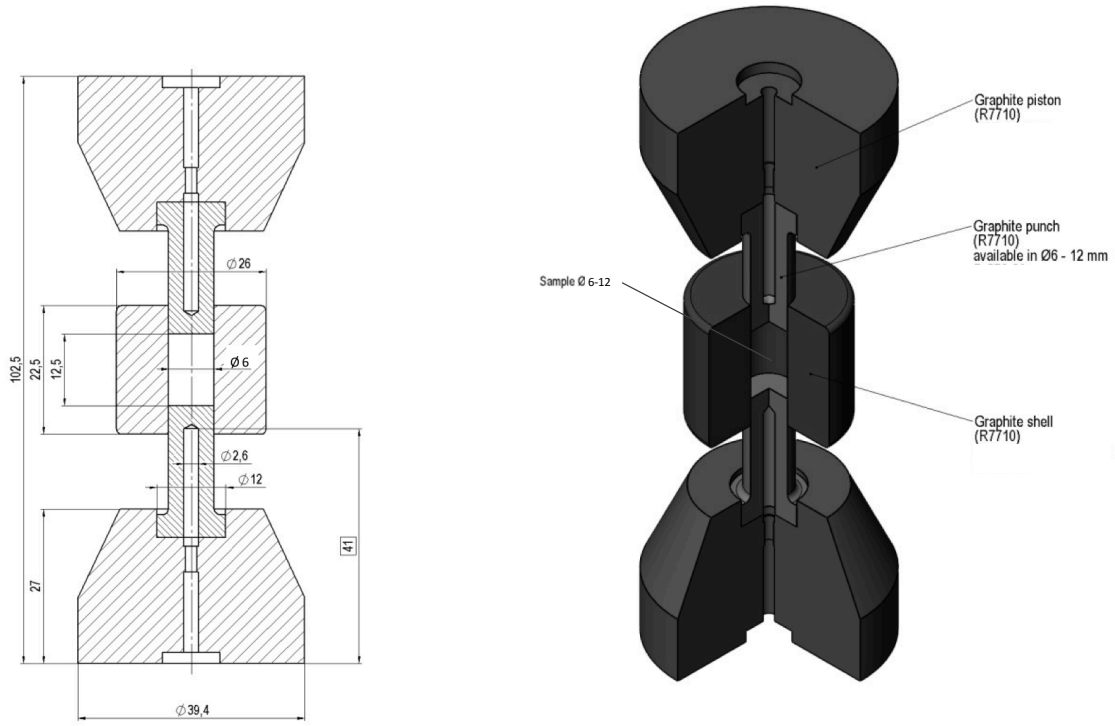

Figure 10: Technical drawing of the standard SPS set-up used for reactive-sintering on UO_2 and C mixture and for the sintering of uranium carbide.

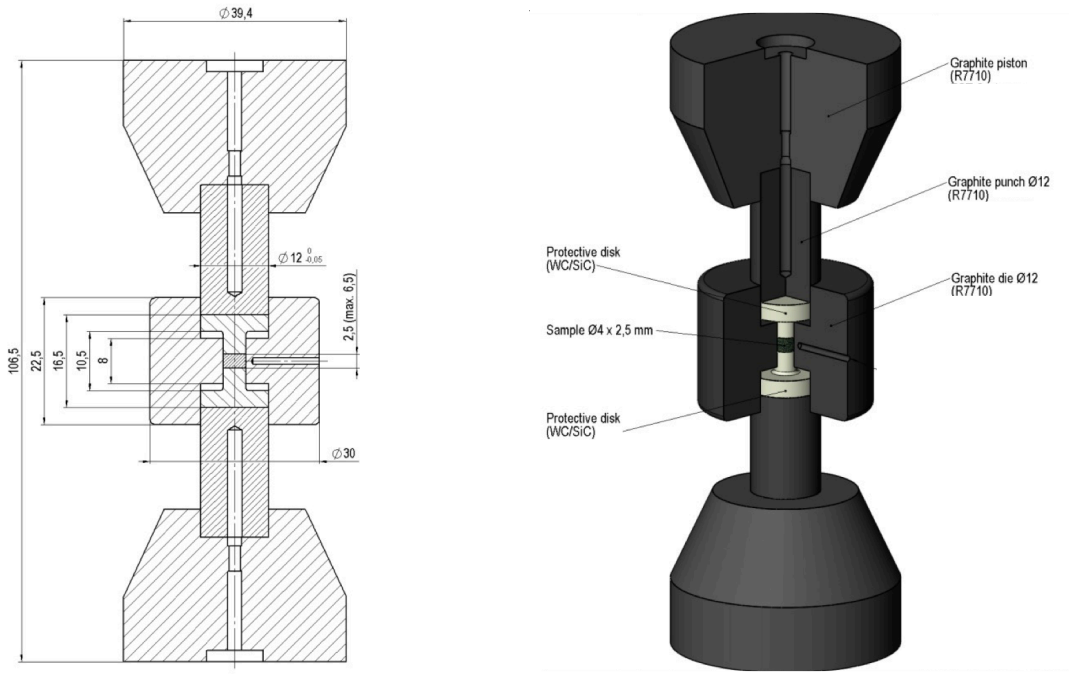

Figure 11: Technical drawing of the high pressure set-up used for the sintering of uranium carbide. Silicon carbide punches (in white) allow increasing the pressure over 500 MPa.

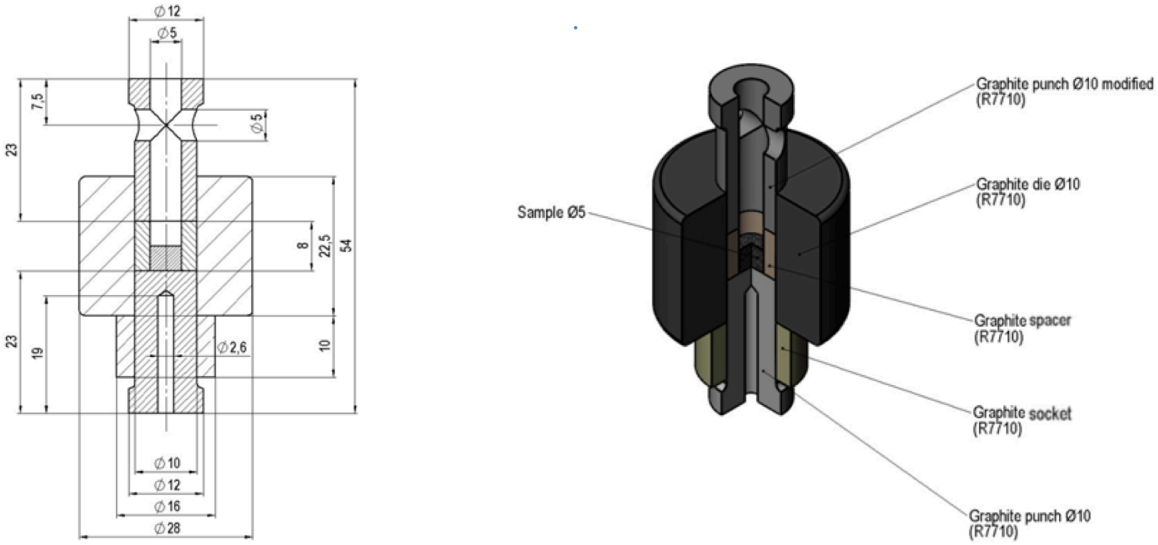

Figure 12: Technical drawing of the set-up developed for performing the CTR in SPS. The upper graphite punch contains a hole to enhance the release of CO as soon as is produced. The inner graphite spacer (in brown) is used to avoid any contact between the punches and the treated specimen.

2.4 Concluding Remarks

The adopted techniques turned out to be very efficient for this kind of experimental work. The obtained results were useful to understand what parameters in the process needed to be changed and the effect of these changes, thus allowing a quick and significant optimization of the developed method. Very interesting information has been also acquired from the characterization of the morphology, structure and crystallography of the produced specimens. In fact, a better understanding of the ongoing physical phenomena was thus achievable. Finally, these experiments supported the already known flexibility and efficiency of spark plasma sintering devices to adapt to different materials and different processes.

3 Experimental Procedure

Abstract *A new method for uranium carbide fabrication was tested. This experimental work foresaw the synthesis of UC precursors via a liquid route in order to achieve a better homogeneity of them (without any preliminary milling step), thus reducing the time and temperature usually needed to perform the carbothermal reduction (CTR). CTR studies were conducted in a conventional furnace and in a modified SPS set-up, properly designed to the scope. The as-produced carbides were sintered in SPS to study any influence of the synthesis parameters on the sintering capability of the powder.*

3.1 Introduction

In this chapter, the adopted experimental procedure is described. In particular, the specifications of the used liquid solutions and the calculations performed to find the needed volumes to be mixed are explained. Then, the parameters of all the heating treatments are shown in detail, like the heating and cooling rates, the maximum temperatures, the dwell times, the applied pressures, and the filling atmosphere. As a summary, a flow sheet of the performed experiments is presented in *Figure* 13.

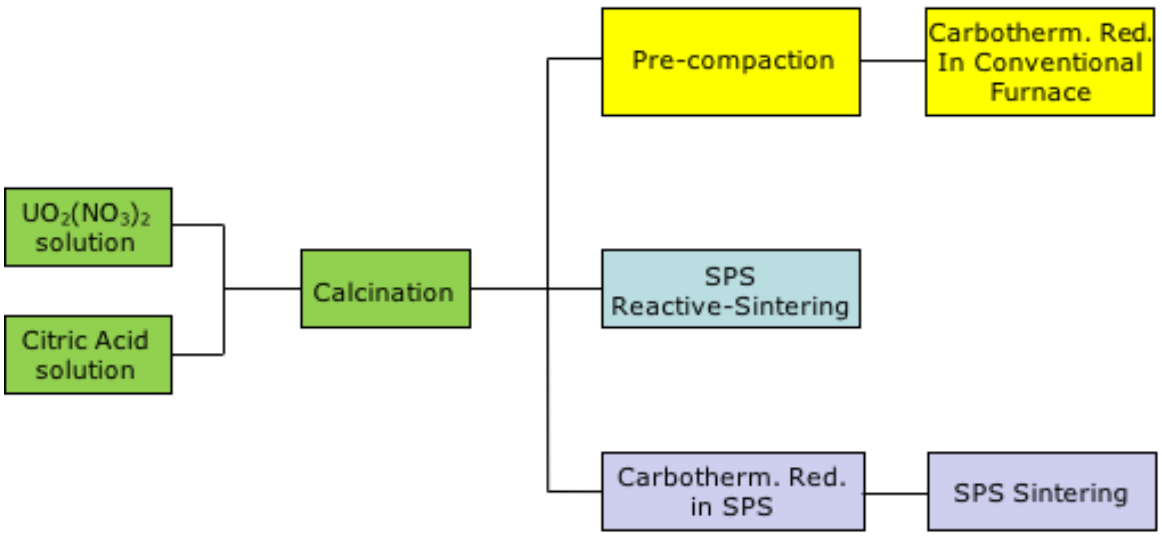

Figure 13: Flow sheet of the conducted experiments for uranium carbide fabrication.

3.2 Sample Preparation

Uranyl nitrate (-$UO_2(NO_3)_2$-) aqueous solution was used as uranium source. The carbon source was a citric acid ($C_6H_8O_7$) solution. The concentrations of the solutions to be mixed are shown in the *Table 1* below.

Table 1: Characteristics of the two starting solutions.

Solution	[g/L]	M [mol/L]
$UO_2(NO_3)_2$	501.6	2.076
$C_6H_8O_7$	494.1	2.611

The uranyl nitrate solution was obtained by dissolving uranyl nitrate hexahydrate powder in deionized water (7 MΩ) in a glove box under air. The second solution was prepared in a flume hood using citric acid (99+%, Alfa Aesar GmbH & Co KG®), which was dissolved in deionized water. To facilitate its dissolution an ultrasonic bath was used.

Targeted ratios between uranium and citric acid were obtained with mixing of controlled volumes of the two solutions. The mixing took place in a plastic container, in a glove box designed for uranium handling. A picture of the resulting liquid is shown in *Figure 14*.

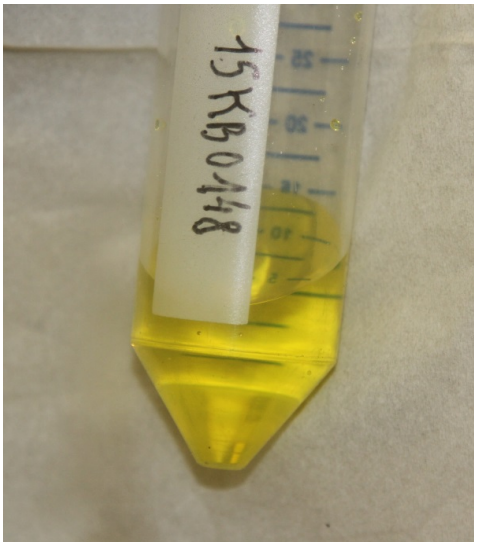

Figure 14: Mixed solution of uranyl nitrate and citric acid.

Different uranyl over citric acid ratios were studied, in order to find the composition that would give a higher percentage of uranium carbide after the carbothermal reduction.

The volumes to be taken were calculated in such a way:

If x is the needed mass of U_{met} in g, r the molar ratio citric acid/U_{met}, V_1 and V_2 the volumes of uranyl nitrate and citric acid, respectively, and M1 and M2 the molar concentrations:

$$V_1 = \frac{x}{MM(U)} * \frac{1}{M1} \quad (5)$$

$$V_2 = \frac{x}{MM(U)} * \frac{1}{M2} * r \quad (6)$$

Using the equations above, the volumes of the two mixed solutions were calculated in order to obtain the desired ratios. In *Table 2*, the values considered are listed.

Table 2: Volumes taken from the two solutions depending on the desired ratio and mass of uranium

Ratio	x [g]	V_1 [mL]	V_2 [mL]
1.10	2	4.050	3.540
1.40	2	4.050	4.505
1.70	2	4.050	5.475
1.90	2	4.050	6.120
1.95	2	4.050	6.285
2.00	2	4.050	6.440
2.00	10	20.250	32.200
2.05	2	4.050	6.600
2.10	2	4.050	6.760
2.20	2	4.050	7.085
2.30	2	4.050	7.445

3.3 Calcination

The above mentioned solutions were placed in quartz crucibles and underwent a heat treatment in a calcination furnace, in argon atmosphere, to get rid of all the volatile substances. During the pyrolysis, different types of molecules were lost, as water, carbon monoxide, carbon dioxide, nitrogen and nitrogen oxides. Then, in the end a black dried material was obtained, as shown in the *Figure 15*.

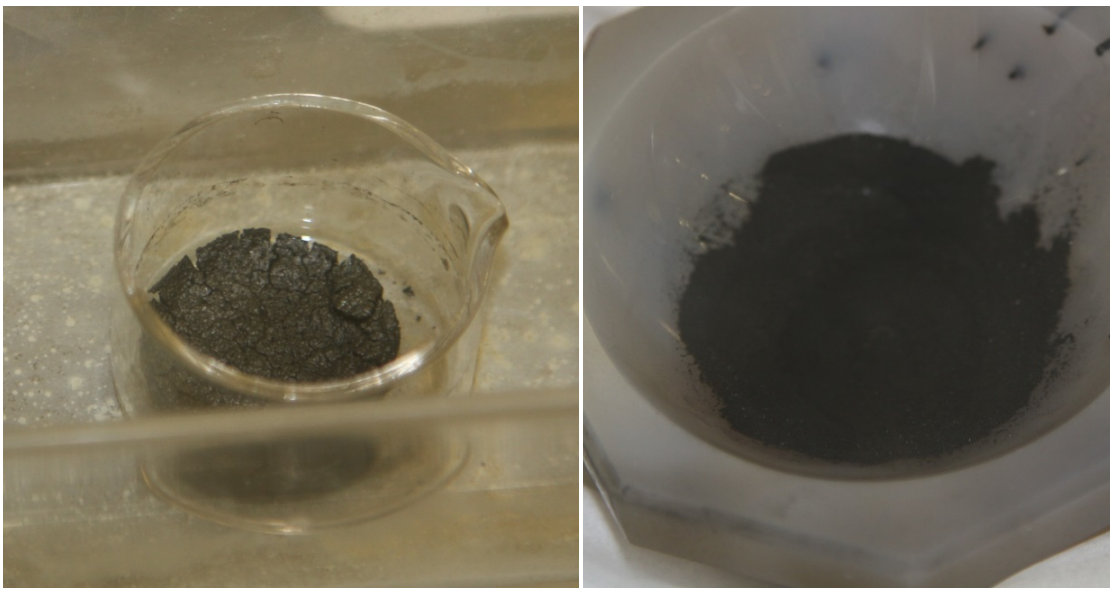

Figure 15: Pyrolysed material, before (left) and after (right) crushing in a mortar.

The solution was heated up to 1000 °C, hold for 2 hours and then cooled. The heating rate was +50 °C/h until 200 °C, and +200 °C/h till the maximum temperature, while the cooling rate was -400 °C/h. The slow heating ramp at the first stage was used for water evaporation. As a summary, a plot of the temperature profile is presented in *Figure 16*.

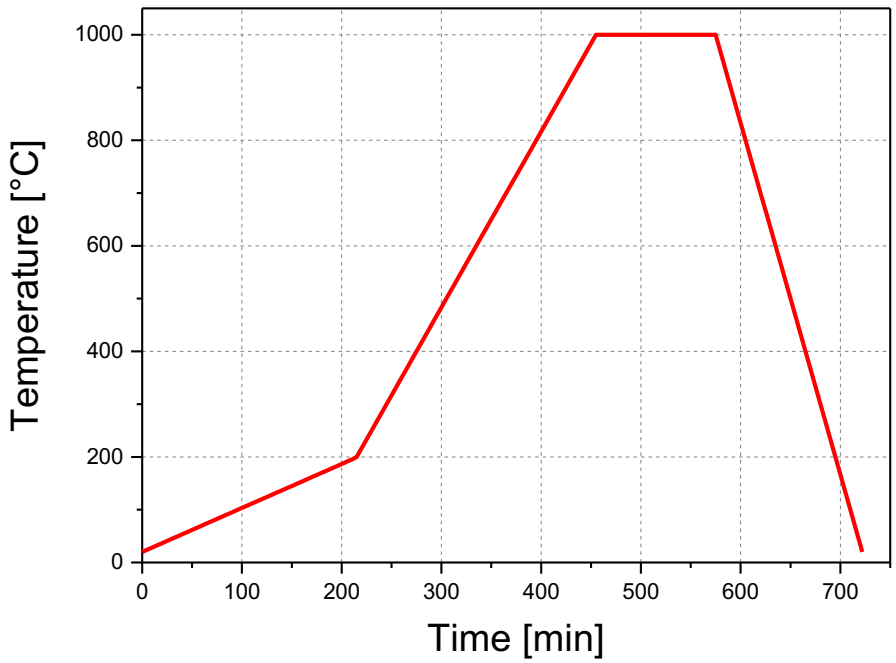

Figure 16: Calcination heating cycle.

During the calcination, different chemical reactions take place. First, after water evaporation, uranyl nitrate is converted into oxide. Similar reaction as described for metallic nitrates combustion into oxide is considered. In this method, nitrates act as a combustive agent and organic compounds (here citric acid) as reductive agent to give oxide and to release N_2, CO_2 and H_2O.

$$UO_2(NO_3)_2 + 5/9\ C_6H_8O_7 \rightarrow UO_3 + N_2 + 20/9\ H_2O + 10/3\ CO_2 \quad (7)$$

Citric acid under inert conditions decomposes at high temperature into carbon:

$$C_6H_8O_7 \rightarrow 3C + 4H_2O + 3CO \quad (8)$$

Finally, the presence of carbon at high temperature under inert atmosphere leads the reduction of uranium oxide into UO_2:

$$UO_3 + C \rightarrow UO_2 + CO \quad (9)$$

Combination of reactions (7), (8), and (9) give the overall reaction (10):

$$UO_2(NO_3)_2 + 17/9\ C_6H_8O_7 \rightarrow UO_2 + 3C + N_2 + 68/9\ H_2O + 10/3\ CO_2 + 5\ CO \quad (10)$$

Following these reactions, about two citric acid molecules per uranyl in the starting mixture are necessary to obtain the final ratio C/UO_2 of 3 required for the carbothermal reduction. Nevertheless, those reactions are probably in competition with other reactions giving for example the release of NOx, CxHy or different ratio CO/CO_2. The appropriate ratio between uranyl and citric acid in the starting materials to give pure uranium carbide UC will be determined experimentally.

To have an overview of the decomposition steps, a thermogravimetric analysis (TGA) was performed on the starting material. In order to focus on the decomposition phenomenon only, the sample analysed in TGA was first dried at 150°C for 2 hours.

Different types of analysis were made on the calcinated powder. Phase composition and crystallinity were analysed with an X-ray diffractometer. To better analyse the morphology and structure of the powder SEM and TEM were performed.

3.4 Carbothermal Reduction

The UO_2 + C powder was subjected to heat treatments at higher temperature in order to obtain uranium carbide. This chemical reaction is called carbothermal reduction (CTR), and it is ideally given by:

$$UO_2 + 3C \rightarrow UC + 2CO \quad (11)$$

Actually, this reaction seems to progress in two steps (Manara *et al.*, 2012). First, uranium dicarbide is formed as intermediate product, and then it reacts with uranium dioxide producing uranium monocarbide.

$$UO_2 + 4C \rightarrow UC_2 + 2CO \quad (12)$$

$$UO_2 + 3UC_2 \rightarrow 4UC + 2CO \quad (13)$$

The kinetics of these reactions has not been deeply studied, but it is known to be strongly dependent on the partial pressure of carbon monoxide (Suzuki *et al.*, 1981). Therefore, the ability of removing the CO strongly affects the completion of the process and the final compositions. For this reason, the carbothermal reduction is usually performed under high vacuum (Duguay *et al.*, 2015), taking the CO away as soon as it is produced, thus forcing the reaction to proceed.

After the heat treatment, the material was analysed by XRD. The Rietveld refinement of the data was made to estimate the phase proportion. In this way, the degree of completeness of the carbothermal reduction was evaluated. Furthermore, SEM was performed on the powder to characterize its morphology.

Three different processes were performed on the UO_2 + C mixture. At first, a conventional heating in a furnace was carried out. Then, we tried to synthesize and sinter the carbide at the same time in a Spark Plasma Sintering (SPS), through a process called reactive-sintering, which has been already performed in conventional industry for different carbides, like ZrC and HfC (Sun *et al.*, 2013). Finally, these two processes were separately performed in SPS. At first, carbides were produced using a particular set-up developed during this work, which has been designed to carry out the carbothermal reduction. Later this powder was subjected to densification through a standard SPS set-up.

3.4.1 Carbothermal Reduction in a Conventional Furnace

Before heating, the calcinated powder was pressed into pellets with a hydraulic and automatic press. The precompaction was needed to enhance the contact between the precursors (Majumdar *et al.*, 2006). The pressure applied was between 400 and 500 MPa. Each pellet had a mass of ca. 500 mg and a diameter of 5 cm. Approximately 1 wt.% of Zinc Stearate ($C_{36}H_{70}O_4Zn$) was added as lubricant during the pressing.

A maximum temperature of 1600°C was reached, as usually done for the conventional fabrication of uranium carbide. The dwell time was only one hour, much less than in the described conventional routes, where the maximum temperature is hold for several hours (4-12h) (Duguay *et al.*, 2015). The heating and cooling rates were ±200°C/h. Another peculiarity of the treatment was the atmosphere in the chamber. Argon was chosen to fill the furnace, because the latter was not suitable for vacuum. The use of argon instead of vacuum is believed to drastically affect the kinetics of the reaction (Matzke *et al.*, 1986).

During the heat treatment the CO release was monitored, letting a fraction of the outlet flow through the infrared detector. Thus, information about the starting temperature of the carbothermal reduction and the completeness of the process was collected. The latter was also estimated through weight loss measurements and XRD analysis on the final product.

The temperature history and the furnace used for carbothermal reduction are reported in *Figure 17* and *Figure 18*, respectively. The furnace was flushed with argon for two hours before the heating cycle.

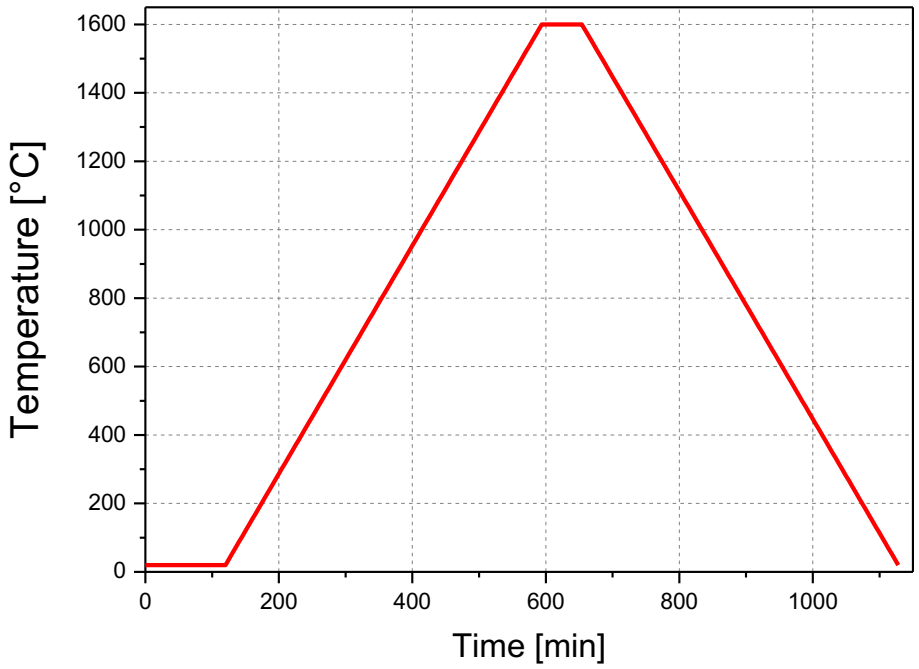

Figure 17: Typical heating cycle for the carbothermal reduction in the conventional furnace.

Figure 18: Conventional furnace.

3.4.2 Reactive-Sintering in SPS

Some tests were made in SPS in an attempt to simultaneously synthesize and densify uranium carbide from the UO_2 + C mixture coming from the mixing of citric acid and uranyl nitrate. This procedure, called reactive-sintering, has been successfully performed in conventional industry for the fabrication of hafnium (Majunmdar *et al.*, 2006), tungsten (Sun *et al.*, 2014), vanadium (He *et al.*, 2010) and silicon carbides (Guo *et al.*, 2012). The adopted set-up (*Figure 20*) was the same one usually used for uranium dioxide sintering (Cologna *et al.*, 2016). Different parameters have been tested, such as the dwell time, the applied pressure, and the atmosphere during the SPS process.

In addition to the measurements of the mass before and after the heat treatment and XRD on the final products, data from the SPS controlling system were used to monitor the evolution of the process. These consisted of the velocity and relative displacement of the piston, which could have given information on CO release and sintering of the sample.

An example of the typical heating ramp and applied pressure performed for this kind of experiment is shown in *Figure 19*.

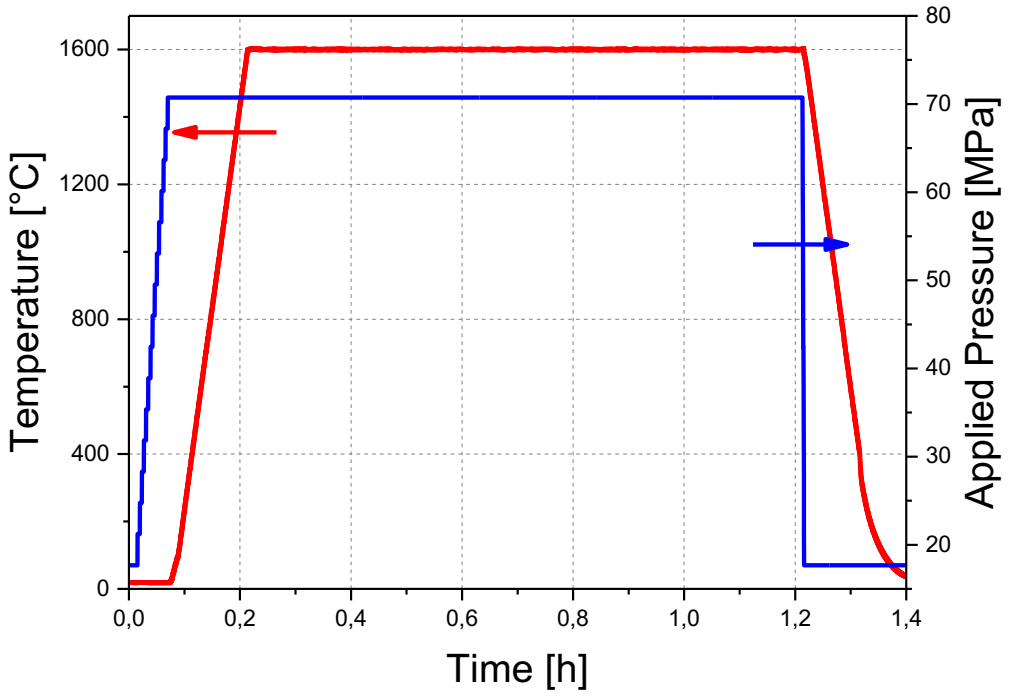

Figure 19: Temperature history and pressure applied on the specimen for the reactive-sintering.

Figure 20: Conventional sintering set-up, used for reactive-sintering tests.

3.4.3 Carbothermal Reduction in SPS

The final part of this work focused on the synthesis of uranium carbide in the SPS through a new set-up (*Figure 21*) and, later, the densification of this powder. Thus, differently from above, these two processes were split into two different steps, as Feng *et al.* made for hafnium carbides (Feng *et al.*, 2015). As explained in Chapter 2, thanks to some modification of the design, the SPS was simply used as a furnace where performing the carbothermal reduction, with the possibility of employing vacuum atmosphere and very high heating rates (>100°C/min).

Thanks to the ease and speed of the procedure, a deep study was done changing the maximum temperature, the dwell time, and the configuration of the SPS. The kinetics of the reaction was then analysed in order to optimize the heating parameters of the process. An example of the heating cycle (10 minutes of dwell at 1200°C) is shown in *Figure 22*.

The amount of uranium carbide synthesized was estimated by XRD of the final material and measurements of the weight losses. SEM was performed on selected samples to see the morphology of the product, studying the effect of the different heating histories on it.

Figure 21: Set-up for carbothermal reduction in SPS.

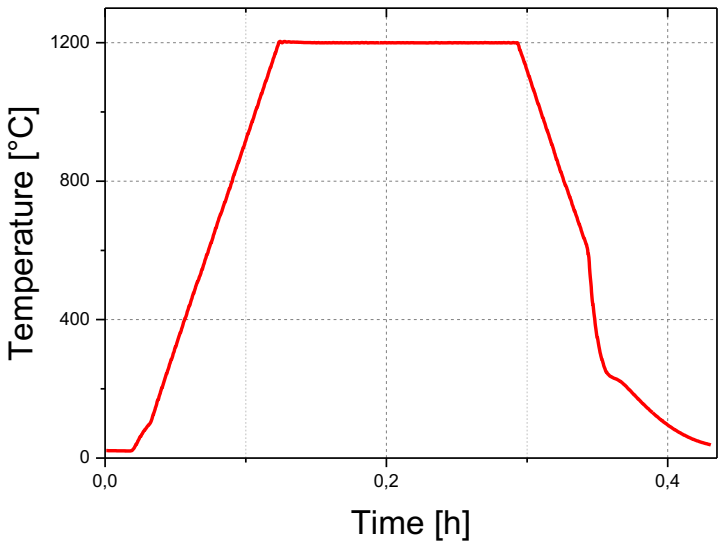

Figure 22: Temperature history in SPS for carbothermal reduction.

3.5 Sintering of Uranium Carbide in SPS

The densification behaviour in SPS of the powder synthesized with the newly developed set-up was studied. The aim of this part was to compare the sinterability of uranium carbide produced at different temperatures and different dwell times. The procedure consisted of crushing the as-synthesized material by manually pestling in a mortar and filling the SPS die with it. Two types of set-up were used: the classical one, which limits the applied pressure to 100 MPa, and the "high-pressure" set-up (Anselmi-Tamburini *et al.*, 2007; Grasso *et al.*, 2010) which allows a maximum pressure of 500 MPa. The sintered pellets were often attached to the graphite punches of the SPS. Then, to avoid any damage on them, the reached density was measured by X-ray tomography on pellets inside the die. After this measure, selected pellets were removed from the die and analysed by SEM. XRD was performed on them before and

after the densification to see any change in the crystallinity and composition due to the heat treatment.

The used recipe consisted of reaching a maximum temperature of 1700 °C, with a heating rate of +200°C/min, a ten minutes dwell, cooling down at -200°C/min till 600°C, and then rapid cooling (power switched off) till room temperature. The entire process was performed under vacuum (<0.05 mbar). Because of the stresses due to the high applied force, for the high-pressure test the maximum temperature was limited at 1600 °C. The two recipes are shown in *Figure 23* and *Figure 24*, where the temperature and the applied pressure are plotted.

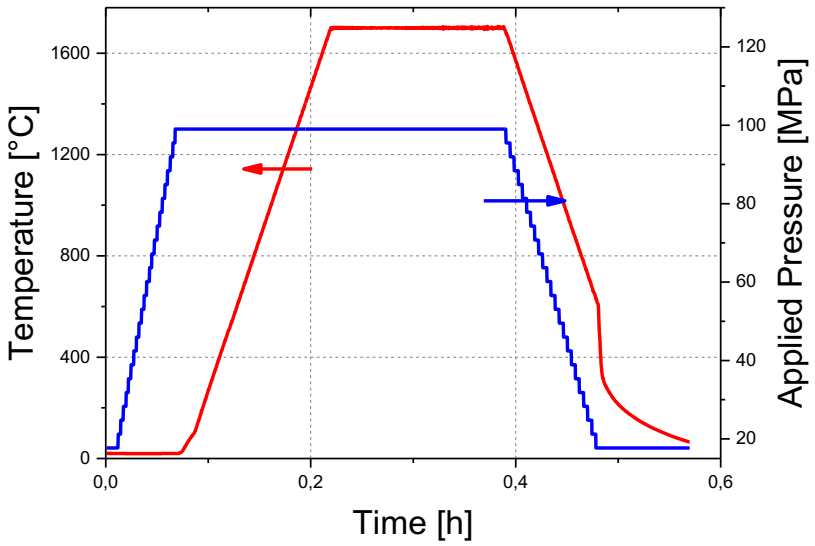

Figure 23: Applied pressure and temperature trends during the sintering with normal set-up.

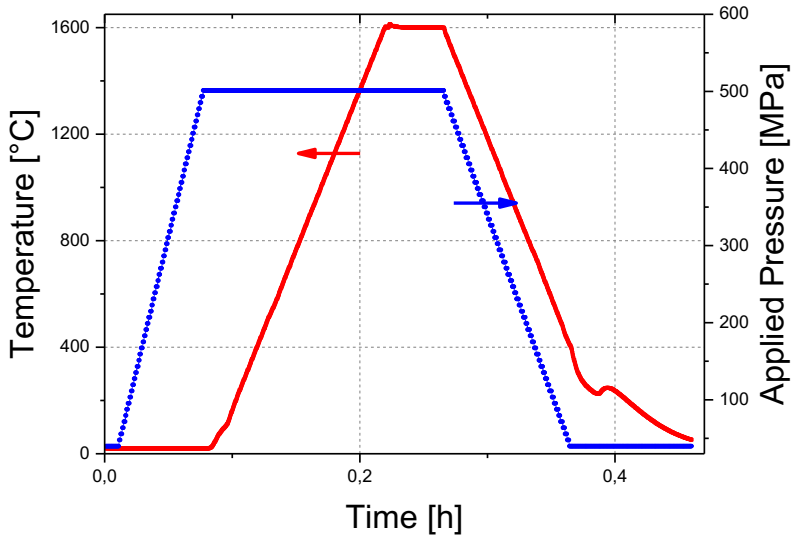

Figure 24: Applied pressure and temperature trends during the high-pressure sintering.

3.6 Concluding Remarks

In the presented experimental work, a new method for uranium carbide fabrication has been developed. All the required steps have been performed and some of them optimized, namely: the sample preparation through a liquid route, the synthesis in both conventional furnace and SPS, and the sintering of pellet in SPS. The interesting reactive-sintering has been tested too.

4 Results and Discussion

Abstract *Preparation of uranium carbide by carbothermal reduction and its sintering to dense pellets by conventional means require high temperature for long periods. We have developed a preparation route yielding fine UC powder in very short time with significantly increased sinterability. At first, a mixture of nanocrystalline UO_2 embedded in amorphous carbon (nano-UO_2/C) was obtained by thermal decomposition of gel obtained from solutions of uranyl nitrate and citric acid. Later, the nano-UO_2/C powder was treated in a conventional furnace or modified spark plasma sintering facility at elevated temperatures (≥1200°C) in order to obtain uranium carbide. The effect of initial composition, temperature, gas/vacuum atmosphere and the overall reaction kinetics were studied. Finally, the sinterability dependence from the temperature production was analysed performing the densification in SPS of the synthesised fine carbide powder.*

4.1 Introduction

Typically, the preparation of U(Pu)C involved UO_2 (PuO_2) powder mixing and blending with graphite followed by CTR under vacuum at temperatures above 1450°C for several hours. This method can be defined as "conventional" carbide preparation route, which adopts oxide/graphite blend as a starting material. Recently, a big step has been made in the preparation of non-nuclear carbides. Organic species are used as a source of fine carbon with high surface area that consequently leads to milder conditions needed for the CTR (Matovic *et al.*, 2013; Chen *et al.*, 2011; Sinha *et al.*, 2002; Onoki *et al.*, 2013).

In the present work, a preparation of uranium carbide derived from solution of uranyl nitrate and citric acid is described. Complexation of uranyl by citrate (Lenhart *et al.*, 2000; Bailey *et al.*, 2005) assures perfect homogenous distribution of the carbon and metal source after decomposition in argon at 1000°C, thus forming nanocomposite UO_2/C mixture. Suzuki *et al.* (1981) performed a kinetics study of the CTR and found that the most limiting factors are oxygen diffusion in UO_2 particles to the reaction interphase or the diffusion of the CO gas out through a compact layer. The developed nanocomposite can overcome both limiting factors thanks to the maximally enlarged interphase area and interconnected porosities after liquid decomposition. The reduction of time and temperatures needed for carbide synthesis may lead to the production of a very sinterable fine powder, thus overcoming another issue concerning uranium carbide fuel: the long time and high temperature needed for sintering.

This chapter is organized as follows. At first, the product of the decomposition of uranyl nitrate and citric acid solution has been characterized to evaluate the occurred phenomena and to confirm the enhanced homogeneity between the carbide precursors. Then, the results of the CTR in conventional furnace were analysed to find the optimal ratio between citric acid and uranyl nitrate. Later, a discussion on the SPS reactive-sintering tests is presented. After this part, the CTR in the developed SPS set-up is examined focusing the attention on the influence of the different citric/uranium ratios, maximum temperature, and holding times.

Eventually, the densification of the powder produced in SPS at different temperatures is discussed, highlighting the onset temperatures of the sintering and the reached final densities.

4.2 Decomposition of Uranyl Citrate Solution

The thermal decomposition of the mixed solutions of uranyl nitrate and citric acid consists of water evaporation, nitrogen and nitrate release as N_2 and NO_x and citric acid decay into carbon and $CO/CO_2/H_2O$. Different types of measurements were performed to estimate what happened during the heat treatments and to characterize the final materials: weight losses, XRD after the process, Thermogravimetric Analysis (TGA), Scanning Electron Microscopy (SEM), and Transmission Electron Microscopy (TEM).

4.2.1 Characterization of the Decomposition Product

After the heat treatments an agglomerated cake was obtained and crushed into fine powder with a mortar. The phase composition and crystallinity of this powder were studied by XRD. Diffractogram of the decomposition product obtained at 1000°C is shown in *Figure 25*.

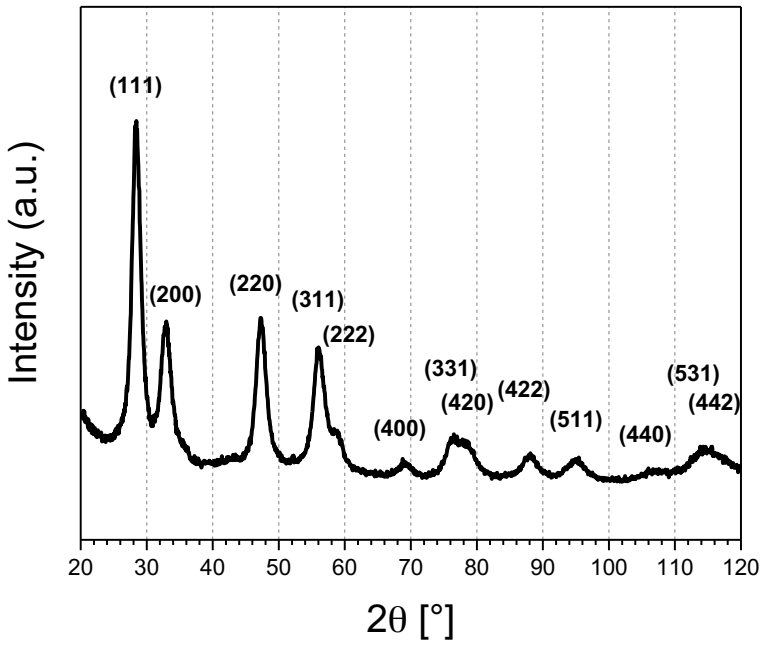

Figure 25: XRD diffractogram of the decomposition product obtained at 1000°C under argon atmosphere. Diffraction lines are marked with Miller indices corresponding to a fluorine structure.

As could be seen in the figure above, only UO_2 diffraction lines are present. Then, it could be deduced that the carbon did not crystallize, but, instead, stayed as amorphous carbon

embedding UO_2 crystals. Considerations should be done on the position and Full Width at Half Maximum (FWHM) of the UO_2 peaks. In fact, the Rietveld refinement gave a lattice parameter of 5.435 Å, which is significantly lower than the actual value for stoichiometric uranium dioxide (5.471 Å (Leinders *et al.*, 2015)). Typically, decreased lattice parameter implies overstoichiometric UO_{2+x}. In particular, using the formula (14) suggested by Teske *et al.* (1983), the O/M ratio estimation is 2.27

$$a = 5.4705 - 0.132x \tag{14}$$

However, the low value of the lattice parameter could be caused also by highly defective structure due to the carbon inclusion in the fluorite lattice of UO_2. The estimated value is probably due to a combination of both effects. Then, it is worth noting the broadness of the peaks in the diffractogram. As explained in Chapter 2, the FWHM could be correlated to the average crystallite size through the Williamson-Hall equation. Calculations gave a value of ca. 10 nm, which is considerably small for the high temperature (1000°C) reached during the calcination. Thus, carbon matrix seems to prevent the grain growth by diffusion during annealing.

The SEM (*Figure 26*) performed on the powder showed big agglomerates with sizes up to 100 µm, where the uranium dioxide and carbon are organized in thin flake shape structures. A high open porosity characterizes these agglomerates, thanks to the release of different gaseous phases during the decomposition of the starting solutions. The hypothesis of a morphology in which nanoparticles of uranium dioxide are embedded in amorphous carbon was confirmed by TEM images, shown in the *Figure 27*. Here, agglomerates of UO_2 with a maximal crystallite size up to 100 nm are surrounded by carbon, which is observable as a thin fuzzy film at the borders of the agglomerates. Then, the developed method provides a highly porous structure which would help the proceeding of the following carbothermal reduction, enhancing the release of CO and an intimate blending of the two precursors without any ball milling step, which, instead, is usually performed for 24/48h in conventional fabrication route (Suzuki *et al.*, 1981).

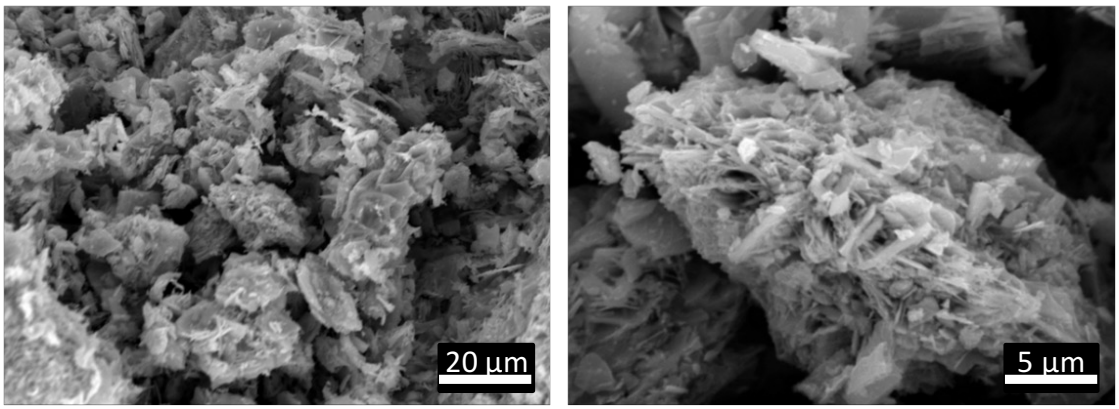

Figure 26: SEM images of the UO_2/C powder obtained at 1000°C under argon atmosphere.

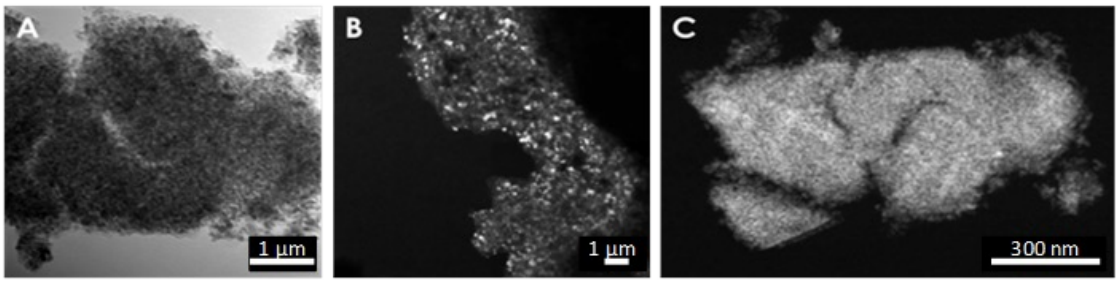

Figure 27: Transmission electron microscopy of the nanocomposite UO_2/C obtained at 1000°C. The crystallites can be seen in the bright (A) and dark field (B) images. The overall morphology and porosity was captured by scanning transmission mode (C).

TGA was performed on the mixed solution to study its pyrolysis. The analyzed sample was characterized by a ratio citric acid/uranyl nitrate equal to 2. As already explained in Chapter 2, the liquid was first dried at 150°C for 2 hours. The weight losses after this initial treatment were 64%, and were mostly due to water evaporation. During the TGA the dried sample was heated up to 1200°C in Argon atmosphere. The weight losses in function of the temperature are shown in *Figure 28*. The trend is characterized by different steps, which correspond to different chemical reactions. The total weight losses are ca. 45% and are completed already at 550°C.

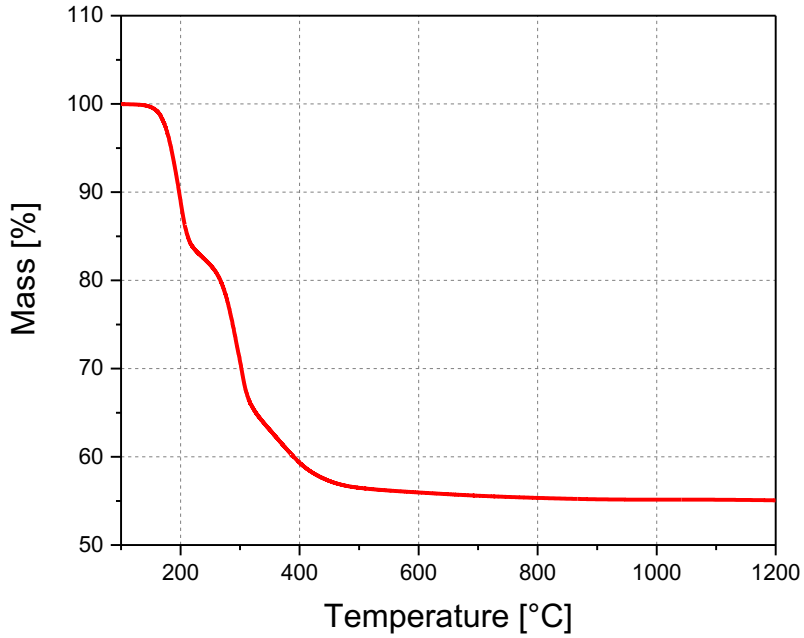

Figure 28: TGA in argon of the sample with 2.00 ratio.

An oxidation study (in air) was performed on the sample already decomposed in argon with a 2.0 ratio. Thanks to this analysis, the carbon content in the powder before the carbothermal

reduction could be estimated. As shown in *Figure 29*, weight gain ~ 4% (A→B) corresponds to oxidation of UO_2 to U_3O_8 (theoretically 3.95%). The weight loss ~ 9% (B→C) corresponds to burning of carbon; the calculated UO_2/C ratio is 1:2.24. Thus, for this specific case (chemical compounds, concentrations, U/C ratios etc.) 1 mol of citric acid after all decomposition, combustion, reduction reactions leaves about 1.12 mol of free carbon available for CTR.

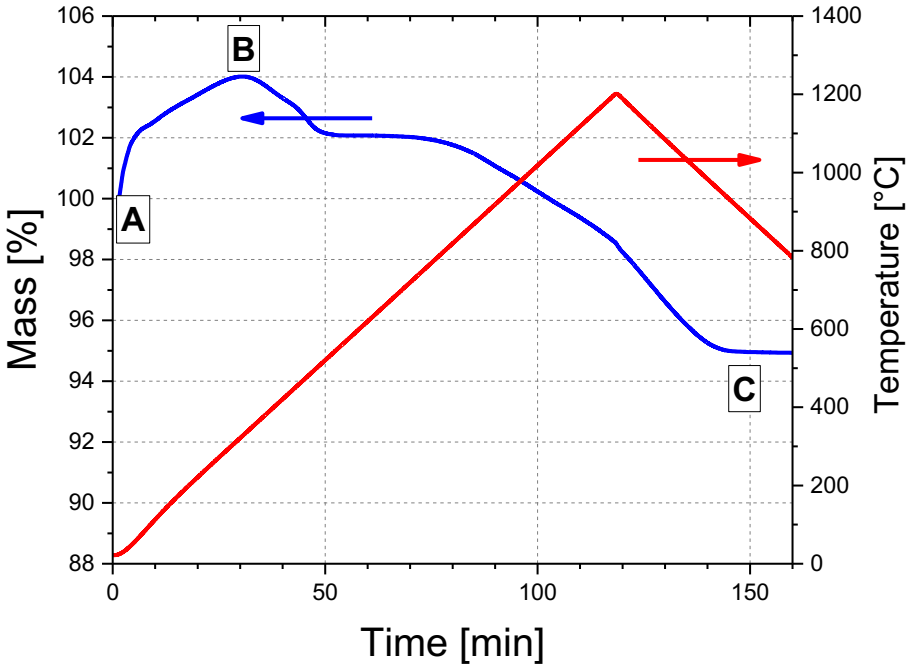

Figure 29: TGA oxidation study under air of the sample with a 2.00 ratio.

Then, since the carbothermal reduction performed on the samples with a ratio 2.00 was always almost complete, it could be supposed that less carbon is needed through this particular method than the conventional one, enhancing the release of CO_2 instead of CO. Then, the production of uranium carbide should be split into two competitive reactions (11), (15):

$$UO_2 + 3C \rightarrow UC + 2CO \quad (11)$$

$$UO_2 + 2C \rightarrow UC + CO_2 \quad (15)$$

The result of the oxidation study was also confirmed by the weight of the product of the calcination process. For a proper comparison, only the mass of the samples with a ratio equal to 2.00 are reported in the *Table 3*. The amount of metallic uranium is the only quantity known in the final powder, if we suppose that no uranium losses occurred during the heat treatment and neglect the instrumental errors during the preparation of the mixed solution. Since the XRD showed that uranium is present only as uranium dioxide and hypothesizing that the

latter is stoichiometric, the mass of oxygen could be estimated. Then, subtracting the mass of uranium and oxygen to the total mass of the calcinated sample, the amount of free carbon could be calculated. Since higher is the mass, lower is the error associated with the measure, the above calculated amount of carbon should be weighted on the mass of uranium contained in the mixture. The averaged UO_2:C is then 2.19, in agreement with the one coming from the oxidation study if all the uncertainties are taken into account.

Table 3: Calculations to estimate the amount of C.

m_U [g]	mol_U	m_{total} [g]	m_O [g]	m_C [g]	mol_C	C : UO_2
2	0.0084	2.436	0.269	0.167	0.0139	1.66
2	0.0084	2.514	0.269	0.245	0.0204	2.43
2	0.0084	2.477	0.269	0.208	0.0173	2.06
10	0.0420	12.5	1.346	1.155	0.0963	2.29

4.3 Optimization of the Ratio Citric Acid/Uranium

An optimization of the ratio between citric acid and uranyl nitrates was needed to find the proportion that would lead to higher amount of uranium carbide after carbothermal reduction. Phase composition was estimated by XRD, analysing few mg of the treated powder. Three different phases could have been found in the diffractograms, namely uranium dioxide, uranium dicarbide and uranium monocarbide. The refinement of the patterns performed with the software JANA2006 provided the relative proportion in weight. The amount of not-reacted oxide in the powder and the potential presence of dicarbide were correlated to a defect or excess of carbon in the starting powder, respectively. Apart from the incompleteness of the reaction, another reason of the oxide phase could be an oxidation of the as-produced carbide, which is known to be very sensitive to oxygen and moisture in the atmosphere, even at room temperature (Berthinier *et al.*, 2011).

As explained in chapter 2, following the sequence of chemical reactions that theoretically could occur, about 1.9 mol of citric acid are needed for one mole of uranyl nitrate. However, there could be some not-considered competitive reactions which could lead to a different needed molar ratio between the two precursors. Thus, in a preliminary optimization study, five solutions were prepared with ratios between 1.1 and 2.3. The pyrolised powders were heated in a conventional furnace in argon up to 1600 °C, for one hour. The samples were not precompacted before the carbothermal reduction. The lack of pelletization before the heat treatment is supposed to affect only the completeness of the reaction and not the effect due to the relative amount of carbon (Duguay *et al.*, 2015).

The results are presented in *Figure 30*, where the composition in wt.% for the five initial samples after the reaction is shown. The highest amount of uranium monocarbide was found in the sample with a molar ratio 2.0 (85% UC, 6% UC_2, 9% UO_2). This is showing that the

chemical reactions occurring during the uranyl nitrate/citric acid thermal decomposition are not far from the foreseen theoretical ones. In the lowest ratios (1.1 and 1.4) carbide was present only as UC_2. This dicarbide phase is supposed to come from the first reaction of the carbothermal reduction (12), when uranium dioxide reacts with the surrounding carbon. The absence of UC phase is attributed to the lack of carbon. The carbon may be not enough to go through the second reaction (13) giving uranium monocarbide, since only small spot of uranium dicarbide are formed inside a matrix of oxide. Moving to higher ratios UC phase appears, while UO_2 is consumed. Unlike the UC_2 in the ratio 1.4, the UC_2 in the 2.3 ratio is most likely due to an excess of carbon leading to the reaction showed below, which would gradually reduce the UC amount.

$$UC + C \rightarrow UC_2 \qquad (16)$$

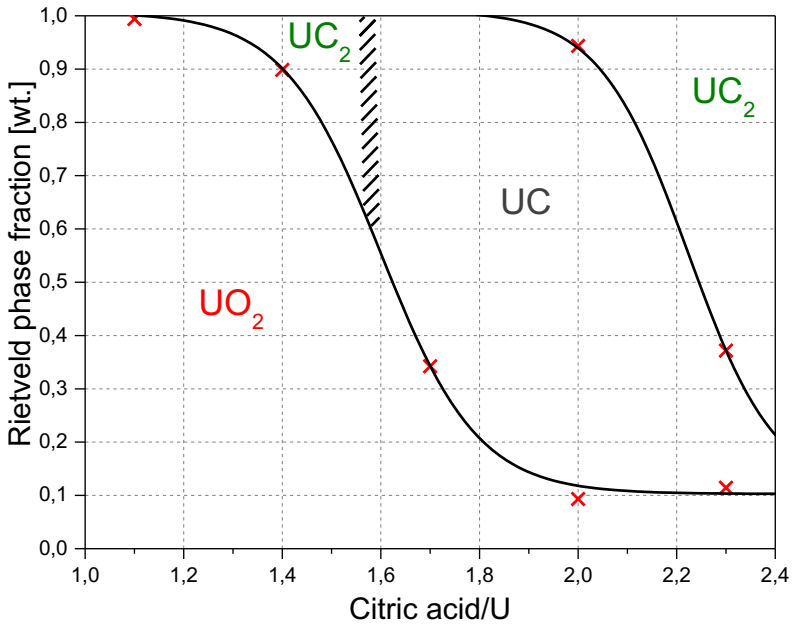

Figure 30: Phase proportion from the Rietveld refinement on the XRD pattern of the carboreduced powder with different citric acid/U ratio.

A deeper investigation of the optimal ratio was then performed around the value 2.0. Other five samples were thus analysed, studying the ratios 1.90, 1.95, 2.00, 2.05, and 2.10. The results are shown in *Figure 31*. In this case, the calcinated powders were pressed up to 400-500 MPa before the heat-treatment. The highest amount of uranium carbide was found in the 2.00 sample, whose composition showed almost 96% of the target phase. An increasing percentage of UC was expected with an increase in the ratio till the optimal value was reached, and after that a decrease in UC should have been compensated by an increase of UC_2 phase, because of the reaction (16). As shown in the figure, the bigger ratios gave a lower amount of UC but no UC_2 was found. Thus suggesting that an oxidation occurred in those samples during the

storage until the XRD analysis was carried out. Another consideration could be pointed out comparing the compositions after CTR for the sample 2.0 with and without precompaction. In agreement with Duguay *et al.* (2012), prepressing the starting powder resulted in improving the effectiveness of the reaction. This is attributed to a better contact between the two precursors, namely UO_2 and C, thus enhancing their reactivity.

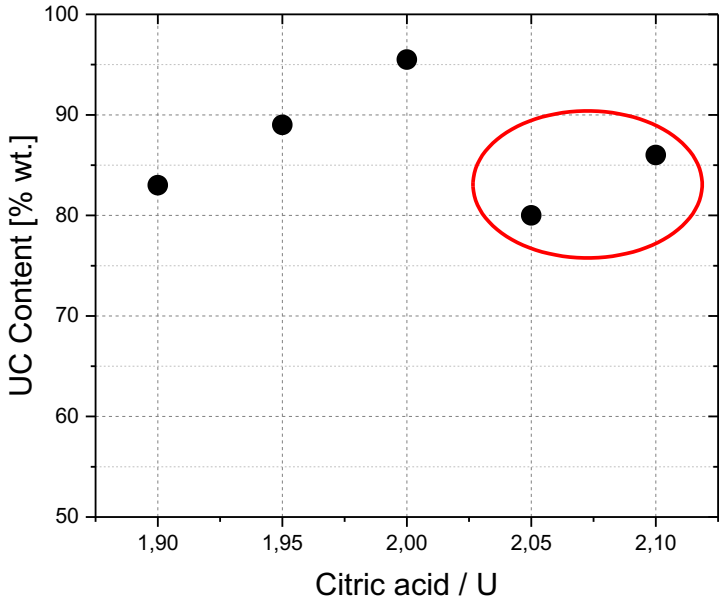

Figure 31: Amount of uranium carbide obtained by XRD after a finer investigation on the citric acid/U ratio. In the red circle the ratios suspected of oxidation.

4.4 Observations during Carbothermal Reduction

The carbothermal reduction was conducted in a conventional metallic furnace, in argon atmosphere, heating up to 1600°C and holding this temperature for one hour. Despite the very short dwell time almost 100% of uranium carbide was produced. The low amount of oxide phase found in the final product from the 2.00 ratio could be ascribed to different reasons. The most important is the oxidation of the specimen during the storage between the production and XRD analysis. In facts, the concentration of oxygen impurities in the nitrogen atmosphere filling the glove box sometimes could reach 0.5-2%. These values are highly above the specification for uranium carbide fabrication (less than 25 ppm (Sengupta *et al.*, 2012)). Then, even if these high concentrations are held for short periods, oxidation could take place, in particular if the sample is in powder form. In this case, the high-surface area avoids the formation of a passivating oxide layer, which could slow down the reaction (Duguay *et al.*, 2012).

The XRD diffractogram of the sample after the heat treatment is presented in *Figure 32*. The peaks are attributable to the face-centred cubic structure (F*m*3-*m*) of uranium monocarbide.

The presence of UO_2 is suggested by the peaks of its fluorine structure, whose most intense peak is located around 2θ ≈ 28°. The UC lattice parameter calculated by Rietveld refinement was 4.9594 ± 0.0005 Å, which is in good agreement with the value stated in literature for stoichiometric $UC_{1.00}$ (4.9600 Å (Williams *et al.*, 1960)).
The measured weight losses were 19%. Slightly higher than the theoretical ones (18.5%). Part of this excess was due to the thermal decomposition of zinc stearate, which was 1% of the total mass. Furthermore, another reason could be the unavoidable losses of powder during the extraction of the pellet from the furnace.

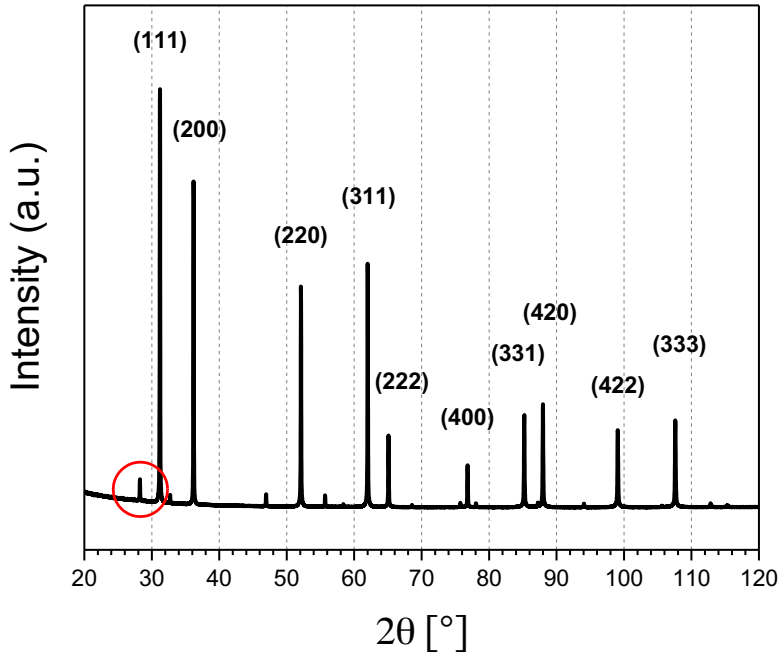

Figure 32: XRD diffractogram of the 2.0 sample heat treated in conventional furnace up to 1600°C, dwell time 1h, in argon atmosphere. The peaks of UC phase are indicated and UO_2 most intensive line is marked with red circle.

During the heat treatment the CO release was monitored splitting part of the argon flow at the outlet of the furnace into an infrared detector. The CO trend in function of time and temperature is shown in *Figure 33*. It is noteworthy that the delay of the CO detection due to gas movement through the pipeline from furnace to the detector was omitted. However, this delay is negligible compared to the thermal inertia of the furnace. Different information about the kinetics of the reaction is obtainable analysing the plot. The starting temperature and the completeness of the carbothermal reduction could be estimated. Regarding the onset of the reaction, no differences were foreseen if compared with the conventional route, since this parameter is not influenced by the morphology of the treated powder. In the proposed experiment, the temperature at which the CO starts to be release is located around 1200°C, in agreement with the literature (Sengupta *et al.*, 2012). Actually, a first release of CO is detected between 400°C and 600°C because of the decomposition of zinc stearate, used as lubricant

during the precompaction. Looking at the overall evolution, the high degree of completeness deduced by XRD analysis is confirmed, since no significant change in the slope is detected when the cooling starts. A picture of the synthesized carbide is shown in *Figure 34*. The material is grey with a metallic shine. The darkness of the colour suggests the formation of a thin oxide layer on the surface. The material kept the pellet shape during CTR, but big cracks were formed, which were possibly formed due to the stresses arising from volumetric transformations (shrinkage) during the reaction and from release of CO, coming from both the thermal decomposition of the lubricant and the production of carbide.

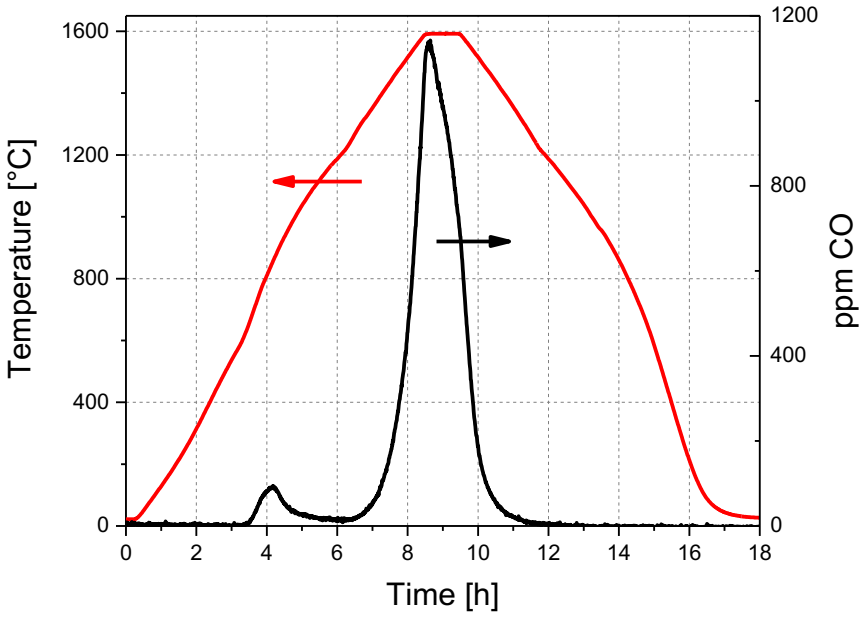

Figure 33: Recorded CO release during carbothermal reduction in conventional furnace.

Figure 34: Picture of the sample after carbothermal reduction in conventional furnace.

4.5 Reactive-Sintering in SPS

Different tests were performed with the purpose of synthesize and sinter uranium carbide at the same time in a spark plasma sintering (SPS) device. This kind of experiment has been successfully carried out in conventional ceramic industry producing hafnium (Majunmdar *et al.*, 2006), zirconium (Sun *et al.*, 2013), or tungsten (Sun *et al.*, 2014) carbides in very short times.

The influence of dwell time, pressure applied on the specimen, and atmosphere filling the SPS chamber were studied in an attempt to find the optimal conditions allowing the fabrication of dense uranium carbide pellets.

The applied conditions are shown in *Table 4*, where the maximum temperature, the heating rates, the holding times, the pressure and the used gas are presented. The use of vacuum instead of argon should have enhanced the reactivity of the nanocomposite UO_2/C powder, as Sun *et al.* (2013) demonstrated in their work. The reduction of the pressure applied on the pellet by the graphite punches was performed for the same reason (Sun *et al.*, 2014). The main supposed effect induced by these changes would be the facilitation of the release of CO produced during the synthesis of carbide. In fact, the partial pressure of CO is one of the most important thermodynamical factors governing the kinetics of the carbothermal reduction (Suzuki *et al.*, 1981).

Table 4: Specifications of the performed reactive-sintering tests.

# Sample	Tmax [°C]	Dwell [min]	T rate [°C/min]	Pressure [MPa]	Atmosphere
RST1	1600	10	±200	70	Ar
RST2	1600	20	±200	70	Ar
RST3	1600	60	±200	70	Ar
RST4	1600	60	±200	70	Vacuum
RST5	1600	120	±200	17	Vacuum

In *Figure 35*, the SPS piston displacement velocity is displayed together with the temperature history during the test performed in argon with a dwell time of one hour (sample RST3). Usually, the displacement of the piston could be correlated to different physical phenomena, like a densification/sintering or a solid state chemical reaction occurring in the sample. In particular, in the considered test, apart from the first peak, which is due to the initial pressing from 17 MPa up to 70 MPa, two main peaks are present. The first one (a) is located between 200°C and 400°C, and it is most probably due to a desorption of water, caught by the powder during the storage. The second and last peak (b) is characterized by a smaller intensity, it starts at 600°C and last till the maximum temperature is reached. This peak was not fully explained, but, considering the starting temperature (which is lower than the usual onset of carbothermal

reduction) it is supposed to be caused by an overall sintering of the material. However, taking into account the measured density after the heat treatment (shown in *Table 5*), the degree of densification was very limited. Furthermore, no traces of uranium carbide were found in the XRD pattern shown in *Figure 36*. Only uranium dioxide's peaks are present. These peaks display a high FWHM, thus suggesting a small crystallite size. Adopting the Williamson-Hall formula, this was estimated to be 20 nm. Then, if we compare it to the value calculated on the starting nano-crystallized UO_2/C (10 nm), no significant increase in the uranium dioxide crystallite-size happened, despite of the very high temperature (1600°C).

The absence of any carbide formation, the low density and the low crystals growth could be justified by difficulties in CO release. Indeed, if the CO is not efficiently released, small produced quantities are enough to let its partial pressure reach significant value, thus stopping the proceeding of the reaction. Then, if UO_2 and C do not react and if these two precursors are blended at a nanometric scale, the diffusion of uranium dioxide embedded in the amorphous carbon would be prevented, thus avoiding any crystal growth too. However, the produced CO should not come from the carbothermal reduction, since the XRD analysis exhibit only UO_2 phase. Instead, a reduction of overstoichiometric UO_2 is more credible following the chemical reaction (17). Here the reducing agent could be the carbon in the starting powder or the carbon coming from the graphite punches and die. This hypothesis is also supported comparing the estimation of the lattice parameters coming from the Rietveld analysis before and after the heat treatment in the SPS. As mentioned above, the calcinated powder was characterized by a lattice parameter: a = 5.435 Å; while the one after the reactive-sintering test was: a = 5.448 Å. In fact, this increase in the lattice parameter could be due to a reduction in the overstoichiometry and/or in the disorder of the UO_2 lattice caused by carbon inclusions. Both phenomena lead to a formation of small quantities of CO that, blocked in the vicinity of the powder, may have drastically slowed down the carbide production.

$$UO_{2+x} + yC \rightarrow UO_{2+x-y} + yCO \qquad (17)$$

Another proof that the problem affecting these tests was the limited CO release comes from the analysis of the experiments performed in vacuum. In fact, under this condition the gas is supposed to be more easily released from the vicinity of the pellet when it is produced. The piston speed in function of time and temperature of sample RST4 is shown in *Figure 37*. The two initial peaks are similar to the ones present in the previous experiment, thus showing that the same physical phenomena took place. However, something different happened when the maximum temperature was reached. During the dwell, the piston speed did not stay around zero, but exhibited a group of low intensity peaks until the cooling started. These periodic peaks have been explained as an intermittent release of carbon monoxide. In particular, the CO is believed to accumulate between the pellet and the top of the punches until it reaches a pressure high enough to allow its release through the plays of the graphite die. This event should occur in the argon experiment too: the vacuum only facilitates and enhances this process, allowing it to be visible in the time scale considered.

The XRD pattern of this powder is presented in *Figure 38* (zoom in *Figure 39*). Apart from the fluorine structure of UO_2, peaks of the tetragonal (CaC_2 type) structure of uranium dicarbide have been recognised. The phase composition analysis performed through the software Jana2006 estimated almost 1 wt.% of UC_2. This carbide formation demonstrates an improvement in the process, even if the produced quantity was very small. Concerning the lattice parameter of the oxide phase, this was found to be a = 5.4617 ± 0.0005 Å. Then, a further increase was noted if compared with the argon experiments, thus suggesting a further reduction of the UO_{2+x} phase and decrease of the supposed carbon inclusions in its lattice. The achieved final density was slightly higher too, but anyway not adequate (as shown in *Table 5*). The fact that UC_2 and not UC was formed, its low percentage, together with the low density suggest that the kinetics of the reaction was very slow to consider this kind of experiment successful. No significant improvements were found in the tests performed applying a lower pressure on the pellet or increasing the dwell times.

Table 5: Reached density after the reactive-sintering tests.

# Sample	Reached Density [g/cm^3]
RST1	4.36
RST2	4.27
RST3	4.65
RST4	5.61
RST5	3.13

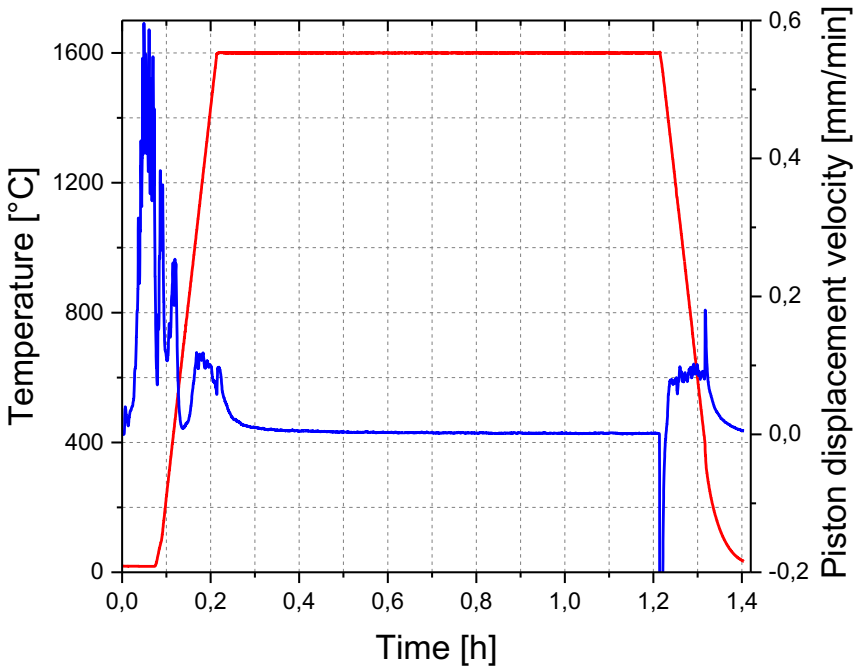

Figure 35: Temperature history and piston displacement velocity (not corrected by the thermal expansion and contraction of the system) of the test performed in argon with 1hour dwell time at 1600°C (RST3).

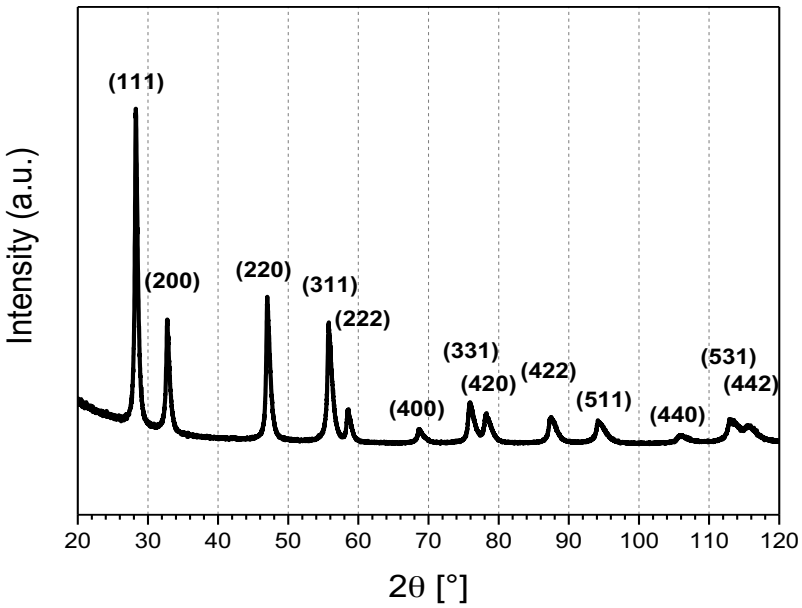

Figure 36: XRD pattern of the powder after the reactive-sintering test in argon and with a dwell time of one hour at 1600°C. The diffraction peaks of UO_2 are shown.

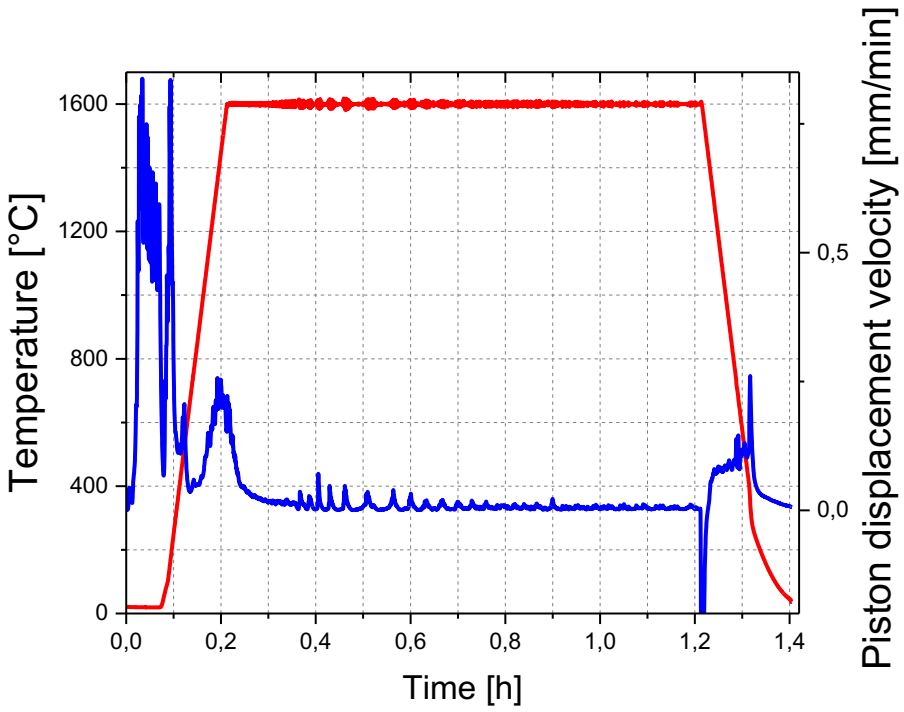

Figure 37: Temperature history and piston displacement velocity (not corrected by the thermal expansion and contraction of the system) of the reactive-sintering test performed in vacuum with a dwell time of one hour.

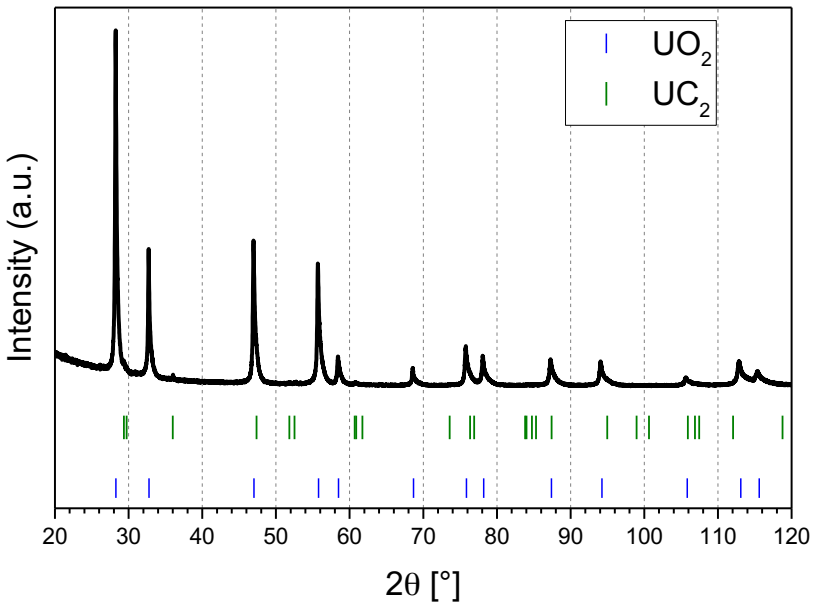

Figure 38: XRD pattern of the powder after the reactive-sintering test performed in vacuum with a dwell time of one hour at 1600°C. The diffraction lines of UO_2 and UC_2 are shown.

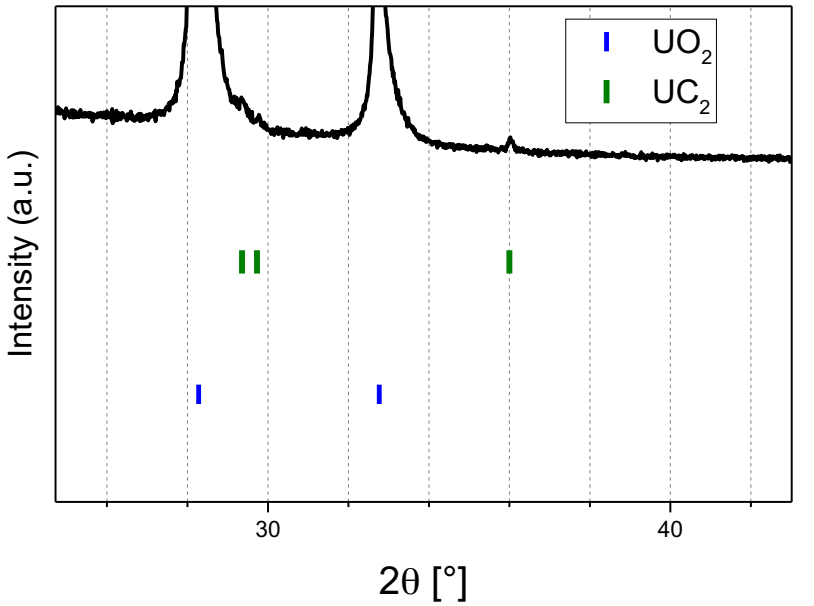

Figure 39: Zoom of the XRD pattern of the powder from the reactive-sintering test performed in vacuum with a dwell time of one hour at 1600°C. The diffraction lines of UO_2 and UC_2 are shown.

4.6 Carbothermal Reduction in Modified SPS

The reactive-sintering experiments pointed out that the most detrimental factor influencing the proceeding of the carbothermal reduction in SPS was the release of CO/CO_2, coming from the reduction of UO_{2+x} and the carbide synthesis. Thus, efforts were made to develop a particular SPS set-up optimized for this kind of reaction, which is described in Chapter 2. The use of a perforated punch and a graphite spacer inside the die are the main characteristics of the modified apparatus. The first is useful to ensure the removal of the gas as soon as it is produced. The other one is introduced to avoid any contact between the punches and the treated powder, thus similarly helping the CO release. Since no pressure is applied on the precompacted specimen, the SPS is simply used as a furnace where carrying out the carbothermal reduction. Contrary to conventional furnaces, like the one described before, fast heating and cooling rates are achievable (> 100°C/min), thus allowing very short durations of the experiments. The big advantage of pursuing the carbide synthesis with this device would be the prevention of grain growth and necking during the heat treatment. Therefore, an increased sinterability of the resulting powder is expected.

4.6.1 Effect of the Initial Ratio Citric Acid/Uranyl Nitrate

The carbothermal reduction in SPS was characterized by different operating conditions which could have a great impact on the proceeding of the reaction and, then, on the achievable results. Namely, the use of vacuum instead of argon and the reducing environment given by the graphite pieces surrounding the powder. For these reasons, the optimal ratio between the two starting solutions could be slightly different from the one estimated for the conventional furnace.

The effect of the initial ratio citric acid/uranyl nitrate was studied, with a small range of composition based on the results obtained for CTR in conventional furnace. It was observed that ratios ≥ 1.9 gave satisfactory UC purity. The highest amount of UC (≈99.7%), measured by XRD, was given by the sample with ratio 2.2 at 1600°C, with a dwell time of 20 minutes. The results are shown in *Figure 40* and *Figure 41*. The tendency to give higher yield of UC with higher carbon content is more visible for samples obtained at 1600°C for 5 minutes. For longer time (20 minutes) the UC yield is generally higher, over 97 wt.%, but results are scattered with no observable tendency. If compared with the experiments conducted in conventional furnace, traces of UC_2 were rarely observed. The only exception was the carbothermal reduction of the ratio 2.3 in 5 minutes. An explanation could be that under SPS condition, the rate of the equation giving UC from UO_2 and UC_2 interaction is much higher than the one through with UC_2 is formed. Then, the concentration of UC_2 is constantly very small or negligible.

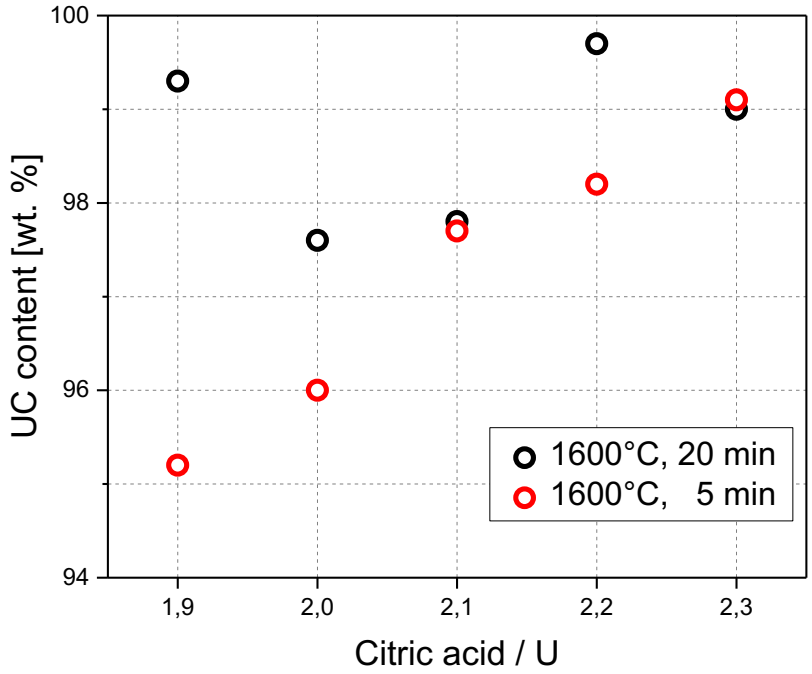

Figure 40: UC yield from Rietveld refinement of XRD data after carbothermal reduction in SPS, influence of the ratio citric acid/ U.

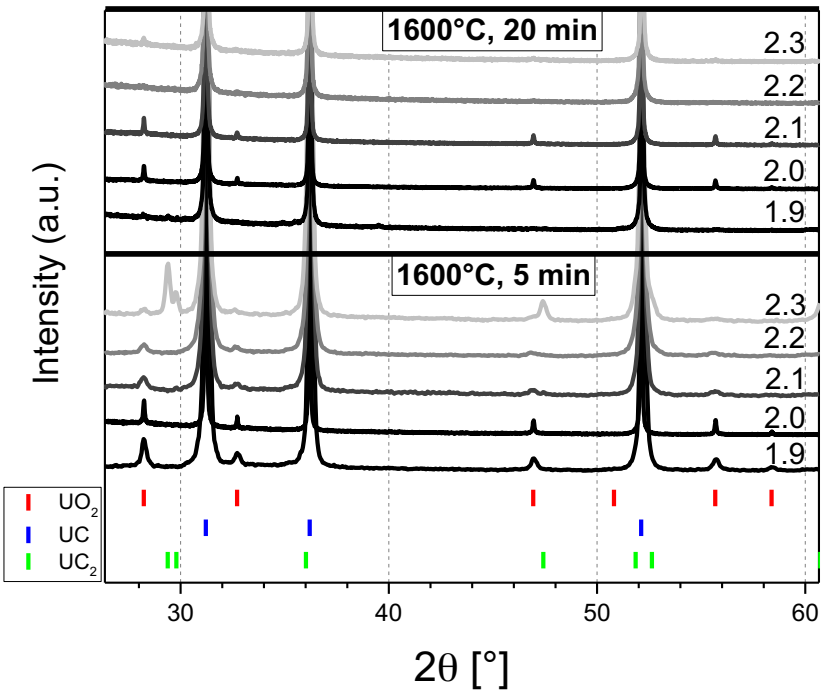

Figure 41: XRD pattern of the powder with different ratio carboreduced in SPS with 5 (top) or 20 minutes (bottom) of dwell time. The diffraction lines of UO_2, UC, and UC_2 are shown.

4.6.2 Kinetics Study

The high heating rates implemented and the efficiency of the developed method permitted to successfully perform the carbothermal reduction in less than one hour (including the whole heating and cooling ramp). Therefore, a deep study of the kinetics of the reaction was possible, evaluating the effect of the maximum temperature and dwell time. In particular, the tested temperatures were 1000°C, 1200°C, 1400°C, and 1600°C, while the holding times were 0, 1, 5, 10, 20, and 30 minutes.

As shown in *Figure 42* and *Figure 43*, for the experiments at 1600°C, the production of carbide was almost completed with no dwell time. Thus showing that the carbothermal reduction advanced significantly already during the heating and cooling ramps (±200°C/min). Only decreasing the temperature, a progression is visible for the shortest durations. However, at 1200°C and 1400°C the reaction yield was over 90% within 5 minutes. Regarding the 1000°C test, no carbide was formed, as can be deduced by the XRD diffractograms in *Figure 44*. Then, the starting temperature in the SPS conditions is located between 1000°C and 1200°C.

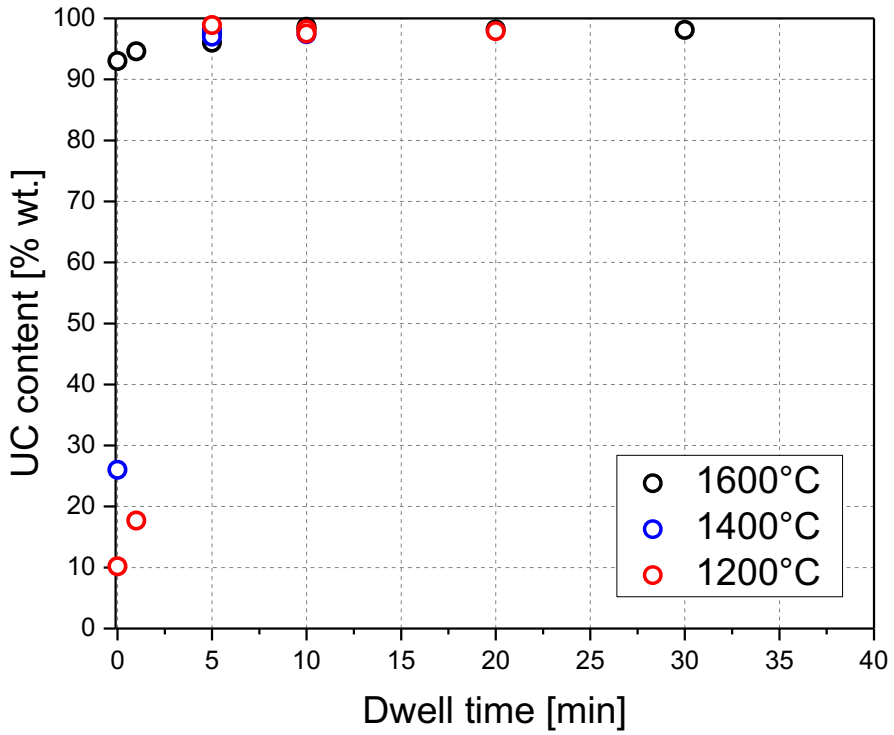

Figure 42: UC yield from Rietveld refinement of XRD data of the kinetics study on carbothermal reduction in SPS.

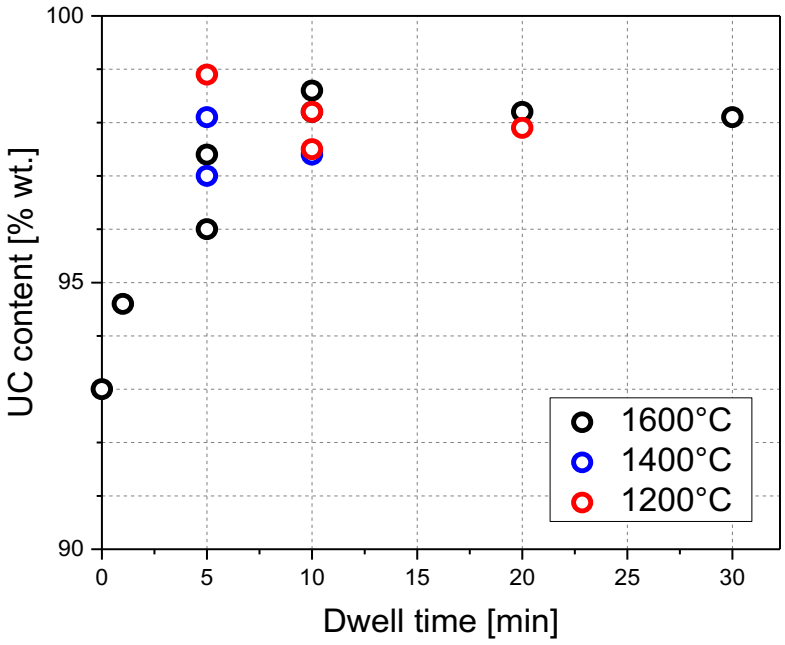

Figure 43: Zoom of UC yield from Rietveld refinement of XRD data of the kinetics study on carbothermal reduction in SPS.

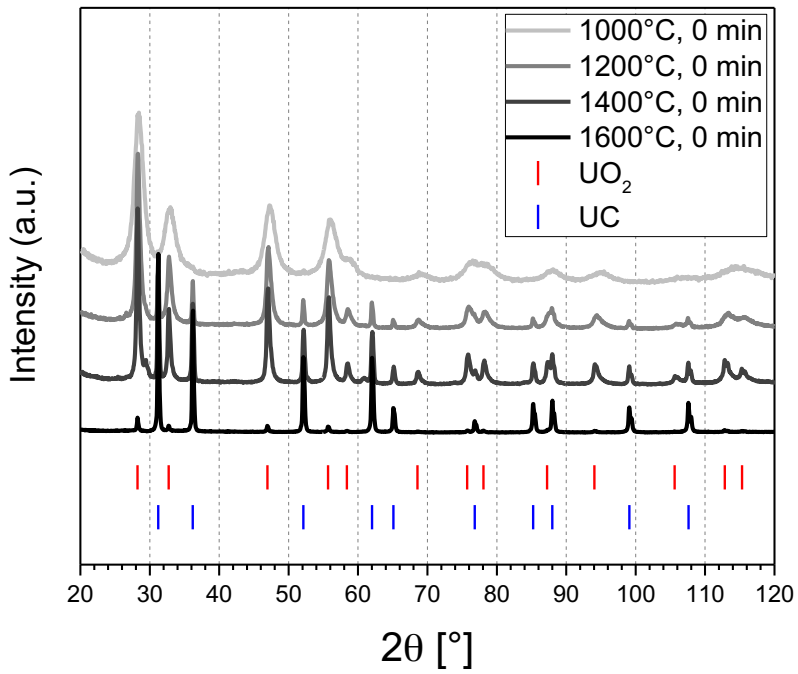

Figure 44: XRD pattern of the powder after the SPS heat treatment with 0 minutes of dwell time at different temperatures. The UO_2 and UC diffraction lines are shown.

4.6.3 Characterization of the Obtained Carbide Powder

The morphology of the carbide produced by SPS was analysed by scanning electron microscopy. In particular, the powders synthesised at 1200°C, 1400°C, and 1600°C with a 10 minutes dwell time are compared in *Figure 45*.

The overall morphology is characterized by porous agglomerates with size of $10^1 \div 10^2$ μm, independently from the temperature. The porous shape is most probably caused by the formation and removal of gas during the carbothermal reduction. The individual grain sizes are up to 1 μm for the powder obtained at 1200°C, and above 1 μm for higher temperatures. The most important difference between the three considered powders is the degree of necking, which becomes more accentuated increasing the temperature of production. Thus, the average grain size tends to be higher. For this reason, the sinterability of the carbide produced at 1200°C is supposed to be higher than the one at 1400°C and 1600°C, if no milling would be performed.

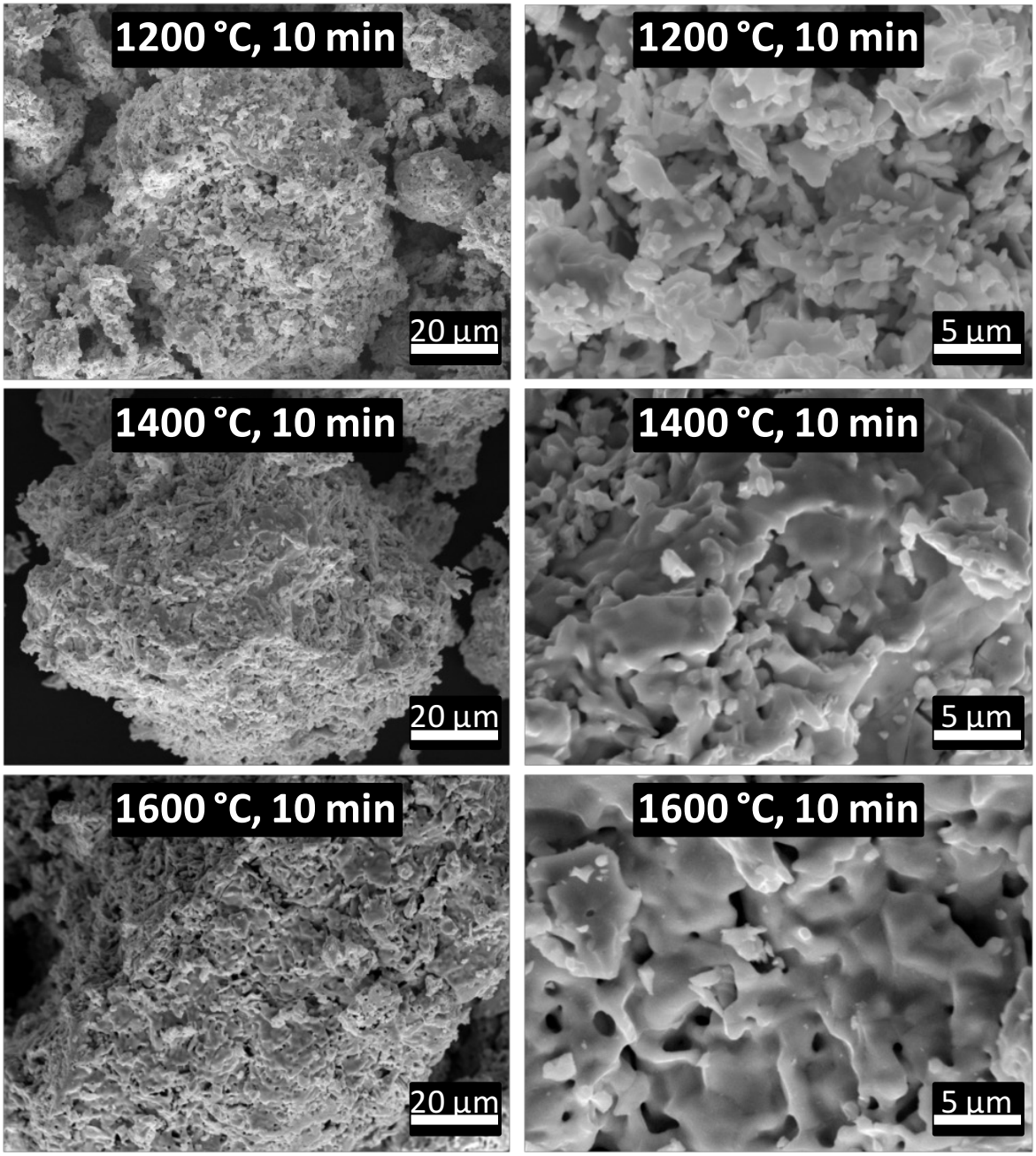

Figure 45: SEM images of the powder produced in SPS. From left to right: increase in the magnification. From top to bottom: increase in the temperature of production.

In *Figure 46*, the lattice parameter of uranium carbide phase obtained by the refinement of the XRD pattern is shown. In detail, the lattice parameter is analysed in function of the different temperatures and different holding times. First of all, it is important noting that deviations from the value for stoichiometric UC (a = 4.9600 ± 0.0005 Å (Williams *et al.*, 1960)) could be caused by different factors. As already stated in Chapter 1, the most influential are: a deficiency of carbon leading to hypostoichiometric UC, strains in the lattice which depend on the particular heating treatments underwent by the specimen (Williams *et al.*, 1960), and

oxygen impurities coming from oxidation or uncompleted carbothermal reduction (Manara *et al.*, 2012).

The majority of the lattice parameters are acceptably in agreement with the value found in literature (Williams *et al.*, 1960). However, for the sample produced at 1200°C for short dwell time (≤ 5 minutes) a systematic shift is visible. The reason for this deviation could be the presence of oxygen dissolved in the lattice of UC, thus giving more properly a $UC_{1-x}O_x$ phase (Magnier *et al.*, 1966), which is not easily recognisable with XRD. In this case, the dissolution of oxygen is likely due to an incompleteness of the reaction, since its intensity goes down as the holding times increases. On the contrary, an oxidation should have affected all the samples unconditionally from their thermal history. Another deviation is found for the sample treated at 1600°C for 30 minutes. A lower lattice parameter is a symptom of a hypostoichiometry (Manara *et al.*, 2012), or a very high oxygen inclusion in the lattice (as shown in *Figure 60*). Here, both of the alternatives are plausible: a random carbon deficiency in the UO_2/C starting mixture or a strong oxidation of the sample occurred during the preparation for the XRD experiment (rather than a partial carbothermal reduction, since this experiment was performed at the highest temperature with the longest dwell time).

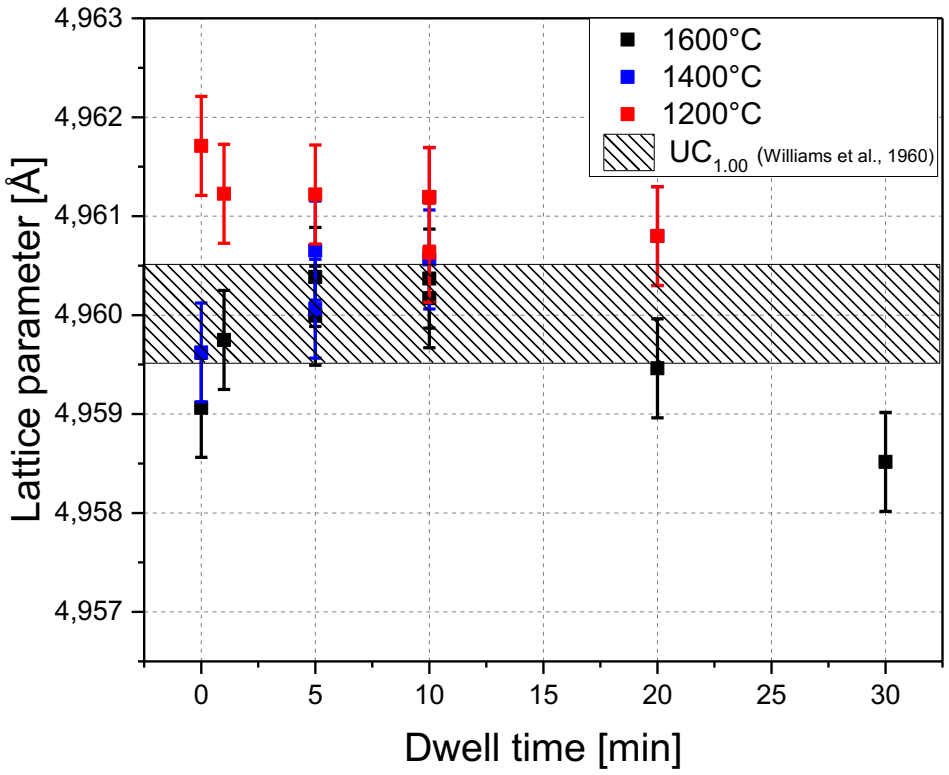

Figure 46: UC lattice parameter in function of the temperature of production and the dwell time.

4.6.4 Discussion on the Kinetics of the Carbothermal Reduction in SPS

The carbothermal reduction in SPS of the nanocrystalline UO_2/C powder was performed in unprecedented short times. The best result (UC 99.7 wt.%) was obtained in less than 40 minutes, including the heating and cooling periods. High amount of carbide (>98 wt.%) were produced even in less than 20 minutes. These durations should be compared with the times usually spent by conventional carbothermal reduction to produce uranium carbide. As already stated in the Chapter 1, the typical dwell times are 4-15 hours. Considering also the time needed to heat till the maximum temperature is reached and then cool down to room temperature, a total duration of 20-35 hours is expected. Thus, the developed method of synthesis allows a reduction in time of more than 95%.

This enormous saving is attributed to different reasons. First of all, the SPS permit to reach the high temperatures needed to start the carbothermal reduction in few minutes. Then, the designed set-up turned out to be very efficient in the removal of the produced CO/CO_2, thus thermodynamically helping the proceeding of the reaction. Finally, the high reactivity of the starting powder should be considered. The importance of the last factor is confirmed by the experiments in the conventional furnace mentioned above. In fact, high percentage (>95 wt.%) of uranium carbide were found after only one hour at 1600 °C in argon atmosphere, which is still considerably shorter than the usually performed 4-15 hours under vacuum. In the following two subparagraphs the effect of the used set-up and the initial powder on the achievable results will be further analysed.

4.6.4.1 Influence of the Set-up

The used set-up has been fully described in Chapter 2. However, another set-up was realized and tested. The main difference was the use of a 12 mm upper punch, with a restriction in the final part to 10 mm. Thus, no spacer was used, since the graphite piston leant directly on the die. This modification allowed doubling the diameter of the chamber where to place the powder, leading to an increase of the capacity of the set-up. Another peculiarity of the modified set-up was the diameter of the punch holes, which was reduced from 5 mm to 4 mm, in an attempt to strengthen the mechanical resistance of the graphite piece. In *Figure 47*, the two different set-ups are displayed.

Figure 48 and *Figure 49* clearly show that the experiments performed with the bigger set-up gave generally less amount of uranium carbide. This difference is negligible at higher temperatures (1600°C), while it is significant in the tests at 1200°C. The lower efficiency (at low temperatures) of the second set-up could be attributed to a combination of two factors. An increase of the treated mass (250mg → 500mg), thus leading to an increase of the CO/CO_2 produced, and a reduced gas removal effectiveness, caused by the lower diameter of the holes.

These comparisons lead us to underline the importance of designing a good set-up, appropriate to the particular device (SPS devoted to hazardous material), reaction (carbothermal reduction), and conditions (treated mass).

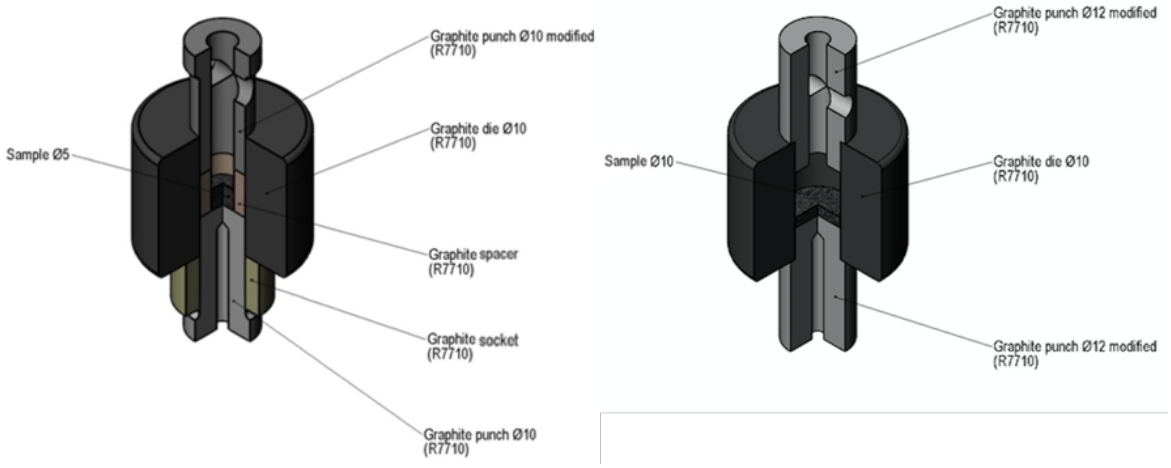

Figure 47: Comparison between the two different set-ups for CTR in SPS. On the right, the set-up modified to achieve a higher treatable mass.

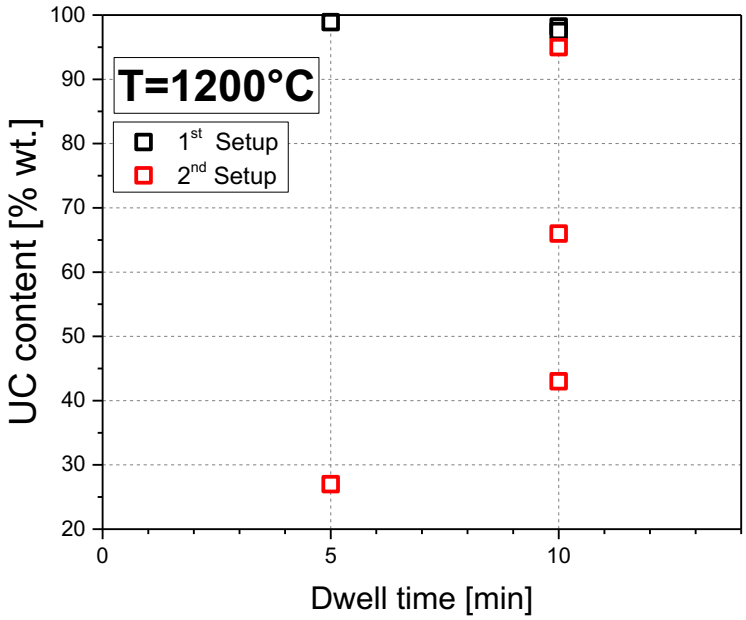

Figure 48: UC yield with the two different SPS set-up at 1200°C in 5 and 10 minutes of dwell time.

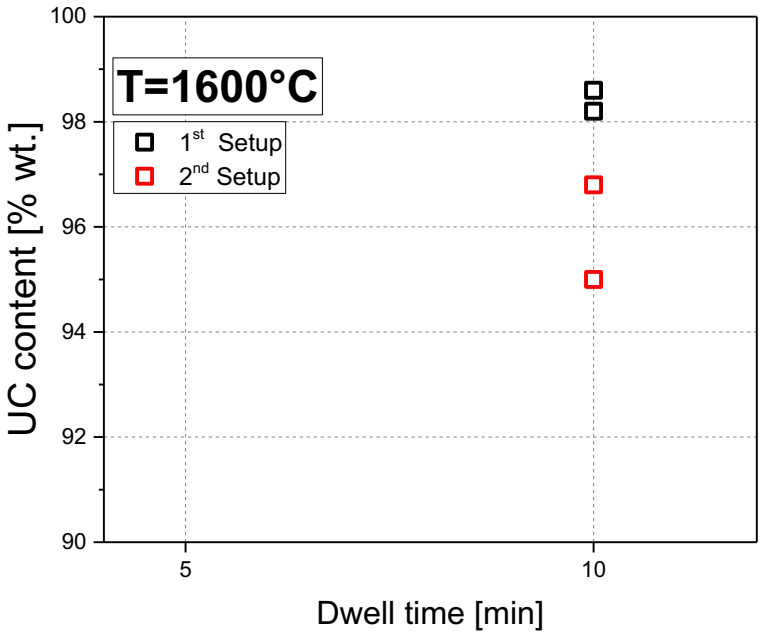

Figure 49: UC yield with the two different SPS set-up at 1600°C in 10 minutes of dwell time.

4.6.4.2 Reactivity of the Nanocrystalline UO_2/C Powder

To have a further confirm of the enhanced reactivity of the powder coming from the decomposition of citric acid/uranyl nitrate solution, one test was performed in SPS using the conventional UO_2/C powder. The precursors were manually mixed with a mortar (instead of the conventionally performed ball milling) in a UO_2:C ratio of 3:1 and heat treated up to 1600°C, with a dwell time of 10 minutes. In order to properly compare the two materials, the same set-up and total mass were adopted, thus avoiding any secondary effect.

The result of the experiment is presented in *Figure 50*, where it is directly compared to one test on the nanocrystalline UO_2/C mixture in the same heating condition. The carbothermal reduction of the conventional powder was clearly not completed. A big amount of uranium dioxide was still present. This phase should not come from an oxidation of the sample, since carbon is still present too, thus demonstrating the incompleteness of the reaction. In particular, the phase composition obtained with XRD analysis is presented in *Table 6*.

This test demonstrated the better performances of the proposed liquid route for powders synthesis, compared to a solid-state route where powders are mixed in a mortar. The peculiarity of the liquid method is the achievement of an intimate contact between the precursors for the carbothermal reduction, thus enhancing the kinetics of the reaction, rending unnecessary the ball milling step. Then, the homogeneous dispersion of UO_2 and carbon at a nanometric scale, together with the velocity and efficacy of the heating treatment in the

developed SPS set-up contributed to successfully produce uranium carbides in very short times.

Table 6: XRD phase compositions of the carboreduced powders in SPS coming from conventional uranium dioxide and carbon blending and citric acid/ uranyl nitrate precursors

Sample	UC [wt.%]	UC_2 [wt.%]	UO_2 [wt.%]	C [wt.%]
Citric acid + Uranyl nitrate	98	-	2	-
Conventional UO_2 + C	42	11	28	19

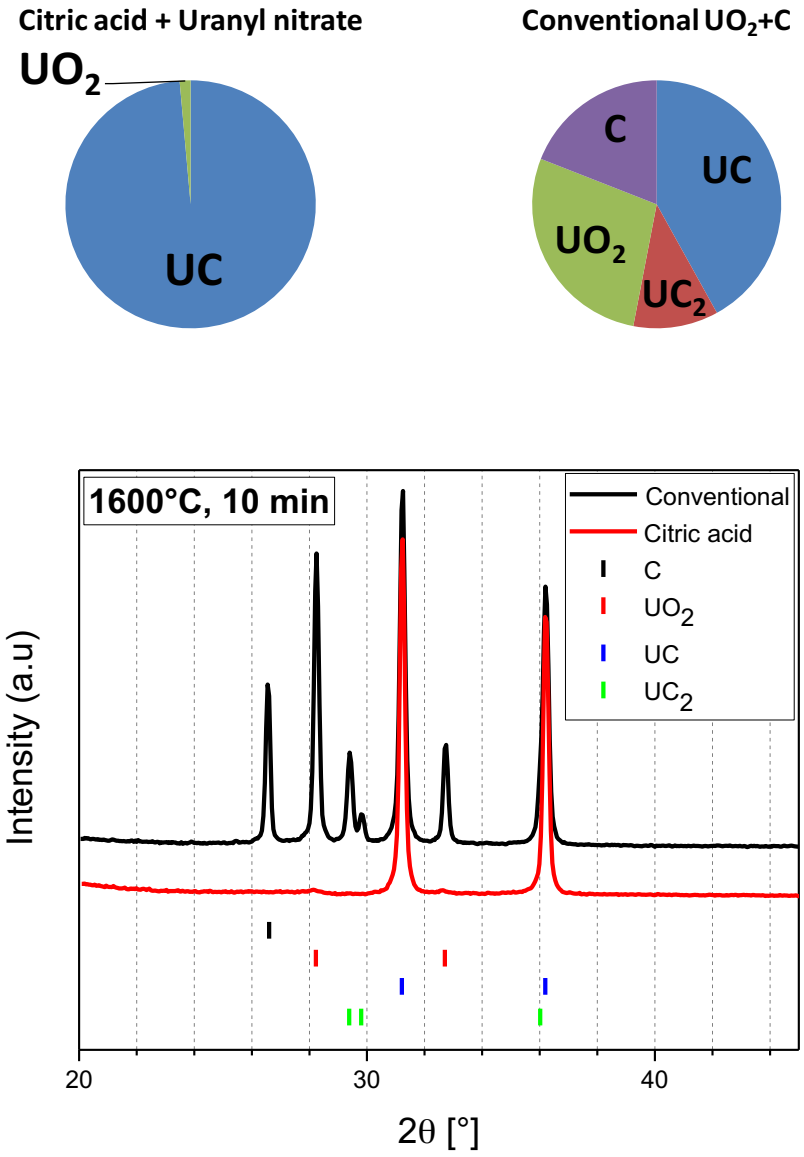

Figure 50: Comparison between XRD diffractograms and phase composition of the carboreduced powder in SPS coming from conventional uranium dioxide and carbon blending and citric acid/ uranyl nitrate precursors. The diffraction lines of UO_2, UC, UC_2, and C are shown.

4.7 Sintering in SPS

The carbide synthesized in SPS at different temperatures where then sintered in the same device. The main purpose of these experiments was to study the effect of the temperature of production on the sinterability of the powder. As described in Chapter 1, carbides are usually densified at 1750°C for 4h (Duguay *et al.*, 2012). Here, the specimens were heated until 1700°C, with a heating rate of 200°C/min, holding of 10 minutes and then cooled to room temperature. During the treatment a pressure of 100 MPa was applied on the pellets.

Relatively high densities were obtained despite the very short duration of the process. Several reasons could justify it. First of all, the SPS itself is known to facilitate the sintering, thanks to the application of pressure and the current passing through the material (McWilliams *et al.*, 2008). Then, the treated carbides were produced in very short times, at relatively low temperature, thus limiting the degree of grain growth (Guillon *et al.*, 2014).

The SPS software tracks the densification during the heat treatment, showing the displacement of the pistons and its derivative. Then, measuring the density at the end, the density in function of time could be estimated. However, to have the real trend, a blank experiment would have been needed using an already sintered ($\varrho \approx 100\%TD$) uranium carbide pellet, with a mass comparable to the mass of the analysed samples. In this way it would have been possible to correct the displacement subtracting the part due to the thermal expansion of the whole system (SPS pistons and treated pellet). Because of the unavailability of such a reference sample, this correction was not conducted on the proposed tests. However, this fact does not affect the interpretation of results, since, here, the attention was focused only on the final reached density and, above all, the onset temperature of the densification.

4.7.1 Sinterability Dependence on the Temperature of Synthesis

The samples that underwent the sintering process were the ones produced at 1200°C, 1400°C, 1600°C with a 10 minutes' dwell. In the *Figure 51*, the densification history of the three pellets is shown in function of time and temperature, uncorrected for the thermal expansion and contraction. The density trend was obtained from the recorded relative displacement of the SPS pistons, using the following formula:

$$\varrho(t) = m \,/\, [\, \pi \bullet r^2 \bullet (h_f + (d_f - d(t))) \,] \qquad (18)$$

Where m is the treated mass, r the radius of the pellet, h_f the final height of the pellet, d_f the final relative displacement of the pistons, and $d(t)$ the relative displacement in function of the time (values recorded by the SPS software).

The final height, and then the final density, was measured by X-Ray Tomography, since difficulties were found in the removal of the pellets from the graphite die. The reason for this

inconvenience was attributed to a chemical reaction occurring between uranium carbide and the carbon from the punches.

The estimated final densities are shown in *Figure 52*, together with the onset temperatures of the sintering, and confirmed what was above supposed: the lower is the temperature of synthesis, the higher is the sinterability of the powder, thus resulting in a lower starting temperature of the densification and a higher reachable density. Furthermore, it is also important to underline the value of the reached densification. In very short experiments, densities higher than 88% TD were obtained, thus demonstrating the good sinterability of the carbides produced through the proposed method (for $T_{production} \leq 1400°C$) and the efficacy of the SPS as a sintering tool.

SEM images of the three sintered pellets are presented in *Figure 53* (right side). The progressive increase of the density calculated by tomography is clearly visible. Looking at the morphology of the analysed samples, before and after the treatment, information about the sintering process could be deduced. The carbide produced at 1600°C showed agglomerates of grains with a high degree of grain coarsening. This resulted in a low sintering efficiency, with difficulties in closing both intra- and inter-agglomerate porosity. The pores in this case has a characteristic dimension ≥1 μm. On the other hand, the sample synthesized at 1200°C was characterised by smaller grain sizes and necking, thus allowing a better densification with less residual porosity. The few found pores had a characteristic dimension of 10^2 nm. The carbothermal reduction performed at 1400°C gave a pellet that lay in between the ones above described: few pores are visible, with sizes smaller than 1 μm.

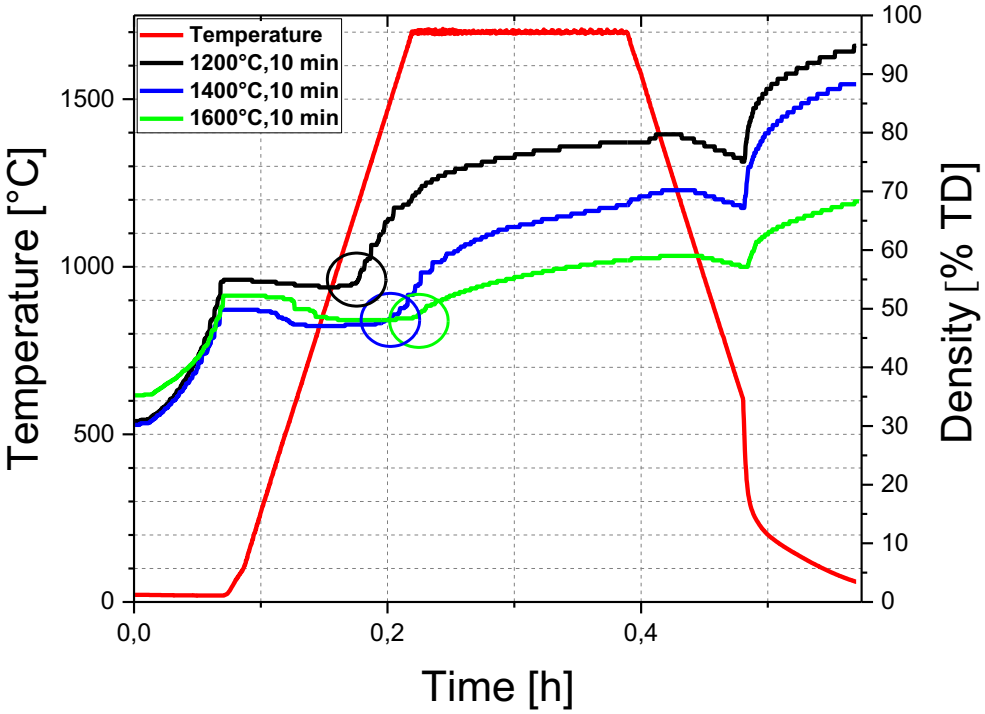

Figure 51: Temperature history and theoretical density trends (not corrected by the thermal expansion and contraction of the system) during the SPS sintering of the powders carboreduced in SPS at 1200°C, 1400°C, and 1600°C. The onset of sintering of the three different powders is marked with circles.

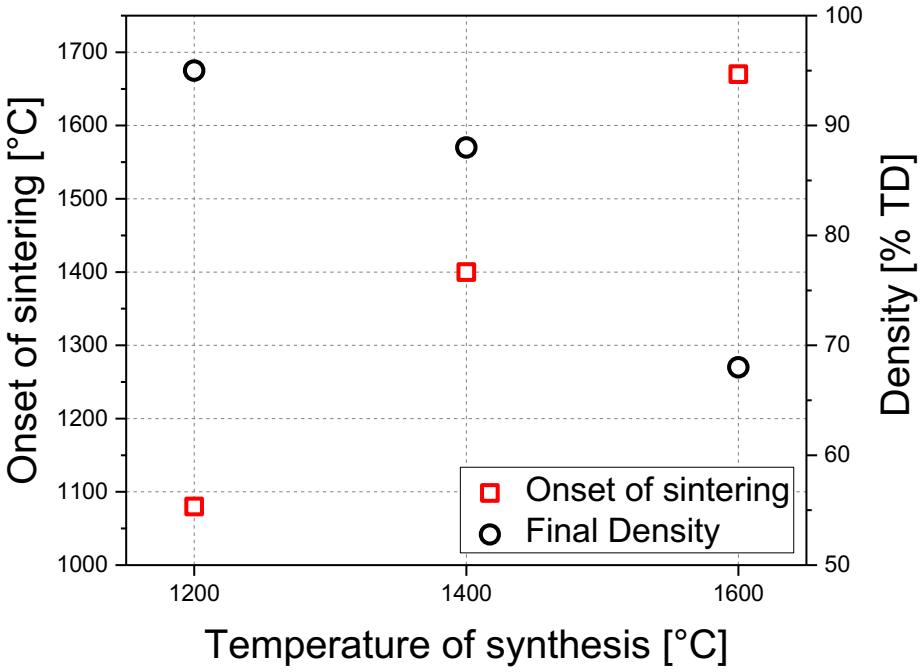

Figure 52: Final densities and onset of sintering for the powder synthesised at 1200°C, 1400°C, and 1600°C.

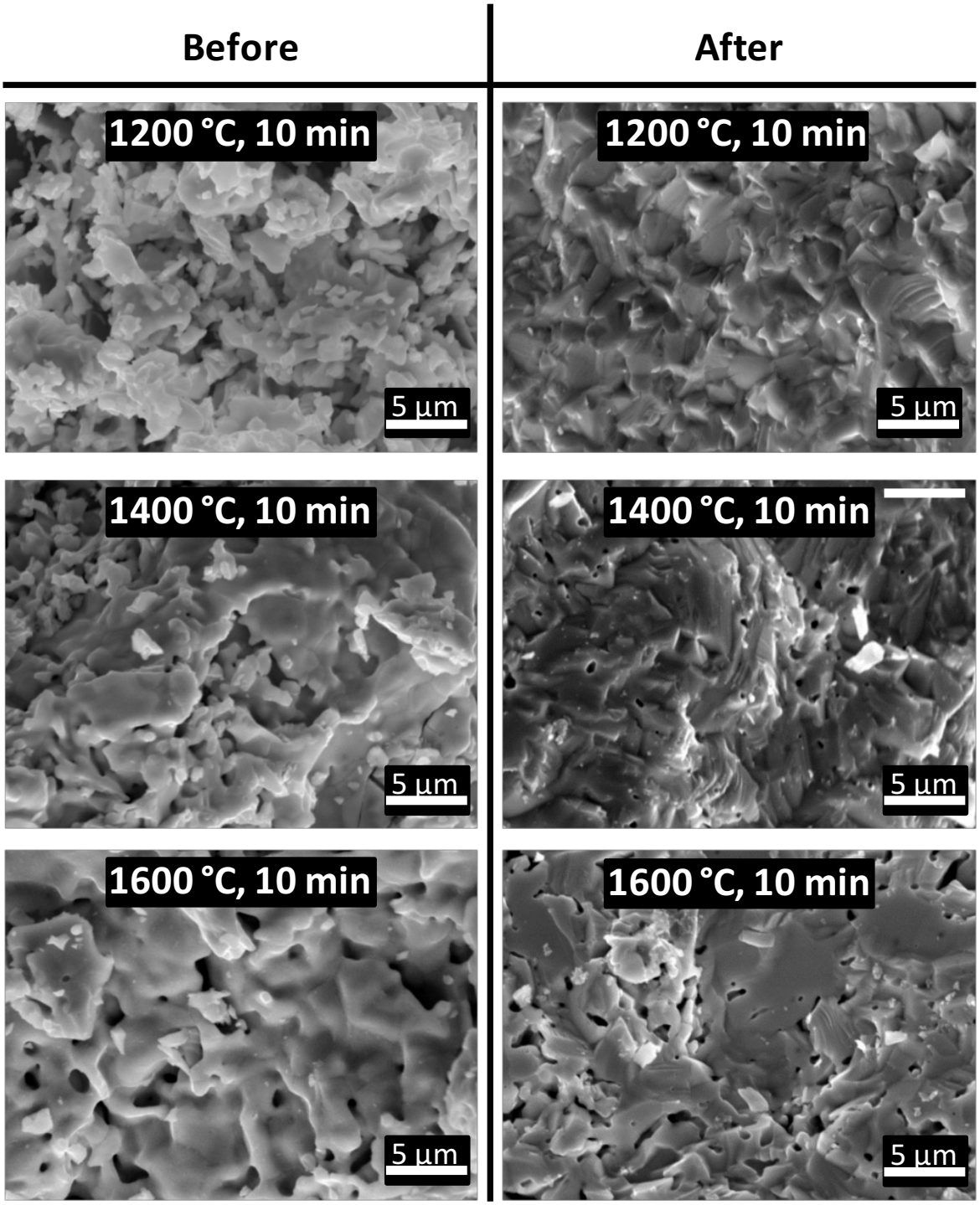

Figure 53: Comparison between SEM images of the carbides produced at different temperatures before (left) and after (right) the sintering.

4.7.2 Difference in Composition Before and After Sintering

After the X-Ray tomography, pieces coming from the middle of the pellets were analysed by XRD to check any modification in the phase composition. The comparison between the

diffractograms before and after the sintering is shown in *Figure 54*, *Figure 55*, and *Figure 56*. In all the three pellets there was a decrease in the amount of uranium monocarbide associated with a substantial increase in the uranium dicarbide phase. The small traces of UC_2 found after the carbothermal reduction turned into more than 5 wt.% in the densified material. Different reasons could be given to this phenomenon. Some not-reacted carbon still present in the powder may have reacted with UC leading to the formation of UC_2, following the reaction (16). Another source of carbon could be the graphite environment where the reaction took place. This last explanation was confirmed analysing a further piece of one pellet which stayed attached to the graphite punch. In *Figure 57*, the two patterns of the two different located parts are compared. The weight percentage of the uranium dicarbide phase increases going from the middle of the pellet to the part in contact with the graphite piston, suggesting that the cause was a diffusion of the carbon from the graphite SPS set-up to the treated specimen. Another occurring phenomenon is the small increase in the amount of oxide phase. Here, the main cause may be an oxidation of the uranium carbide occurred during the storage and/or the sample preparation for XRD analysis.

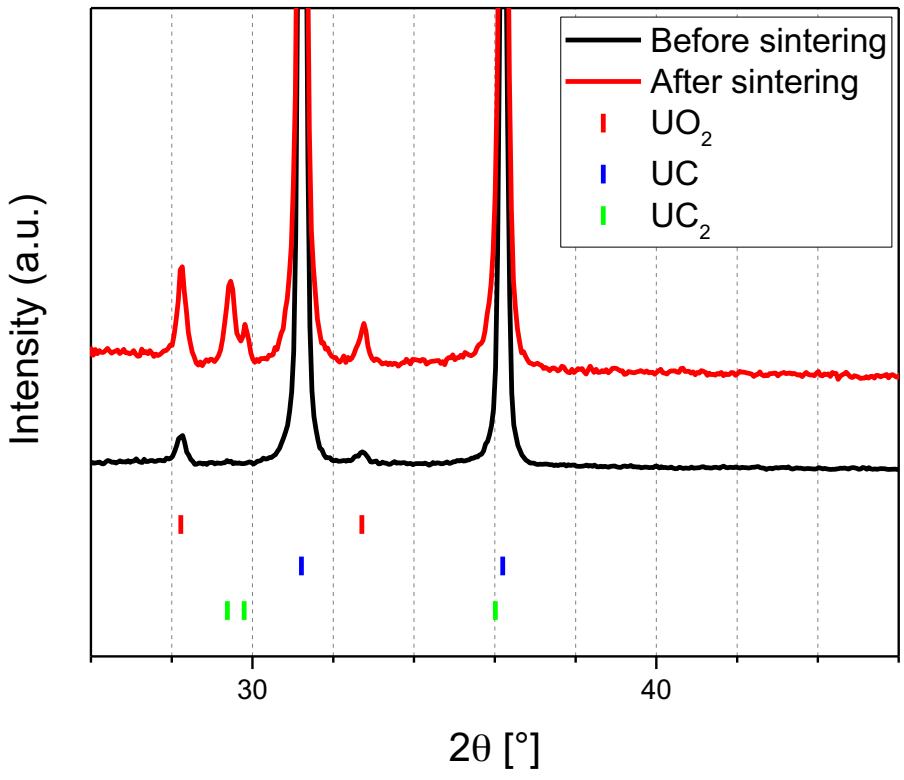

Figure 54: XRD pattern of the sample produced at 1200°C, before and after the sintering.

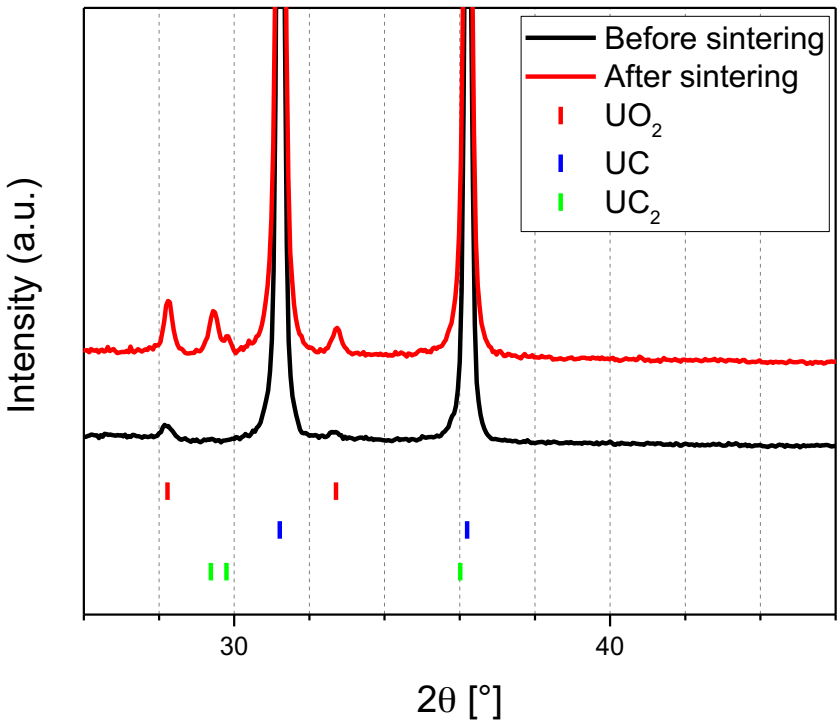

Figure 55: XRD pattern of the sample produced at 1400°C, before and after the sintering.

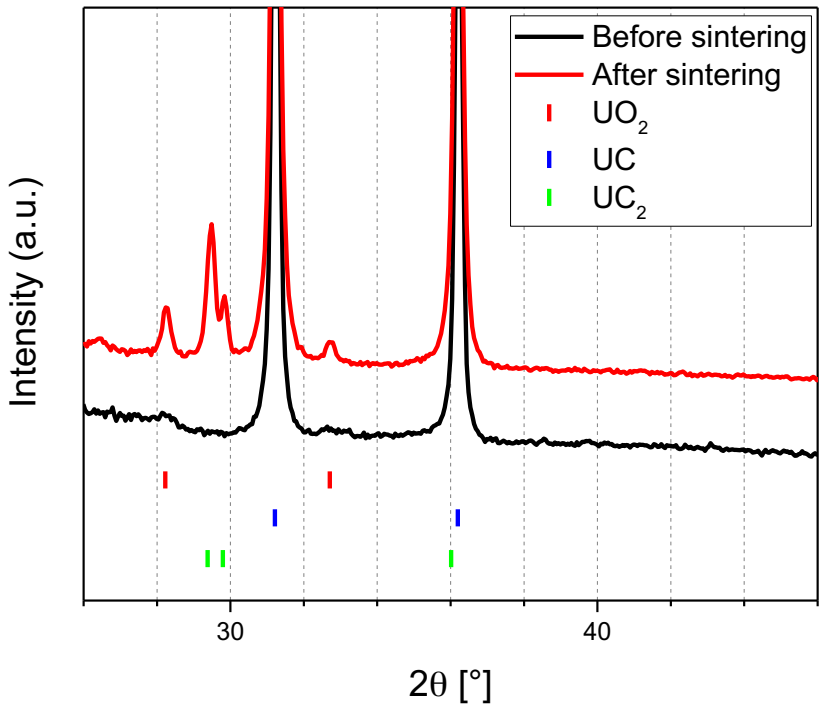

Figure 56: XRD pattern of the sample produced at 1600°C, before and after the sintering.

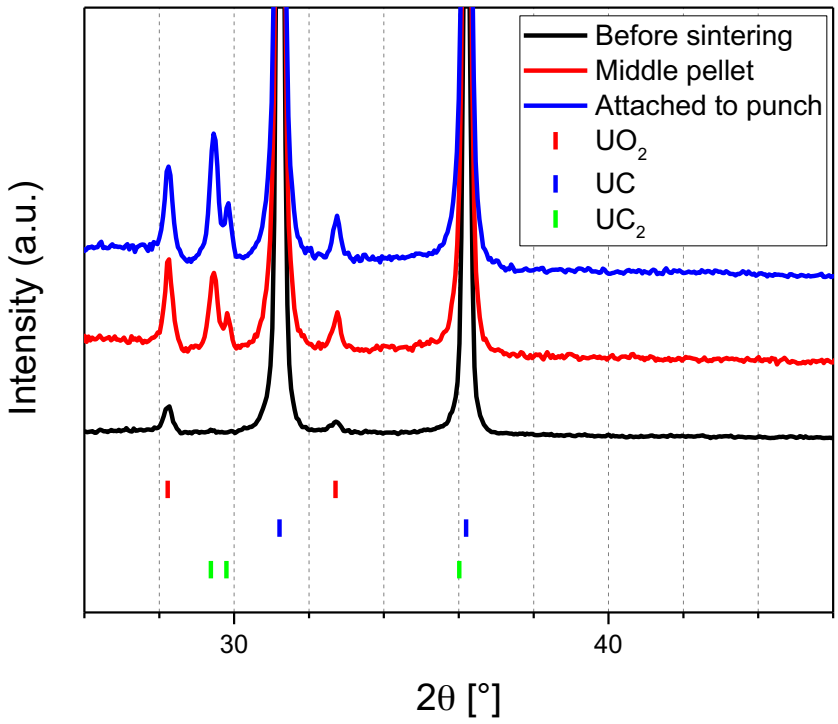

Figure 57: XRD pattern of the sample produced at 1200°C, before the sintering and after the sintering in the middle and extremity of the pellet.

4.7.3 Comparison between Normal and High Pressure Sintering

Apart from the normal sintering test mentioned above, the carbide produced at 1200°C in 10 minutes was sintered in SPS using the high pressure set-up. It was expected that the higher pressure applied (500 MPa vs. 100 MPa) would have enhanced the sintering efficiency causing an anticipation of the starting temperature of the densification, as already demonstrated in UO_2 pellets by Cologna *et al.* (2016). However, the result was the opposite. The high pressure sintering started 400°C later than the normal one, as shown in *Figure 58*. A possible explanation could be obtained analysing the components of the high pressure set-up. In fact, to manage to increase the pressure to such high values, silicon carbide punches are used, characterised by a higher mechanical resistance than the graphite ones. The silicon carbide has a higher electrical resistivity if compared to graphite (10^{2}-10^{4} vs. 10^{-4}-10^{-1} Ω•cm), thus lower current flows through the pellet during the heat treatment. The density in function of time during a sintering process in SPS is influenced by different factors: the temperature, the grain size, the applied pressure and the flowing current (Guillon *et al.*, 2014). Then, it could be that for uranium carbide the current has a more important effect than the applied pressure, contrary to what has been observed for uranium dioxide pellets. However, this is only a hypothesis coming from the analysis of one single test. To properly demonstrate this

affirmation, a sintering test using silicon carbide pistons and applying the same pressure of a normal sintering test (100 MPa) would be needed.

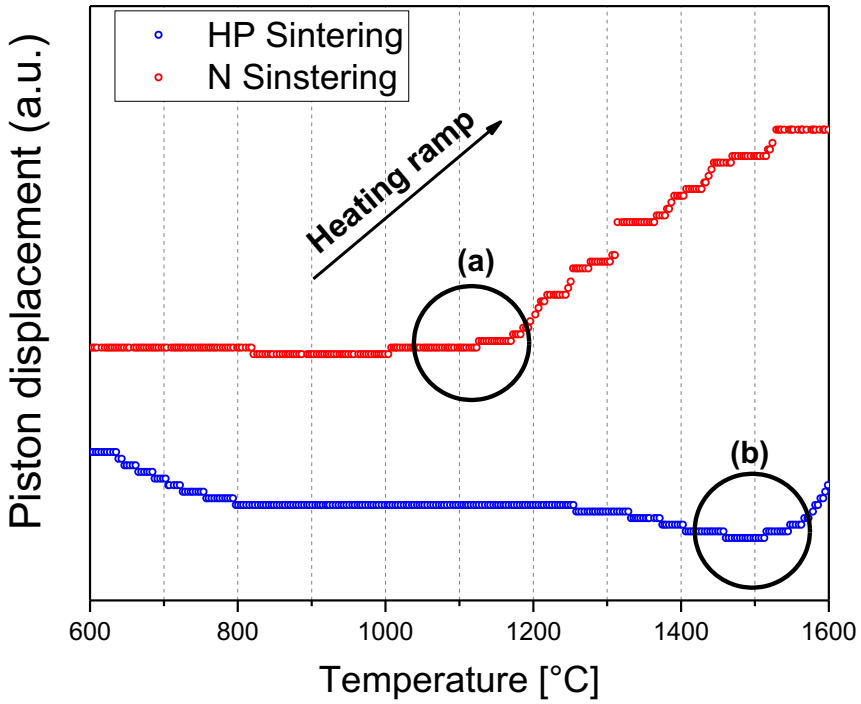

Figure 58: Piston displacement (not corrected by the thermal expansion and contraction of the system) in function of temperature for the same sample but in different sintering set-up: the normal (N) set-up and the high pressure (HP) set-up. The onset of sintering is marked with the black circles (a) and (b) for normal and high pressure set-up, respectively.

4.8 Sensitivity of the Powder to Glove Box Atmosphere

Finally, a study on the sensitivity of the carbide powder synthesised in SPS is presented. The samples were analysed by XRD one month after the production. The phase compositions and lattice parameter were compared in order to see if a degradation of the powders occurred in contact with the controlled atmosphere of the glove box. It is important to underline that the samples were in powder form and stored inside plastic container in the SPS glove box, equipped with a dedicated nitrogen supply system. The evolution of the amount of uranium carbide is shown in *Table 7*, while the one of the cell parameters in *Figure 59*. A small decrease in the fraction of UC was registered (<2 wt.%) followed by a slight increase in the lattice parameters, usually associated with an increase of oxygen impurities dissolved in the UC lattice (Manara *et al.*, 2012). It is difficult to directly link the cell parameter to the amount of dissolved oxygen, since different parameters affect it. However, looking at the *Figure 60* proposed by Magnier *et al.* (1963), some considerations could be suggested. In fact, since after one month the lattice parameter increased, it could be concluded that the area where the fresh analysed

samples are placed is before the maximum of the proposed trend. Then, the oxygen amount should be lower than 2000 ppm. However, to confirm these hypotheses other measurements in time are needed.

These tests suggested that the produced material is not heavily oxidized by the SPS glove box atmosphere, even if the concentration of oxygen was higher than the advised specification. These results are not extendable to the powder produced in the conventional furnace, since the latter is served by another nitrogen supply system, with other characteristics.

Table 7: Yield of UC in function of time for five different samples. An oxidation study.

Sample	% UC as produced	% UC after one month
	91.7	91.6
	98	98
	98.2	97.6
	98.2	97.1
	97.7	96.5

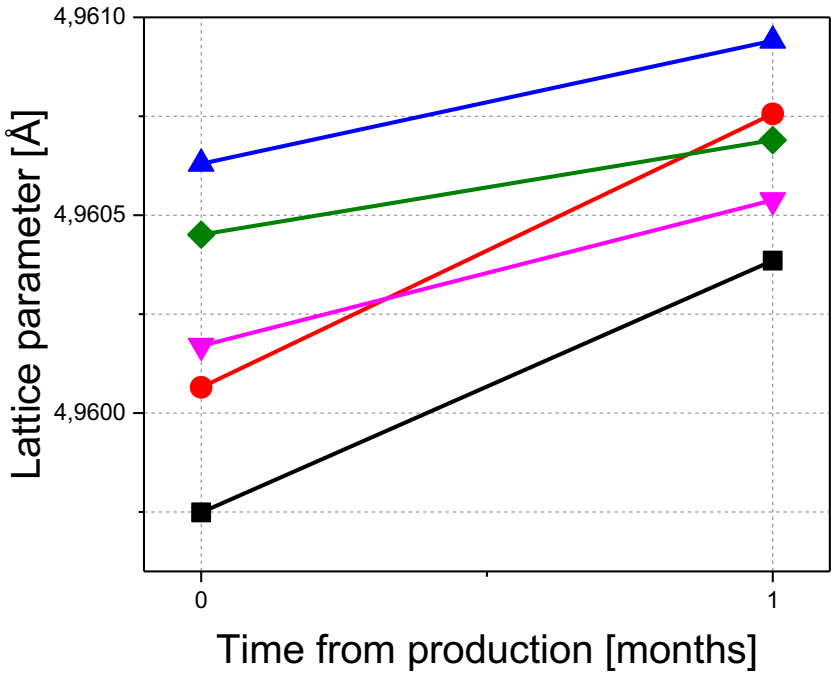

Figure 59: Lattice parameter of five UC samples produced in SPS registered at different times. An oxidation study.

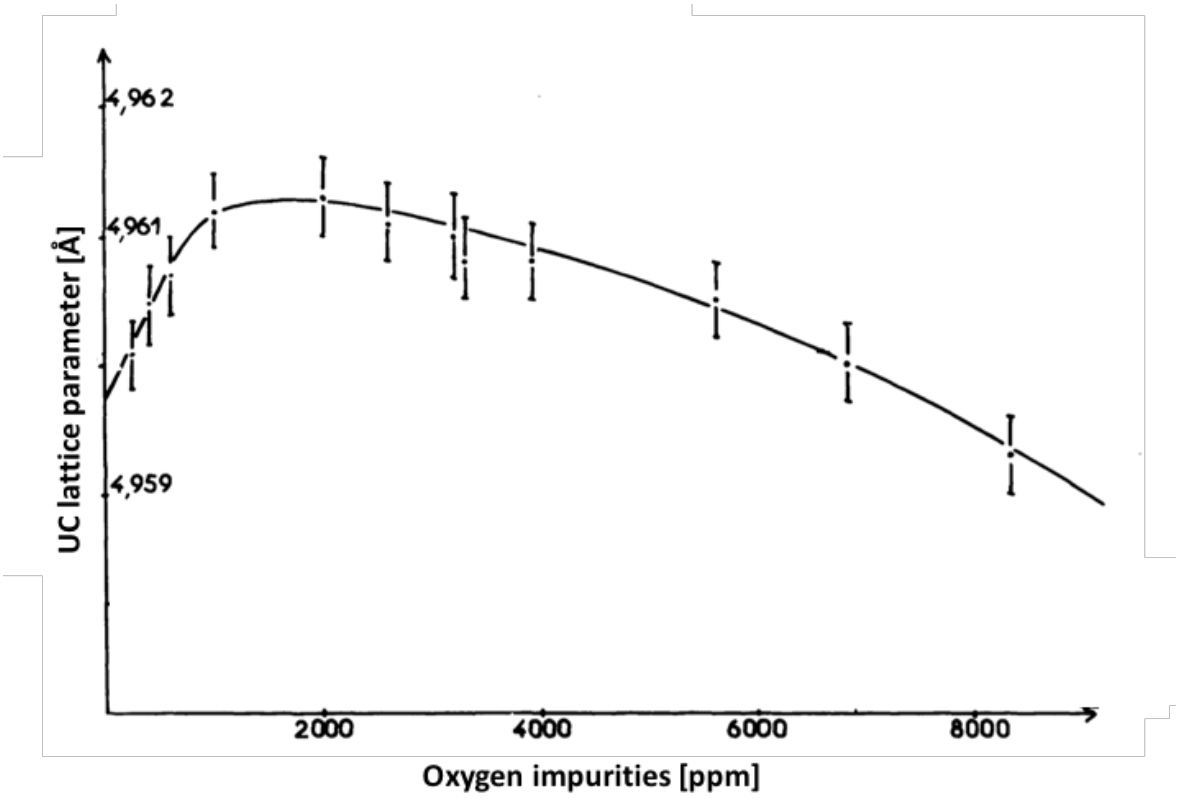

Figure 60: UC lattice parameter in function of oxygen impurities.

4.9 Concluding Remarks

SEM and TEM on the calcinated UO_2/C, and the UC yield after CTR at very low temperature and for very short dwell time demonstrated the enhanced reactivity of the precursors prepared through this new liquid route. An appropriate SPS set-up design for CTR has been developed, thus also justifying the achieved results. The short duration and low temperature of the CTR experiments conducted in SPS allowed the production of a high sinterable carbide, as predicted. In fact, very high density (≈ 95 %TD) were reached in only ten minutes at 1700°C.

Conclusions

In this work, we achieved a simple and efficient synthesis route for uranium carbide preparation. Carbothermal reduction (CTR) using nanocomposite of UO_2 and carbon as a starting material has been tested under conventional conditions and in a modified spark plasma sintering (SPS) set-up. In a conventional furnace, using argon atmosphere at 1600°C and one hour dwell, the nano-UO_2/C powder gave uranium carbide of 96 wt.% purity. An UC_2 intermediate has been observed in these conditions. The yield of CTR has been found to be critically sensitive to partial pressure of CO. In the modified spark plasma sintering set-up (under vacuum), the CTR occurs under much milder conditions, namely 1200°C within 5 minutes were enough to give almost 99 wt.% of uranium carbide. No UC_2 intermediate was observed during the CTR in SPS, which may be due to the vacuum and easy release of CO.

Thanks to the fast heating/cooling ramps of SPS, the produced powder is finer and therefore more sinteractive. In particular, the powder produced at 1200°C and 1400°C in 10 minutes revealed to have a great sinterability: densities higher than 88% TD were reached in 10 minutes at 1700°C. The extraction of the pellets from the graphite die was difficult and always resulted in their damage, probably due to a chemical reaction occurring between the treated carbide and the surrounding graphite pieces at high temperatures. Apposite separator materials will have to be studied to address this issue, as explained in the next section. In *Figure 61*, a flow sheet of the adopted experimental procedure together with the main considerations coming from the analysis of the obtained results are presented.

The main achievements of the thesis work can be summarised as follows:

- For the first time, the citric acid route has been developed for the synthesis of UC.
- The calcination of the liquid precursors allows the formation of well-dispersed nanocrystalline UO_2 particles in an amorphous carbon matrix.
- Thanks to the nanometric nature of the reactants and to the quality of dispersion, an unprecedented high reactivity in carbothermal reduction was achieved, considering also non-nuclear carbides.
- The carbothermal reduction can take place in a conventional furnace, or, even more effectively, in SPS in a set-up specifically developed during this thesis.
- The obtained UC powders are highly sinteractive and can be directly compacted in SPS to high density without any milling step.
- The new process developed has the potential to simplify considerably the synthesis of carbide fuels, which is one of the factor limiting their use, by rendering all laborious traditional ball milling steps unnecessary, and drastically reducing the time and energy needed for the synthesis.

Further R&D activities are needed to make the developed method suitable for nuclear fuel production, such as thermo-physical and mechanical characterizations, and out-of-pile and in-pile experiments on the produced samples, but this was out of the scope of the present work.

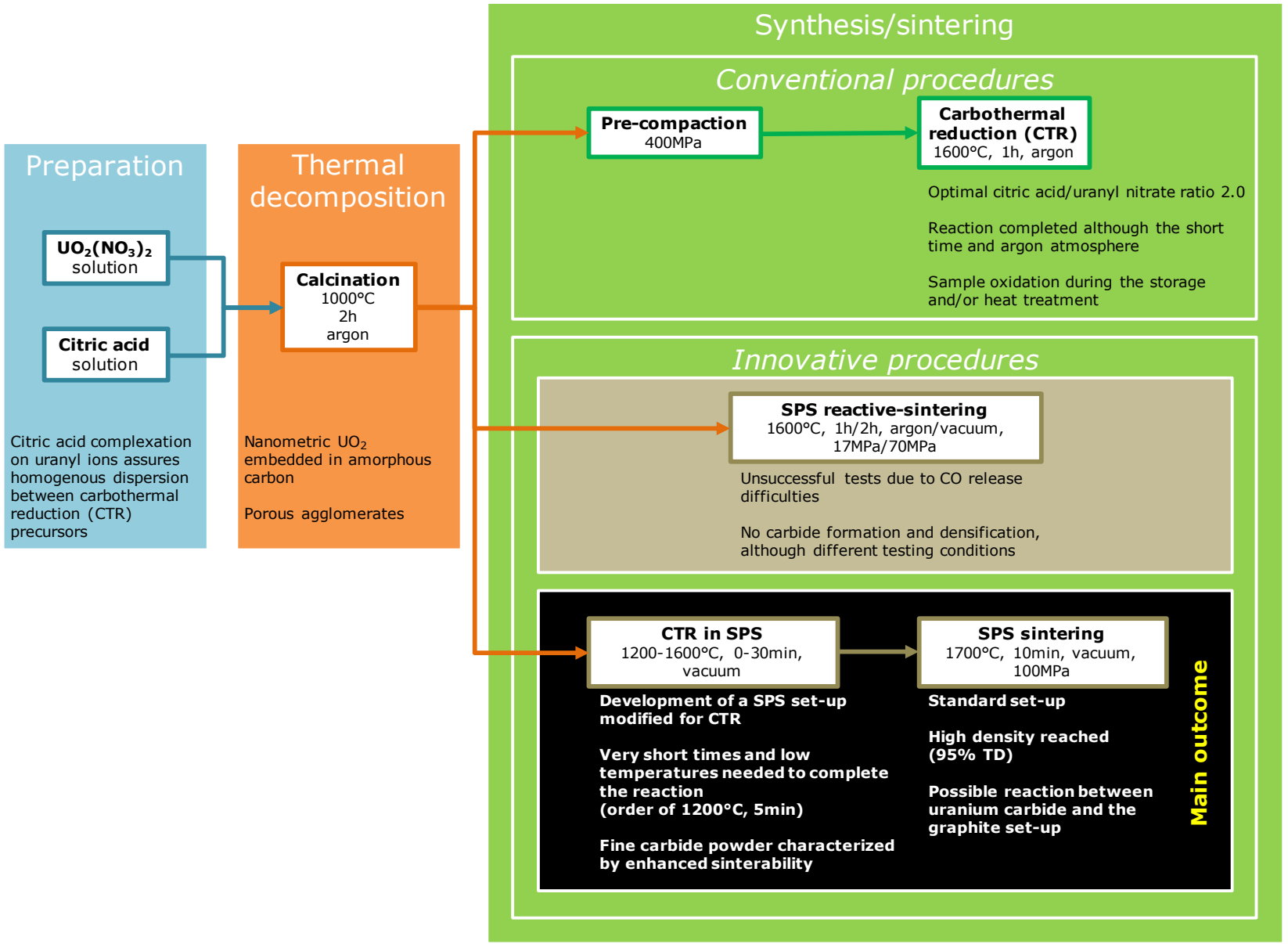

Figure 61: Flow sheet of the adopted experimental procedure. The main achieved results are included.

This page is intentionally left blank

Possible Future Steps

Different improvements and further studies may be planned starting from the achieved results.

- First of all, actions should be taken to minimize the oxidation of the produced carbides in order to clearly know if the small (<2 wt.%) amount of oxide comes from a carbon deficiency in the starting material. Furthermore, the presence of oxygen impurities could heavily affect carbide behaviour, from irradiation, chemical, and thermo-mechanical viewpoints. To reach this goal, fully hermetic metallic containers should be adopted for the storage, and the handling of the specimen (especially when in powder form) should occur only when the oxygen content in the glove box atmosphere fulfils the advised specifications (< 25 ppm).

- Another issue is the extraction of the carbide pellet from the SPS die, which resulted to be difficult for a presumed chemical interaction between the graphite and the specimen. Thus, an appropriate modification may be adopted. For example, the contact between the SPS parts and the pellet should be avoided placing a non-reactive material between them. This material needs to be highly electrically conductive, since it has been found in this thesis that the flowing current may enhance the carbide sintering. Apart from the unequivocal convenience of handling full pellets, this achievement would allow having a more precise density measurement through an Archimedes' balance with bromobenzen, which also allows estimating the fraction of open porosity (that is an important parameter to be monitored in fuel pellets).

- A further improvement would be the development of a new SPS set-up for CTR to increase the mass of the treated material without compromising the kinetics of the reaction.

- Performing the CTR in SPS under argon would be useful to properly evaluate the effect of the filling gas in the developed method. Furthermore, the influence of the chosen atmosphere during the sintering (vacuum, argon, argon/hydrogen) on the final density would be interesting to be studied. Further improvements may be achievable.

- As done for the CTR, an optimization of the temperature and holding times at which the sintering is performed is recommended to check if the desired densities (80-85% TD) may be reached with even milder conditions.

- Of course, a further crucial step is the demonstration of the feasibility to produce mixed carbides, in order to produce pellets that could fuel a fast reactor. Apart from the allowed reduction in time, the proposed method, decreasing also the temperatures of the CTR, should limit the plutonium losses by volatilization, that heavily affect the conventional routes.

This page is intentionally left blank

References

Anselmi-Tamburini, U., Woolman, J.N., Munir, Z.A., 2007. *Transparent Nanometric Cubic and Tetragonal Zirconia Obtained by High-Pressure Pulsed Electric Current Sintering*, Advanced Functional Materials 17, 3267-3273.

Anselmi-Tamburini, U., Spinolo, G., Maglia, F., Tredici, I., Holland, T.B., Mukherjee, A.K., 2012. in *Sintering: Mechanism of Convention Nanodensification and Field Assisted Process*, (Editors: Castro, R., van Benthem, K), Springer, Berlin/Heidelberg 2012, Chapter 8, 159-193

Bailey, E.H., Mosselmans, J.F.W., Schofield, P.F., 2005. *Uranyl-citrate speciation in acidic aqueous solutions-an XAS study between 25 and 200°C,* Chemical Geology 216, 1-16

Bart, G., Botta, F.B., Hoth, C.W., Ledergerber, G., Mason, R.E., Stratton, R.W., 2008. *AC-3-irradiation test of sphere-pac and pellet (U,Pu)C fuel in the US Fast Flux Test Facility*, Journal of Nuclear Materials 376. 47-5

Basak, U., 2009. *Fabrication, properties and irradiation behaviour of MOX, carbide and nitride fuels, inert matrix fuels with and without minor actinides*, Joint ICTP/IAEA School on Physics and Technology of Fast Reactors Systems, Nov. 17, 2009

Benz, R., Stone, P.L., 1969. *Carbon-Thorium Binary Alloy Phase Diagram*, High Temperature Science 1, 342-359

Berthinier, C., Coullomb, S., Rado, C., Le Guyadec, F., Chatillon, C., Blanquet, E., Boichot, R., 2009. *Experimental thermal analysis of Uranium Carbide Powder Ignition*, Proceedings of Global 2009, Paris, France, September 6-11, 2009, Paper 9131

Berthinier, C., Coullomb, S., Rado, C., Blanquet, E., Boichot, R., Chatillon, C., 2011. *Experimental study of uranium carbide pyrophorocity*, Powder Technology 208. 312-317

Bokelund, H., Caceci, M., Ougier, M., 1982. *Dissolution of Mixed Carbide in Nitric Acid*, Radiochimica Acta 30, 49-55

Boutard, J.L., de Novion, C.H., 1974. *Etude par RMN et rayons X de sesquicarbure d'uranium*, Solid State Communications 14, 181-185

Bowman, A.L., Arnold, G.P., Witteman, W.G., Wallace, T.C., Nereson, N.G., 1966. *The crystal structure of UC_2*, Acta Crystallographica 21, 670-671

Burkes, D. E., Fielding, R. S., Porter, D. L., Meyer, M. K., Makenas, B. J., 2009. *A US perspective on fast reactor fuel fabrication technology and experience. Part II: Ceramic fuels*, Journal of Nuclear Materials 393. 1-11

Chen, Y., Zang, H., Ye, H., Ma, J., 2011. *A simple and novel route to synthesize nano-vanadium carbide using magnesium powders, vanadium pentoxide and different carbon source*, International Journal of Refractory Metals and Hard Materials 29, 528-531
Chevalier, P.Y., Fischer, E., 2001. *Thermodynamic modeling of the C–U and B–U binary systems*, Journal of Nuclear Materials 288, 100-129

Cologna, M., Tyrpekl, V., Ernstberger, M., Stohr, S., Somers, J., 2016. *Sub-micrometre grained UO_2 pellets consolidated from sol gel beads using spark plasma sintering (SPS)*, Journal of Nuclear Materials 42, 6619-6623

Crawford, D.C., Porter, D.L., Hayes, S.L., 2007. *Fuels for sodium-cooled fast reactors: US perspective*, Journal of Nuclear Materials 371. 202-231

Duguay, C., 2012. *Mastery of (U,Pu)C carbide fuel: from raw materials to final characteristics*, MINOS Workshop: Materials Innovation for Nuclear Optimized System, CEA-INSTN Saclay, France, Dec. 5-7, 2012

Duguay, C., Pelloquin, G., 2015. *Fabrication of mixed uranium-plutonium carbide fuel pellets with low oxygen content and an open-pore microstructure*, Journal of the European Ceramic Society 35. 3977-3984

Feng, L., Lee, S.H., Wang, H., Lee, H.S., 2015. *Synthesis and densification of nano-crystalline hafnium carbide powder*, Journal of the European Ceramic Society 35, 4073-4081

Frost, B.R.T., 1963. The Carbides of Uranium, Journal of Nuclear Materials 10. 265-300

Ganguly, C., Hegde, P. V., 1997. *Sol-gel microsphere palletisation process for fabrication of (U,Pu)O2, (U,Pu)C and (U,Pu)N fuel pellets for the prototype fast breeder reactor in India*, Journal of Sol-Gel Science and Technology 9. 285-294

Ganguly, C., Jain, G.C., Ghosh, J.K.; Roy, P. R., 1988. The role of ``process control'' and ``inspection'' steps in the quality assurance of SS 316 clad mixed plutonium-uranium carbide fuel pins for FBTR, Journal of Nuclear Materials 153, 178-188

Ge, L., Subhash, G., Baney, R.H., Tulenko, J.S., McKenna, E., 2013. *Densification of uranium dioxide fuel pellets prepared by spark plasma sintering (SPS)*, Journal of Nuclear Materials 435, 1-9

Ge, L., Subhash, G., Baney, R.H., Tulenko, J.S., 2014. *Influence of processing parameters on thermal conductivity of uranium dioxide pellets prepared by spark plasma sintering*, Journal of the European Ceramic Society 34, 1791-1801

Grasso, S., Kim, B.N., Hu, C., Maizza, G., Sakka, Y., 2010. *Highly transparent pure alumina fabricated by high-pressure spark plasma sintering,* Journal of the American Ceramic Society 93, 2460–2462

Guillon, O., Gonzalez-Julian, J., Dargatz, B., Kessel, T., Schierning, G., Rathel, J., Herrmann, M., 2014. *Field-Assisted Sintering Technology/Spark Plasma Sintering: Mechanism, Materials, and Technology Developments*, Advanced Engineering Materials, DOI: 10.1002/adem.201300409

Guo, Q., Li, J., Shen, Q., Zhang, L., 2012. *Preparation and characterization of ZrB_2–SiC–$Zr_2Al_4C_5$ composites by spark plasma sintering-reactive synthesis (SPS-RS) method*, Material Science & Engineering A 558, 186-192

Hall, A.R., 1970. *Elastic moduli and internal friction of some uranium ceramics*, Journal of Nuclear Materials 37, 314-323

He, L., Liu, Y., Li, B., Cao, H., Li, J., 2010. *Reaction synthesis of in situ vanadium carbide particulates-reinforced iron matrix composites by spark plasma sintering*, Journal of Materials Science 45, 2538–2542

Holleck, H., Kleykamp, H., 1987. In *Gmelin Handbook of Inorganic Chemistry: U supplement Volume C12,* Springer-Verlag, Berlin

IAEA, 2003. *Development status of metallic, dispersion and non-oxide advanced and alternative fuels for power and research reactors*. IAEA TECDOC No. 1374

Lamarsh, J.R., Baratta, A.J., 2001. *Introduction to Nuclear Engineering, 3rd Edition,* Prentice Hall. 117-128

Lauguer, J., Blum, P.L., 1971. *Le diagramme metastable UC-UC_2*, Journal of Nuclear Materials 39, 245-252

Leinders, G., Cardinaels, T., Binnemans, K., Verwerft, M., 2015. *Accurate lattice parameter measurements of stoichiometric uranium dioxide*, Journal of Nuclear Materials 459, 135-142

Lenhart, J.J., Cabaniss, S.E., MacCarthy, P., Honeyman, B.D., 2000. *Uranium(VI) complexation with citric, humic and fulvic acids*, Radiochimica Acta 88, 345-353

Kumar, R., Chaubey, A.K., Bathula, S., Jha, B.B., Dhar, A., 2016. *Synthesis and characterization of Al_2O_3-TiC nano-composite by spark plasma sintering*, International Journal of Refractory Metals and Hard Materials 54, 304-308

Magnier, P., 1966. *Influence de l'oxygène, de l'azote et du carbone sur le paramètre reticulaire du monocarbure d'uranium,* Report Commissariat a l'Energie Atomique, Centre d'études nucléaires de Saclay, CEA - R 2852

Majumdar, S., Sengupta, A.K., Kamath, H.S., 2006. *Fabrication, characterization and property evaluation of mixed carbide fuels for a test Fast Breeder Reactor*, Journal of Nuclear Materials 352. 165-173

Manara, D., De Bruycker, F., Sengupta, A.K., Agarwal, R., Kamaath, H.S., 2012. *Comprehensive Nuclear Materials*, Chapter 2.04. Elsevier. 87-137

Matovic, B., Babic, B., Bucevac, D., Cebela, M., Maksimovic, V., Pantic,J., Miljkovic, M., 2013. *Synthesis and characterization of hafnium carbide fine powders*, Ceramics International 39, 719-723

Matthews, R.B., Herbst, R. J., 1983. *Uranium-plutonium carbide fuel for fast breeder reactors*, Nuclear Technology 63. 9-22

Matzke, H.J., 1986. *Science of Advanced LMFBR Fuels, A monograph on solid state physics, chemistry and technology of carbides, nitrides, and carbonitrides of uranium and plutonium*, Elsevier Science Publishers, Amsterdam

Mazaudier, F., Tamani, C., Galerie, A., Marc, Y., 2010. *On the oxidation of (U, Pu)C fuel: Experimental and kinetic aspects, practical issues*, Journal of Nuclear Materials 406, 277-284

McWilliams, M., Zavaliangos, 2008. *Multi-phenomena simulation of electric field assisted sintering*, Journal of Materials Science 43, 5031-5035

Munir, Z.A., Quach, D.V., Ohyanagi, M., 2012. In *Sintering: Mechanism of Convention Nanodensification and Field Assisted Process*, (Editors: Castro, R., van Benthem, K), Springer, Berlin/Heidelberg 2012, Chapter 7, 137-158

Muta, H., Kurosaki, k., Uno, M., Yamanaka, S., 2008. *Thermal and mechanical properties of uranium nitride prepared by SPS technique*, Journal of Materials Science 43, 6429-6434

Natarajan, R., Raj, B., 2007. *Fast reactor fuel reprocessing technology in India*, Journal of Nuclear Science and Technology 44, 393-397

O'Brien, R.C., Jerred, N.D., 2013. *Spark Plasma Sintering of W–UO_2 cermets*, Journal of Nuclear Materials 433, 50-54

Ohse, R.W., Capone, F., 1976. In *Plutonium and Other Actinides*; Blank, H., Lindner, R., Eds.; North-Holland: Amsterdam, 1976; pp 245–256

Onoki, T., Ueoka, Y., Xu, B., Shiota, N., Naganuma, Y., Matusoka, A., Minamibori, Y., Tagami, T., 2013. *Synthesis and classification of WC and W metals via organic and inorganic complex precursors*, Journal of the Ceramic Society of Japan 121, 572-574

Petrícek, V., Dusek, M., Palatinus, L., 2014. *Crystallographic Computing System JANA2006: General features*, Crystalline Materials 229, 345-352

Quach, D.V., Avila-Paredes, H.J., Kim, S., Martin, M., Munir, Z.A., 2010. *Pressure effects and grain growth kinetics in the consolidation of nanostructured fully stabilized zirconia by pulsed electric current sintering*,, Acta Materalia 58, 5022-5030

Rahaman, M.N., 2003. *Ceramic Processing and Sintering*, 2nd Edition, Marcel Dekker, Inc., New York

Raj, R., Cologna, M., Francis, J.S.C., 2011. *Influence of externally imposed and internally generated electrical fields on grain growth, diffusional creep, sintering and related phenomena in ceramics*, Journal of the American Ceramic Society 94, 1941-1965

Reavis, J.G., 1966. *Quarterly Status Report on the Advanced Plutonium Fuels Program*; Los Alamos Scientific Laboratory of the University of California, LA-3607-MS, Project 807; July 1966

Reavis, J.G., Reese, L., 1969. *Quarterly Status Report on the Advanced Plutonium Fuels Program*, Los Alamos Scientific Laboratory of the University of California, Project 463 LA-4073-MS (1969); LA-4193-MS (1969)

Richter, K., Coquerelle, M., Gabolde, J., Werner, P., 1974. In Proceedings of a Symposium on Fuel and Fuel Elements for Fast Reactors, Brussel, 1973; IAEA: Vienna, 1974; Vol. 1, 71–84

Rosen, S., Nevitt, M.V., Barker, J.J., 1963. *The U-Pu-C ternary phase diagram below 50 atomic percent carbon*, Journal of Nuclear Materials 9, 128-136

Schwesig, D., Schierning, G., Theissmann, R., Stein, N., Petermann, N., Wiggers, H., Schmechel, R., Wolf, D.E., 2011. *From nanoparticles to nanocrystalline bulk: percolation effects in field assisted sintering of silicon nanoparticles*, Nanotechnology 22, 135601

Sengupta, A.K., Agarwal R., Kamath H.S., 2012. *Comprehensive Nuclear Materials*, Chapter 3.03 - Carbide Fuel. Elsevier. 55-86

Shen, Z.J., Johnsson, M., Zhao, Z., Nygren, M., 2002. *Spark Plasma Sintering of Alumina*, Journal of the American Ceramic Society 85, 1921–1927

Sinha, A., Mahata, T., Sharma, B.P., 2002. *Carbothermal route for preparation of boron carbide powder from boric acid and citric acid gel precursor*, Journal of Nuclear Materials 301, 165-169

Stahl, D., Strasser, A., 1964. In *Carbides in Nuclear Energy*, Proceedings of a Symposium, Harwell, London, Nov 1963; Russell, L. E., Bradbury, B. T., Harrison, J. D. L., Hedger, H. J., Mardon, P. G., Eds.; Macmillan and Co.: London, 1964; Vol. 1, pp 373–391

Stratton, R.W., Ledergerber, G., Ingold, F., Latimer, T.W., Chidester, K.M., 1993. *Fuel fabrication processes, design and experimental conditions for the joint US-Swiss mixed carbide test in FFTF (AC-3 test)*, Journal of Nuclear Materials 204. 39-49

Sun, S.K., Zhang, G.J., Wu, W.W., Liu, J.X., Suzuki, T., Sakka, Y., 2013. *Reactive spark plasma sintering of ZrC and HfC ceramics with fine microstructures*, Scripta Materialia 69, 139-142
Sun, S.K., Zhang, G.J., Wu, W.W., Liu, J.X., Zoua, J., Suzuki, T., Sakka, Y., 2014. *Reactive spark plasma sintering of binderless WC ceramics at 1500°C*, International Journal of Refractory Metals and Hard Materials 43, 42-45

Suzuki, Y., Sasayama, T., Arai, Y., Watanabe, H., 1981. *Fabrication of uranium-plutonium mixed carbide pellets*, Journal of Nuclear Science and Technology. 61-70

Tagawa, H., 1970. *The variation of lattice parameter with carbon content of non-stoichiometric uranium dicarbide,* Journal of Nuclear Materials 34, 116-118

Teske, K., Ullmann, H., Rettig, D., 1983. *Investigation of the oxygen activity of oxide fuels and fuel-fission product systems by solid electrolyte techniques. Part I: Qualification and limitations of the method.* Journal of Nuclear Materials 116, 260-266

Tyrpekl, V., Holzhauser, M., Hein, H., Vigier, J.F., Somers, J., Svora,P., 2014. *Synthesis of dense yttrium-stabilised hafnia pellets for nuclear applications by spark plasma sintering*, Journal of Nuclear Materials 454, 398-404

Tyrpekl, V., Berkmann, C., Holzhäuser, M., Köpp, F., Cologna, M., Wangle, T., Somers, J., 2015. *Implementation of a spark plasma sintering facility in a hermetic glovebox for compaction of toxic, radiotoxic, and air sensitive materials*, The Review of Scientific Instruments 86, p.023904

Valote, C., Bertolus, M., Konings, R., Somers, J., De Groot, S., 2011. *Basic research in support of innovative fuels design for the GEN IV system: the F-BRIDGE project*, Nuclear engineering 241. 3521-3529

Vasudevamurthy, G., Knight, T. W., 2008. *Production of high-density uranium carbide compacts for use in composite nuclear fuels*, Nuclear Technology 163. 321-327

Vaudez, S., Riglet-Martial, C., Paret, L., Abonneau, E., 2008. *GEN IV: Carbide fuel elaboration for the "Futurix Concepts" experiment*, IYNC 2008, Interlaken, Switzerland, Sept. 20-26, 2008, Paper 146

Waltar, A.E., Todd D.R., Tsvetkov, P.V., 2012. *Fast Spectrum Reactors*. Springer

Wangle, T., Tyrpekl, V., Cologna, M., Somers, J., 2015. *Simulated UO_2 fuel containing CsI by spark plasma sintering*, Journal of Nuclear Materials 466, 150-153

Williams, J., Sambell, R.A.J., Wilkinson, D., 1960. *The variation of unit-cell edge of uranium monocarbide in ARC melted uranium-carbon alloys*, Journal of the Less Common Metals 2, 352-356

Yuan, H., Li, J., Shen, Q., Zhang, L., 2012. *In situ synthesis and sintering of ZrB_2 porous ceramics by the spark plasma sintering–reactive synthesis (SPS–RS) method*, International Journal of Refractory Metals and Hard Materials 34, 3-7